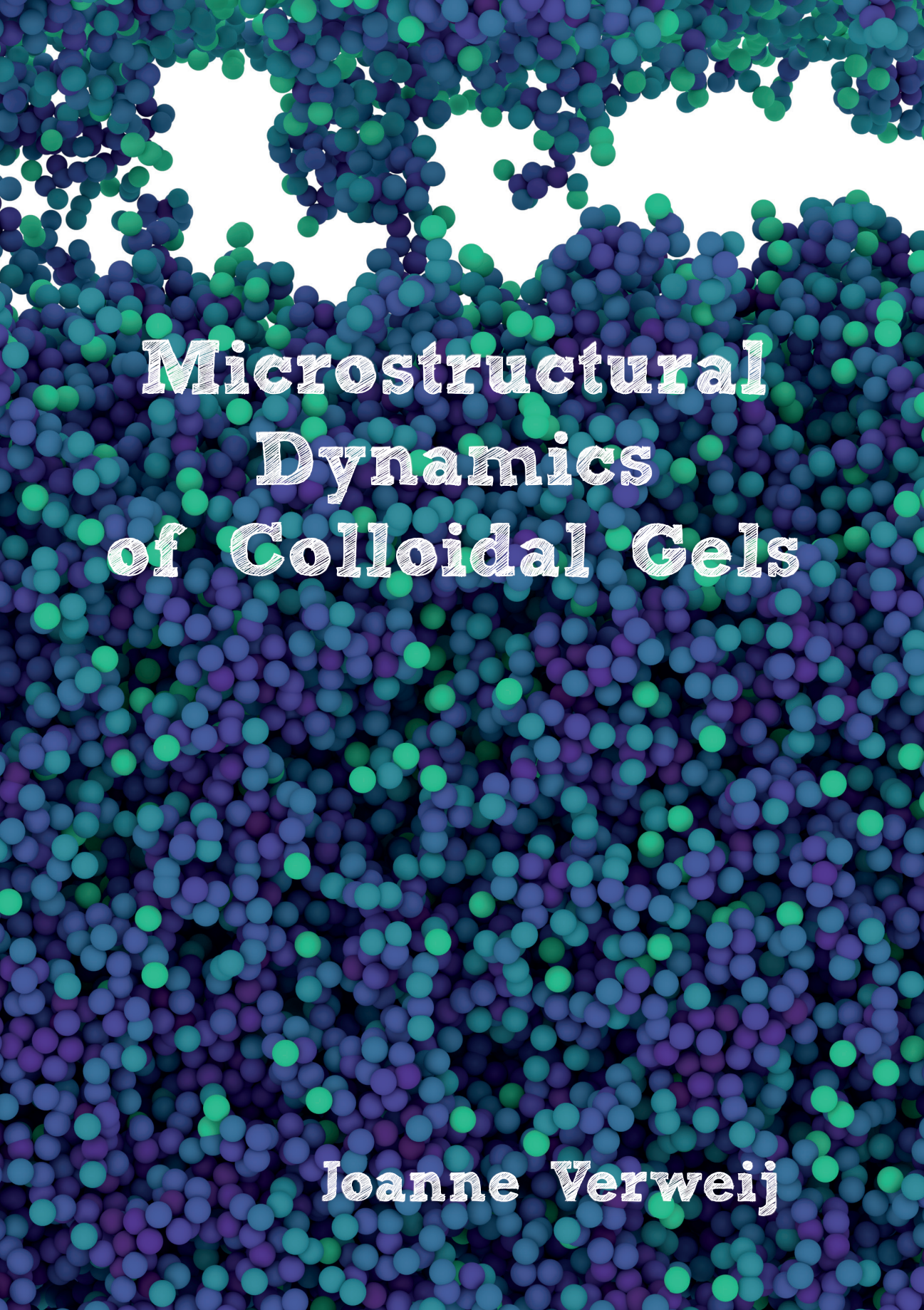
Microstructural
Dynamics
of Colloidal Gels
Joanne Verweij

Propositions

1. Plasticity in colloidal gels cannot be captured by dilute network models (this thesis)
2. Internal stresses play a crucial role in the failure of colloidal gels under external fields (this thesis)
3. Reducing the pressure on academics to publish will lead to an increase in high quality output
4. Cross-disciplinary COVID-19 research shows the value of a broad science agenda
5. Innovative technologies alone are not the solution to climate change
6. It is desirable that children learn to program at the same time when they learn to count and to write

Propositions belonging to the thesis, entitled

Microstructural Dynamics of Colloidal Gels

Joanne Verweij

Wageningen, 16 September 2020

Microstructural Dynamics of Colloidal Gels

Joanne Verweij

Thesis committee

Promotors
Prof. Dr Jasper van der Gucht
Professor of Physical Chemistry and Soft Matter
Wageningen University & Research

Prof. Dr Frans Leermakers
Personal chair, Physical Chemistry and Soft Matter
Wageningen University & Research

Prof. Dr Joris Sprakel
Personal chair, Physical Chemistry and Soft Matter
Wageningen University & Research

Other members
Prof. Dr Erik van der Linden, Wageningen University & Research
Prof. Dr Pavlik Lettinga, KU Leuven, Belgium & Forschungszentrum Jülich GmbH, Germany
Prof. Dr Bela Mulder, AMOLF & Utrecht University
Dr Laura Fillion, Utrecht University

This research was conducted under the auspices of Graduate School VLAG (Advanced studies in Food Technology, Agrobiotechnology, Nutrition and Health Sciences).

Microstructural Dynamics of Colloidal Gels

Joanne Verweij

Thesis
submitted in fulfillment of the requirements for the degree of doctor
at Wageningen University
by the authority of the Rector Magnificus,
Prof. Dr A.P.J. Mol,
in the presence of the
Thesis Committee appointed by the Academic Board
to be defended in public
on Wednesday 16 September 2020
at 4 p.m. in the Aula.

Joanne Verweij
Microstructural Dynamics of Colloidal Gels
163 pages

PhD thesis, Wageningen University, Wageningen, The Netherlands (2020)
With references, with summary in English

ISBN: 978-94-6395-428-0
DOI: https://doi.org/10.18174/523815

“Attention makes the genius; all learning, fancy, and science depend on it. Newton traced back his discoveries to its unwearied employment. It builds bridges, opens new worlds, and heals diseases; without it Taste is useless, and the beauties of literature are unobserved; as the rarest flowers bloom in vain, if the eye be not fixed upon the bed. ”

Robert Aris Willmott - Pleasures, Objects, and Advantages of Literature (1855)

Contents

Introduction

I

Soft matter

All around us, we find soft, elastic materials. One can think of eating pudding, yogurt or ice cream, squeezing toothpaste out of a tube and driving to work in a car with rubber tires. While these materials have very different properties, their microscopic structure share some common features: their building blocks are larger than small molecules but tinier than grains of sand and do not exhibit long-range order [1, 2]. Soft materials can be formed by a rich variety of building blocks, such as polymers, surfactants and colloids [1].

Soft materials are widely used in day to day life. Yet, how the macroscopic behaviour of a material can be explained from the structure and interaction of its individual building blocks remains a complex question in soft matter physics. As follows, the physics of these systems is intensively studied in many disciplines, ranging from material science, food science and nanotechnology to tissue engineering [3–11]. It is especially hard to study the relationship between structure and function when a materials' structure is not in equilibrium and evolves in time. This is the case for the class of soft materials studied in this thesis, so-called colloidal gels.

In this thesis, we use simulations and experiments to study the microstructural dynamics of colloidal gels, both in the presence and absence of external fields. Simulations are suitable to study the microstructural response of colloidal gels in great detail. In addition, recent advances in the synthesis of colloidal particles allow us to quantify large parts of the microstructure of experimental colloidal gels using confocal microscopy. By combining simulations and experiments we aim to get a better understanding of the mechanical (in)stability and the network topology of colloidal gels. But before we dive into this research, several concepts which are key to understand this thesis are explained. This Chapter starts with a description of physical

gels and their applications. Next, concepts such as stress, strain and yield stress are clarified. Subsequently, the use of colloids as a model system, the formation of colloidal gels and their mechanical (in)stability is discussed. The end of this Chapter concludes with a description of the simulation methods used in this thesis.

1.1.1 Gels and their applications

In this thesis, colloidal gels are studied as a class of soft materials. According to the Encyclopedia Britannica the basic definition of a gel is the following:

Gel, *coherent mass consisting of a liquid in which particles too small to be seen in an ordinary optical microscope are either dispersed or arranged in a fine network throughout the mass. A gel may be notably elastic and jellylike (as gelatin or fruit jelly), or quite solid and rigid (as silica gel, a material that looks like coarse white sand and is used as a dehumidifier).* [12]

We can distinguish between two types of gels, depending on their bonding properties, namely chemical and physical gels. The strongest interactions are obtained in chemical gels were covalent bonds create cross-links in a network, for example in vulcanized rubber [13]. In this case, irreversible cross-linking or polymerization is induced by heating the material. Physical gels involve non-covalent bonds, which are often –but not always– reversible and can be tuned in strength [14]. Here, association and dissociation of bonds can be

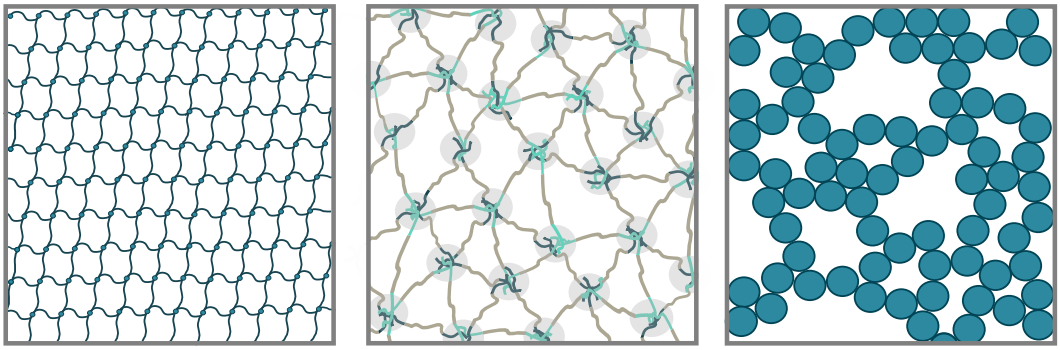

Figure 1.1 – Schematic representation of a hydrogel, block copolymer gel and colloidal gel (from left to right). Hydrogels consist of cross-linked hydrophilic polymers which form a network which can contain large amounts of fluid. Block copolymer gels consist of polymers with different functional groups. Here, we show a network formed through charge-driven assembly. In colloidal gels the network is formed by attractive particles dispersed in a fluid.

induced by varying pH, temperature, concentration, ionic strength, charge composition, the amount of light, magnetic and electric fields and shear [14–17].

Let us now take a closer look at some possible applications of these physical gels. The first class of gels we discuss are hydrogels, which consist of a three-dimensional polymer network in water (see Fig. 1.1 left) and are mechanically soft. These gels can be used for drug delivery and tissue engineering [3, 18–20], as their structure is similar to the extracellular matrix. Specifically, the structure of the gel can be used to control the distribution of cells or medication. Applying stimuli to the gel network can trigger the development of desired tissues [21–25]. However, it is also possible to use the scaffold as a means to selectively transport biomolecules which are vital for tissue growth [26–28]. Recent advances in 3D printing and the development of thougher hydrogels now even open up the possibility to develop materials that mimic cartilage [3, 29–31]. Besides its use in medical applications hydrogels are also suitable as soft actuators and sensors [32–35]. The suitability of hydrogels for actuation is based on the ability of hydrogels to swell and deswell upon applying external triggers [4, 36–38]. Using hydrogels as force sensors is advantageous because they are extremely stretchable and can self heal if the polymer chains form new cross-links [33, 39].

Another class of physical gels are block copolymer gels. The polymer, for instance, consists of two charged outer blocks and a neutral middle block. Combined with oppositely charged block copolymers a transient network will form (see Fig. 1.1 middle). Due to their high connectivity, block copolymer gels can be used in dye solar cells and lithium batteries [40–42] and as thin-film transistors [43, 44]. Other applications range from tissue engineering [45, 46], self healing gels [47], underwater adhesives [48, 49] to flexible displays [50] and soft actuators [51].

The final class of gels we discuss here are colloidal gels – the type of gel we study in this thesis. Colloidal gels consist of a space-spanning network of particles, dispersed in a fluid [52] (see Fig. 1.1 right). Many food products, such as yoghurt, cheese and egg products, are colloidal gels [5]. Particle gels are therefore widely studied in food technology, to improve sensory perception and food texture [5]. However, colloidal gels are also frequently used in other applications such as, dispersion based paints [53, 54], cosmetics [55], moldable and 3D scaffolds for tissue engineering [56–59], self healing gels [60] and to create ultralight and low conductive aerogels used in the production of ceramics [61–63]. Particles in colloidal gels are kinetically arrested, which prevents the system to evolve towards an equilibrium. As a consequence, thermodynamic theories used for polymer gels, like the hydrogels and block copolymer gels described above, cannot be applied directly.

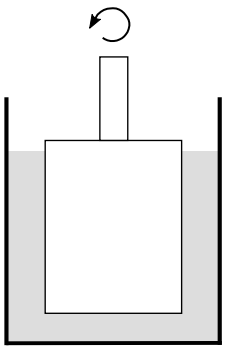

Figure 1.2 – Rheometer with a concentric cylinder geometry.

1.1.2 Stress & strain

One of the characteristics of gels is their elastic response to deformation. Flow and deformation of gels can be systematically studied in a rheometer. The word rheology is credited to Eugene C. Bingham (around 1928), who together with his colleague Marcus Reiner came up with the term inspired by the aphorism of Simplicius' $\pi\alpha\nu\tau\alpha\ \rho\epsilon\iota$ "everything flows" [64]. The studied gel is formed in a round cylinder which contains a rotatable inner cylinder in the middle, the so-called concentric cylinder geometry (see Fig. 1.2). The rotated distance is converted into a strain γ. In this way one can measure how much force it takes to deform a material up to a certain strain. Imagine that you pull on an elastic rubber beam. The initial length of the beam L will get elongated with a certain length δL. In this case, the resulting amount of strain γ can be defined as:

$$\gamma = \frac{\delta L}{L} \tag{1.1}$$

Yet, in the concentric cylinder geometry the gel is sheared, i.e. one of the walls stays stationary whereas the other wall is linearly displaced with δL. We can represent this situation with the schematic picture in Fig. 1.3b. So in case of shear, the amount of strain is calculated by:

$$\gamma = \frac{\delta L}{h} \tag{1.2}$$

Another important quantity in the deformation of a material is the amount of applied stress σ. Stress is defined as a force per unit area. The stress at point P in a material can be described by the the stress tensor (see Figure 1.3a),

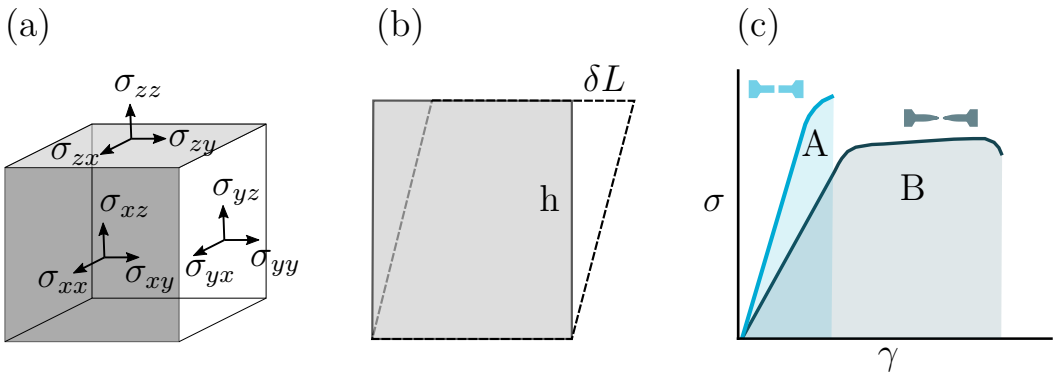

Figure 1.3 – (a) Visual representation of the stress tensor in three dimensions. (b) Shear deformation on a rectangle. The top plate will move whereas the bottom plate stays stationary. (c) Stress-strain curve of a brittle (curve A) and a ductile (curve B) material.

which has 9 different components:

$$\sigma_{ij} = \begin{bmatrix} \sigma_{xx} & \sigma_{xy} & \sigma_{xz} \\ \sigma_{yx} & \sigma_{yy} & \sigma_{yz} \\ \sigma_{zx} & \sigma_{zy} & \sigma_{zz} \end{bmatrix} \tag{1.3}$$

In σ_{ij} the first subscript indicates the direction of the surface normal upon which the stress acts, whereas the second subscript refers to the direction of the stress component. This stress matrix is symmetrical in equilibrium, i.e. $\sigma_{xy} = \sigma_{yx}$, which leaves us with 6 independent components instead of 9. A positive value for these normal components indicates that the force acts outwards and will create a tensile stress. A negative value for the normal component, on the other hand, indicates that the force acts inwards to create a compressive stress [65–67].

1.1.3 Yield stress

Previously we defined the concepts of stress and strain. The modulus of a material can be interpreted as the ratio between this stress and strain. Upon deforming a brittle, stiff material at small strains –such as different metals at low temperature, ceramics or glass- the resulting stress versus strain curve will be linear. At larger deformation brittle fracture occurs or the material starts deforming in a non-linear fashion (see Fig. 1.3c, curve A) [67]. For ductile materials, below a threshold force the material can respond purely elastic, whereas upon exceeding this value –at the so-called yield stress– the material starts to flow [68]. Yield stress materials, such as toothpaste, mayonnaise, foams and paints will return to their original shape when deformation takes place in the elastic regime only. Yet, above the yield point a fraction of the deformation will be permanent and non-reversible (Fig. 1.3c, curve B). We call this plastic deformation.

States of matter can be divided in three major classes; solids, liquids and gasses. A common example to illustrate these states is water, which can exist as ice (solid), water (liquid) and water vapour (gas). Remarkably, gels show characteristics of both liquids and solids. The definition of a gel has therefore been a widely discussed topic amongst scientist. Andrew Keller –a polymer scientist– said the following to its colleagues at the Faraday Discussions Meeting in 1995:

"The fact is that there is no simple and unique definition. In every day usage we may think of a simple jelly as familiar in culinary usage. It embodies the main characteristics of what we associate with the gel state. Its main constituent is a fluid (in this case water) yet it retains its shape, a feature characteristic of the

solid state of matter. Yet it is not an ordinary solid: it can support large strains to a high elastic limit in response to small stresses a consequence of which is the every day experience that a jelly wobbles. In widest generality, the retention of shape implies some connectedness throughout the system which, in view of the fact that the majority component is a fluid, means that there exist connective pathways along the 'non-fluid' component from any chosen point of a macroscopic sample to another, implying, in turn, the existence of a network" [69].

The interesting elastic properties of gels are due to the formation of a space-spanning network of the solid particles within the fluid. Due to this network gels exhibit solid-like properties such as a yield stress. Yet, the gel structure does not show significant order (see schematic state diagram Fig. 1.5). The disorderly and amorphous structure of colloidal gels will show a solid-to-liquid transition upon extensive deformation. This deformation is highly complex as the system is out of equilibrium and the gel undergoes irreversible structural changes.

Colloidal gels

1.2.1 Colloids as big atoms

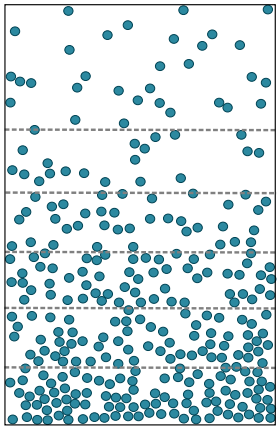

Figure 1.4 – Reproduction of a micrograph taken by J. Perrin of the sedimentation-diffusion equilibrium of resin (gamboge) spheres suspended in water [70].

The description of a gel in the Encyclopedia Britannica indicates that the particles in the liquid are to small to be seen with an optical microscope. Yet, visualization of the solid particles in a gel is crucial to study the microstructure of these gels in experiments. Therefore, we use larger micrometer sized particles: so-called colloids. Colloids can range from 10 nm up to several microns [52].

The proof that colloids provide a model system to study phases displayed by atoms, such as solids, liquids and gases, started with the experimental work of Jean Perrin. In 1909, Perrin showed that the sedimentation equilibrium of particles in a suspension follows an exponential distribution, according to:

$$n(z) = n(0)\exp^{-z/z_0} \tag{1.4}$$

with n the number density of the particle suspension and z the height, were z_0 is defined as:

$$z_0 = k_B T/\Delta m g \tag{1.5}$$

here we consider the Earth's gravitational field g, buoyant mass of the particles Δm, temperature T and the Boltzmann's constant k_B [71]. The distribution of particles in a suspension is governed by a gravitational drift

downwards, assuming that the particles have a higher density than the liquid, and a thermal motion of the solvent molecules (see section Brownian Dynamics simulations) [72]. Jean Perrin showed that this barometric height distribution also holds for gum resin particles which were 240 nm in diameter (Fig. 1.4) [70]. As colloidal particles can also distribute themselves spontaneously, due to Brownian motion, we can use these larger particles to study the phase behaviour of atoms [71]. The concept that colloids to some extent behave as "big atoms" is widely utilized to study phenomena at the atomic scale [71, 73–77].

Colloidal gels form an interesting platform to study particle dynamics of arrested matter, even though there is no real equivalent for colloidal gels at the atomic scale. Colloidal particles are small enough to let the particle dynamics be controlled by the thermal energy, yet it is possible to visualize each individual particle with confocal laser scanning microscopy and follow its motion both in space and time.

1.2.2 Gelation

When the interactions between colloids in a suspension become attractive, particles will meet each other and form fractal aggregates. In time, these growing aggregates fill the entire space with a system-spanning net-

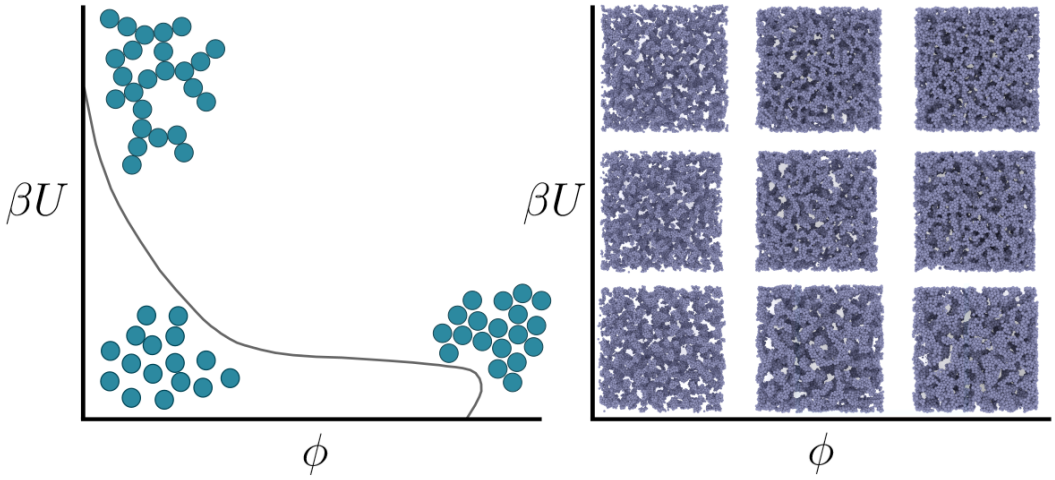

Figure 1.5 – (left) Schematic state diagram of particles with short-ranged interactions, showing a fluid, gel and glass. Here, we plot the volume fraction ϕ on the x-axis versus the interaction energy βU on the y-axis. Figure reproduced from [78]. (right) Visual representation of a small slab of simulated colloidal gels at different volume fractions and interaction energies. From left to right the volume fractions equal $\phi = 0.09$, 0.17 and 0.25, whereas from top to bottom the interaction energies equal 40, 10 and 5 $k_B T$.

work [73, 78, 79]. We call this process gelation and the point when a system-spanning network is reached the percolation point. The formation of a space-spanning network can already happen at low volume fraction ϕ. When we look at the state diagram of particles with a short-ranged interaction (see Fig. 1.5) we observe that at high volume fraction and low interaction energy a different regime appears. Here, particles with short-ranged interactions start to form colloidal glasses [78]. Below the percolation line (in gray), we find a fluid. At low volume fraction above the percolation line, both the interaction energy U/k_BT between particles, the volume fraction ϕ and the range of the attraction determine the obtained gel morphology (see Fig. 1.5) [52].

In the formation of fractal aggregates, two different types of aggregation are distinguished; diffusion-limited cluster aggregation (DLCA) and reaction-limited cluster aggregation (RCLA), respectively. The first type of aggregation is limited by the diffusion time it takes for the particles or clusters to encounter one another. In the second type of cluster formation there is a repulsive energy barrier between the particles, that prevents them from sticking immediately. The rate limiting step in this case is the aggregation reaction itself. Due to the energy barrier that has to be overcome in the latter type of aggregation, more compact clusters are formed. In practice, aggregates form both through DLCA and RCLA rearrangements. However, when particles are likely to stick immediately, it is less probable that they detach again [52, 80–82]. Initially, particles show fast Brownian motion, but this movement slows down due to to aggregation and cluster growth and finally becomes constrained in the gel structure [5]. For short-ranged attractions in the order of the thermal energy, particles can reversibly attach and detach from the network to minimize the free energy of the system [79].

How gels are formed depends on the volume fraction and interaction energy between particles. For low volume fractions and large attractions between colloids gelation is a consequence of diffusion limited cluster aggregation (DLCA) [52, 83–87]. Yet, for intermediate volume fractions and reversible short-ranged attractions in the order of the thermal energy, gels form through a different mechanism. In this regime, gels want to phase separate into colloid-rich and colloid-poor regions through spinodal decomposition. This is due to the fact that the system is thermodynamically unstable and wants to minimize its energy [52, 81, 82]. When particle bonds are formed in these systems, gelation occurs as a consequence of dynamic arrest which hinders further phase separation [52, 88–94]. The transient networks that form in this way thus result from dynamic arrest of bicontinues spinodal decomposition.

1.2.3 Depletion interaction

Colloidal gels typically comprise of particles with attractive interactions. This attraction can be induced in different ways, for instance through charge-based interactions [60, 95], supramolecular interactions [96, 97] or DLVO interactions – a combination of electrostatic and van der Waals forces– [98, 99]. In this thesis we use the concept of depletion to induce attraction between colloids. This method has the advantage that the interaction between particles can be tuned in strength and range.

Depletion occurs when small particles or non-absorbing polymers are added to a colloidal dispersion. The attractive interaction between the particles will be in the range of a few k_BT, depending on the concentration and molecular weight of the polymer. Increasing the strength of the depletion interaction in a colloid-polymer mixture or a colloid-colloid mixture eventually leads to phase separation or aggregation [100, 101].

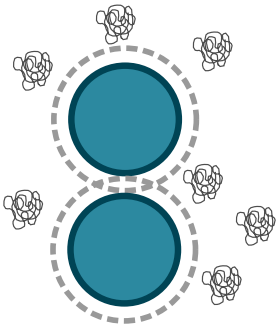

Figure 1.6 – Depletion interaction. The added polymers are excluded from a shell around the colloidal particles, i.e. the depletion zone. Due to the imbalance in osmotic pressure the particles will be pushed together.

The polymer molecules are excluded from the depletion zone near the large colloidal particles (as depicted in Fig. 1.6). When the colloidal particles approach each other the depletion zones will overlap. Consequently, the volume between the particles will have a lower concentration of polymer molecules compared to the bulk solution. This difference in osmotic pressure between the bulk solution and the depletion zone results in a net force pushing the particles together. From a thermodynamic point of view, overlap of the depletion zones reduces the volume from which polymer molecules are excluded, which effectively increases the entropy of the system [100, 102].

The first fundamental work on depletion was carried out by Asakura and Oosawa [103, 104], further elaborated by Vrij [105] and Joanny, Lieber and de Gennes [106]. The original expression for the interaction potential proposed by Asakura & Oosawa neglects the effect of the degrees of freedom of the polymer molecules. To validate a simpler approach, Gast et al. combined thermodynamic perturbation theory and the work of Joanny, Liebler and de Gennes to demonstrate that the free energy of interaction follows from the osmotic pressure of the bulk solution [101, 107]. The approximate interaction potential between particles in the gel is given by:

$$\frac{U(r)}{k_BT} = \Pi(c)V_{overlap}(r) \tag{1.6}$$

with $\Pi(c)$ the osmotic pressure of the depletant and $V_{overlap}(r)$ the volume of overlap between the two depletion layers. Here, the overlap volume can be calculated based on geometric considerations, for instance for equal sized colloids with diameter σ at a center to center separation r [101, 108, 109]:

$$V_{overlap}(r) = \frac{\pi}{6}\sigma^3(1+\xi)^3(1 - \frac{1.5r}{\sigma(1+\xi)} + \frac{0.5r^3}{\sigma^3(1+\xi)^3}) \tag{1.7}$$

were $\xi = R_g/a$ is the polymer-colloid size ratio.

To simulate short-ranged particle interactions for nearly hard spheres, one can use a Asakura-Oosawa (AO) potential. Yet, recent research has shown that the Morse potential –which approaches the one component Asakura-Oosawa interaction– actually better describes the cluster distribution of a full AO fluid than the one-component AO description [110]. Therefore, we use a Morse potential in this thesis to simulate colloidal gels. The equation for the Morse potential reads:

$$\beta U(r) = \beta U \exp[\rho_0(\sigma - r)](\exp[\rho_0(\sigma - r)] - 2) \tag{1.8}$$

were βU determines the well depth of the potential and ρ_0 can be used to vary the range of the potential. The use of the Morse potential as a depletion potential has become more widespread in recent years [111–116].

1.2.4 Aging and mechanical failure

While a colloidal gel is a so-called arrested state, this does not imply that the gel structure does not evolve anymore. In time, a gel will evolve due to particle rearrangements. This process is called aging. Aging is caused by relaxation of internal stresses in the network [117–119], a process which not only occurs in gels, but also in other types of soft matter such as colloidal glasses and concentrated emulsions [117].

There are limits to the stability of colloidal gels. An instability that can happen in weak particle gels is syneresis. In this process the fluid gets expelled from the gel, while the gel gets denser. This phenomena for instance occurs in mayonnaise [120] , cheese [121–124], yoghurt [125, 126] and agar [127]. Syneresis is attributed to rearrangements in the particle network as a response to internal stresses. External stresses, such as gravity or shear, can accelerate or change particle rearrangements in the network. However, it is not yet fully understood how processes, such as syneresis, aging and gravitational collapse are related.

Gravitational collapse is a case in which a gel fails drastically due to external stresses [114, 128–130]. Here, gravity provides a strain on the network which will cause the gel to break. Gravitational collapse can be very rapid –because gravity already prevents the network structure from forming– or slow. In the latter case it is called a delayed collapse. Predictions are that the initial collapse of a gel depends on the speed of fluid backflow through the network, whereas the height of the collapse relates to the network's elasticity [94, 130, 131]. Confocal microscopy data of emulsion gels shows how the network restructures and weakens in time [130]. The reduction in the connectivity of the network eventually triggers a macroscopic collapse.

The mechanical response of colloidal gels can remarkably alter upon

applying shear or if there is fluid flow in a sample. At high shear rates a network can break up into individual particles [132–135], whereas at lower shear rates the network breaks up in clusters [116, 134, 135]. In both cases, the gel loses its mechanical rigidity. Fluid flow through colloidal gels causes hydrodynamic instabilities, which influence both the stability and morphology of the gel [136].

Particle simulations

1.3.1 Brownian Dynamics simulations

At the age of 54, Robert Brown (1773-1858) a Scottish botanist, was studying pollen grains suspended in water [137]. Under his microscope, he observed that particles inside these pollen grains were moving. At first he thought that the particles had a given living force inside of them [138]. Yet, when he repeated the experiment with powders of inorganic materials, such as window-glass and pieces of rock, he still observed particles to move. It took several decades before a satisfying explanation was found. In 1905, Einstein published a paper which explains how particles submerged in a fluid undergo a random walk due to thermal motion of the solvent molecules around them [139]. At that time, the existence of atoms and molecules was still highly debated. Jean Baptist Perrin (1870-1942) proved the theory of Einstein by systematically studying the motion of micrometer sized particles (Fig. 1.7) [140]. For this work he received the Nobel prize for Physics in 1926. Even though Robert Brown was not the first person to describe random motion of particles suspended in a fluid [141, 142], nowadays, this phenomena is known as Brownian motion.

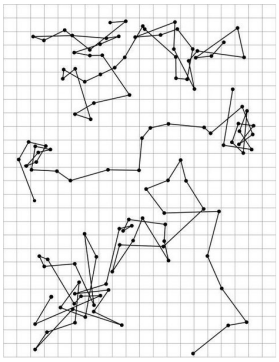

Figure 1.7 – A reproduction from Jean Baptiste Perrin, *"Mouvement brownien et réalité moléculaire," Ann. de Chimie et de Physique (VIII) 18, 5-114, 1909*. Three trajectories of the motion of colloidal particles of radius 0.53 μm are drawn. Successive positions, obtained every 30 seconds, are joined by straight lines (the mesh size equals 3.2 μm).

To describe the highly irregular motion of Brownian particles we use the overdamped Langevin equation. This simplified version of the Langevin equation can be used as we assume that the colloidal systems studied in this thesis are inertia free, i.e. viscous effects play a larger role. The stochastic differential equation is numerically integrated in time using the Euler-Maruyama method [143]. In this way, the motion of a particle i with position $\boldsymbol{r}_i$ is obtained by solving:

$$\dot{\boldsymbol{r}}_i(t) = \beta D[-\nabla_i U(t)] + \sqrt{2D\boldsymbol{\xi}_i(t)} \tag{1.9}$$

The first term on the right of this equation accounts for the particle interactions. Here, U is the interaction potential and β equals the inverse temperature ($1/k_BT$). The second term accounts for the solvent molecules kicking

against the particles. Instead of describing the movement of the solvent molecules explicitly, we use a stochastic force $\boldsymbol{\xi}_i(t)$ to model the thermal fluctuations of the particles. This stochastic force is a random vector with zero mean and unit variance. By treating the solvent molecules implicitly BD simulations become significantly less computationally expensive.

The diffusion D of spherical particles in a liquid can be described by the Stokes-Einstein equation [139, 144]:

$$D = \frac{k_B T}{6\pi\eta r} \tag{1.10}$$

with T the absolute temperature of the system, k_B Boltzmann's constant, η the viscosity of the fluid and r the radius of the particles. Note, that this diffusion constant only holds at low Reynolds number, i.e. when flow is predominantly laminar.

1.3.2 Monte Carlo simulations

The Monte Carlo method has been developed by mathematicians Stanislaw Ulam and John Von Neumann who worked at the Manhattan project during World War II. They did research for the nuclear weapons project at the Los Alamos National Laboratory in the United States, were they tried to develop new methods to predict neutron chain reactions in fission devices. During a game of solitaire Ulam asked himself the question whether or not he could predict the outcome of the game [145]. Here, the idea was born to start with a random configuration and repeat the same experiment hundreds of times to determine the chances of success. John Von Neumann soon realized the importance of this idea and programmed one of the first available computers to carry out these calculations [146]. As the work of Ulam and Von Neumann was classified they gave their work the code name Monte Carlo, referring to the Monte Carlo casino in Monaco where Ulam's uncle would gamble [147].

Statistical sampling was a well-known technique already, yet the development of the computer provided a way to actually use it for large scale calculations after the war [147]. Nowadays, Monte Carlo simulations are used in a wide variety of applications ranging from designing better catalysts, modelling complex road networks to predicting stock price movement.

The Monte Carlo method used in particle simulations is called the Metropolis Method. The basic idea behind this method is to draw samples from a probability distribution $P(x)$. If more and more samples are generated, the values in the end will approximate the desired distribution. The algorithm proceeds by randomly moving a particle in space, through a so-called Markov chain. That is, each particle move is independent from the next one. Based on the old and new position of a particle a move will either be accepted or rejected. Here, the change in energy of the system (ΔE), caused by the move,

determines the acceptance rate. A particle move to a more desired position ($\Delta E < 0$) will always be accepted. If $\Delta E > 0$ the move will be accepted with probability $\exp(\frac{-E}{k_B T})$ [148, 149]. This will continue till the energy of the system does not change anymore.

The advantage of a Monte Carlo simulation is that it allows for discontinued potentials, such as in hard sphere systems. Yet, if one wants to study dynamics of a system Brownian Dynamics is the method of choice.

Outline of this thesis

The central aim of this thesis is to illuminate the structure-function relationship of colloidal gels, both in absence and in presence of external fields. In Chapter 2 we study fatigue in colloidal gels. We investigate the effect of applying small oscillatory deformations to colloidal gels in experiments and colloidal gel strands in computer simulations. In Chapter 3 we extend the simulation study by examining fatigue in gel strands of different diameter, length, interaction strength and interaction range. In Chapter 4, we develop an algorithm to quantify colloidal gels based on the nodes and strands in the network. The network topology is determined by considering particle coordinates and the network's connectivity. We demonstrate that particles undergo different dynamics in nodes and strands close to the percolation point, when no external stresses are applied. In Chapter 5 we perform a simulation study of colloidal gels under shear. We determine the network topology at different interaction strengths and volume fractions to see how the gel structure evolves during shear deformation. We complement the simulation study with shear experiments in which we resolve the three-dimensional structure of colloidal gels using confocal microscopy. In Chapter 6 we experimentally study the gravitational collapse of colloidal gels. By following the structure of the gels in time we can quantify the network response of the gel during failure. Here, the gel collapse is observed to be enhanced by large-scale, shear-like motion in the direction perpendicular to gravity. Finally, Chapter 7 contains a general discussion which connects the research described in the previous chapters and places it in a broader scientific context.

Bibliography

[1] Maurice Kleman and Oleg D Laverntovich. *Soft matter physics: an introduction*. Springer Science & Business Media, 2007.

[2] Pierre-Gilles De Gennes. Soft matter. *Reviews of Modern Physics*, 64(3):645, 1992.

[3] Kenneth R Shull. Materials science: A hard concept in soft matter. *Nature*, 489(7414):36, 2012.

[4] Ryan L Truby and Jennifer A Lewis. Printing soft matter in three dimensions. *Nature*, 540(7633):371, 2016.

[5] Raffaele Mezzenga, Peter Schurtenberger, Adam Burbidge, and Martin Michel. Understanding foods as soft materials. *Nature Materials*, 4(10):729, 2005.

[6] RGM Van der Sman. Soft matter approaches to food structuring. *Advances in Colloid and Interface Science*, 176:18–30, 2012.

[7] Job Ubbink, Adam Burbidge, and Raffaele Mezzenga. Food structure and functionality: a soft matter perspective. *Soft Matter*, 4(8):1569–1581, 2008.

[8] IW Hamley. Nanotechnology with soft materials. *Angewandte Chemie International Edition*, 42(15):1692–1712, 2003.

[9] Satish Nayak and L Andrew Lyon. Soft nanotechnology with soft nanoparticles. *Angewandte Chemie International Edition*, 44(47):7686–7708, 2005.

[10] Ilya Levental, Penelope C Georges, and Paul A Janmey. Soft biological materials and their impact on cell function. *Soft Matter*, 3(3):299–306, 2007.

[11] David Gonzalez-Rodriguez, Karine Guevorkian, Stéphane Douezan, and Françoise Brochard-Wyart. Soft matter models of developing tissues and tumors. *Science*, 338(6109):910–917, 2012.

[12] Encyclopaedia britannica. 2018.

[13] Paul J Flory. Network structure and the elastic properties of vulcanized rubber. *Chemical Reviews*, 35(1):51–75, 1944.

[14] Madeleine Djabourov, Katsuyoshi Nishinari, and Simon B Ross-Murphy. *Physical gels from biological and synthetic polymers*. Cambridge University Press, 2013.

[15] Abdalla Karoyo and Lee Wilson. Physicochemical properties and the gelation process of supramolecular hydrogels: A review. *Gels*, 3(1):1, 2017.

[16] Marc Lemmers, Joris Sprakel, Ilja K Voets, Jasper Van Der Gucht, and Martien A Cohen Stuart. Multiresponsive reversible gels based on charge-driven assembly. *Angewandte Chemie International Edition*, 49(4):708–711, 2010.

[17] Suk-kyun Ahn, Rajeswari M Kasi, Seong-Cheol Kim, Nitin Sharma, and Yuxiang Zhou. Stimuli-responsive polymer gels. *Soft Matter*, 4(6):1151–1157, 2008.

[18] Kuen Yong Lee and David J Mooney. Hydrogels for tissue engineering. *Chemical Reviews*, 101(7):1869–1880, 2001.

[19] Ali Khademhosseini and Robert Langer. Microengineered hydrogels for tissue engineering. *Biomaterials*, 28(34):5087–5092, 2007.

[20] Jeanie L Drury and David J Mooney. Hydrogels for tissue engineering: scaffold design variables and applications. *Biomaterials*, 24(24):4337–4351, 2003.

[21] Lu Han, Xiong Lu, Menghao Wang, Donglin Gan, Weili Deng, Kefeng Wang, Liming Fang, Kezhi Liu, Chun Wai Chan, Youhong Tang, et al. A mussel-inspired conductive, self-adhesive, and self-healable tough hydrogel as cell stimulators and implantable bioelectronics. *Small*, 13(2):1601916, 2017.

[22] Mohamed Alaa Mohamed, Afsoon Fallahi, Ahmed MA El-Sokkary, Sahar Salehi, Magda A Akl, Amin Jafari, Ali Tamayol, Hicham Fenniri, Ali Khademhosseini, Stelios T Andreadis, et al. Stimuli-responsive hydrogels for manipulation of cell microenvironment: From chemistry to biofabrication technology. *Progress in Polymer Science*, page 101147, 2019.

[23] B Hermenegildo, Clarisse Ribeiro, L Pérez-Álvarez, José L Vilas, David A Learmonth,

Rui A Sousa, P Martins, and S Lanceros-Méndez. Hydrogel-based magnetoelectric microenvironments for tissue stimulation. *Colloids and Surfaces B: Biointerfaces*, 181:1041–1047, 2019.

[24] Xifeng Liu, A Lee Miller, Sungjo Park, Brian E Waletzki, Zifei Zhou, Andre Terzic, and Lichun Lu. Functionalized carbon nanotube and graphene oxide embedded electrically conductive hydrogel synergistically stimulates nerve cell differentiation. *ACS Applied Materials & Interfaces*, 9(17):14677–14690, 2017.

[25] Somasundar Mantha, Sangeeth Pillai, Parisa Khayambashi, Akshaya Upadhyay, Yuli Zhang, Owen Tao, Hieu M Pham, and Simon D Tran. Smart hydrogels in tissue engineering and regenerative medicine. *Materials*, 12(20):3323, 2019.

[26] Hyojin Ko, Kasinan Suthiwanich, Héloïse Mary, Somayeh Zanganeh, Shu-Kai Hu, Samad Ahadian, Yunzhi Yang, Goro Choi, Kirsten Fetah, Yuting Niu, et al. A simple layer-stacking technique to generate biomolecular and mechanical gradients in photocrosslinkable hydrogels. *Biofabrication*, 11(2):025014, 2019.

[27] Yun Jung Yang, Danielle J Mai, Thomas J Dursch, and Bradley D Olsen. Nucleopore-inspired polymer hydrogels for selective biomolecular transport. *Biomacromolecules*, 19(10):3905–3916, 2018.

[28] Keely A Heintz, Michael E Bregenzer, Jennifer L Mantle, Kelvin H Lee, Jennifer L West, and John H Slater. Fabrication of 3d biomimetic microfluidic networks in hydrogels. *Advanced Healthcare Materials*, 5(17):2153–2160, 2016.

[29] Sebastián L Vega, Mi Y Kwon, and Jason A Burdick. Recent advances in hydrogels for cartilage tissue engineering. *European Cells & Materials*, 33:59, 2017.

[30] Janani Radhakrishnan, Anuradha Subramanian, Uma Maheswari Krishnan, and Swaminathan Sethuraman. Injectable and 3d bioprinted polysaccharide hydrogels: from cartilage to osteochondral tissue engineering. *Biomacromolecules*, 18(1):1–26, 2017.

[31] Jianqi Wang, Fengjie Zhang, Wing Pui Tsang, Chao Wan, and Chi Wu. Fabrication of injectable high strength hydrogel based on 4-arm star peg for cartilage tissue engineering. *Biomaterials*, 120:11–21, 2017.

[32] Meihong Liao, Pengbo Wan, Jiangru Wen, Min Gong, Xiaoxuan Wu, Yonggang Wang, Rui Shi, and Liqun Zhang. Wearable, healable, and adhesive epidermal sensors assembled from mussel-inspired conductive hybrid hydrogel framework. *Advanced Functional Materials*, 27(48):1703852, 2017.

[33] Guofa Cai, Jiangxin Wang, Kai Qian, Jingwei Chen, Shaohui Li, and Pooi See Lee. Extremely stretchable strain sensors based on conductive self-healing dynamic cross-links hydrogels for human-motion detection. *Advanced Science*, 4(2):1600190, 2017.

[34] Hyunwoo Yuk, Shaoting Lin, Chu Ma, Mahdi Takaffoli, Nicolas X Fang, and Xuanhe Zhao. Hydraulic hydrogel actuators and robots optically and sonically camouflaged in water. *Nature Communications*, 8(1):1–12, 2017.

[35] Wayne Francis, Aishling Dunne, Colm Delaney, Larisa Florea, and Dermot Diamond. Spiropyran based hydrogels actuators—walking in the light. *Sensors and Actuators B: Chemical*, 250:608–616, 2017.

[36] Howon Lee, Chunguang Xia, and Nicholas X Fang. First jump of microgel; actuation speed enhancement by elastic instability. *Soft Matter*, 6(18):4342–4345, 2010.

[37] Etienne Palleau, Daniel Morales, Michael D Dickey, and Orlin D Velev. Reversible patterning and actuation of hydrogels by electrically assisted ionoprinting. *Nature Communications*, 4(1):1–7, 2013.

[38] Leonid Ionov. Biomimetic hydrogel-based actuating systems. *Advanced Functional Materials*, 23(36):4555–4570, 2013.

[39] Zhao Wei, Jian Hai Yang, Jinxiong Zhou, Feng Xu, Miklós Zrínyi, Patrick H Dussault, Yoshihito Osada, and Yong Mei Chen. Self-healing gels based on constitutional dynamic chemistry and their potential applications. *Chemical Society Reviews*, 43(23):8114–8131, 2014.

[40] SS Soni, KB Fadadu, RL Vekariya, J Debgupta, KD Patel, A Gibaud, and VK Aswal. Effect of self-assembly on triiodide diffusion in water based polymer gel electrolytes: an application in dye solar cell. *Journal of Colloid and Interface Science*, 425:110–117, 2014.

[41] Fang Lian, Yan Wen, Yan Ren, and HongYan Guan. A novel pvb based polymer membrane and its application in gel polymer electrolytes for lithium-ion batteries. *Journal of Membrane Science*, 456:42–48, 2014.

[42] Yuzo Kitazawa, Kaori Iwata, Ryosuke Kido, Satoru Imaizumi, Seiji Tsuzuki, Wataru Shinoda, Kazuhide Ueno, Toshihiko Mandai, Hisashi Kokubo, Kaoru Dokko, et al. Polymer electrolytes containing solvate ionic liquids: A new approach to achieve high ionic conductivity, thermal stability, and a wide potential window. *Chemistry of Materials*, 30(1):252–261, 2018.

[43] Jeong Ho Cho, Jiyoul Lee, YU Xia, Bongsoo Kim, Yiyong He, Michael J Renn, Timothy P Lodge, and C Daniel Frisbie. Printable ion-gel gate dielectrics for low-voltage polymer thin-film transistors on plastic. *Nature Materials*, 7(11):900–906, 2008.

[44] Jiang Pu, Yohei Yomogida, Keng-Ku Liu, Lain-Jong Li, Yoshihiro Iwasa, and Taishi Takenobu. Highly flexible mos2 thin-film transistors with ion gel dielectrics. *Nano Letters*, 12(8):4013–4017, 2012.

[45] Christopher S O'Bryan, Christopher P Kabb, Brent S Sumerlin, and Thomas E Angelini. Jammed polyelectrolyte microgels for 3d cell culture applications: rheological behavior with added salts. *ACS Applied Bio Materials*, 2(4):1509–1517, 2019.

[46] Hyuck Joon Kwon, Yoshihito Osada, and Jian Ping Gong. Polyelectrolyte gels-fundamentals and applications. *Polymer Journal*, 38(12):1211–1219, 2006.

[47] Ryota Tamate, Kei Hashimoto, Tatsuhiro Horii, Manabu Hirasawa, Xiang Li, Mitsuhiro Shibayama, and Masayoshi Watanabe. Self-healing micellar ion gels based on multiple hydrogen bonding. *Advanced Materials*, 30(36):1802792, 2018.

[48] Marco Dompé, Francisco J Cedano-Serrano, Mehdi Vahdati, Larissa van Westerveld, Dominique Hourdet, Costantino Creton, Jasper van der Gucht, Thomas Kodger, and Marleen Kamperman. Underwater adhesion of multiresponsive complex coacervates. *Advanced Materials Interfaces*, page 1901785, 2019.

[49] Anton H Hofman, Ilse A van Hees, Juan Yang, and Marleen Kamperman. Bioinspired underwater adhesives by using the supramolecular toolbox. *Advanced Materials*, 30(19):1704640, 2018.

[50] Hong Chul Moon, Timothy P Lodge, and C Daniel Frisbie. Solution processable, electrochromic ion gels for sub-1 v, flexible displays on plastic. *Chemistry of Materials*, 27(4):1420–1425, 2015.

[51] Satoru Imaizumi, Hisashi Kokubo, and Masayoshi Watanabe. Polymer actuators using ion-gel electrolytes prepared by self-assembly of aba-triblock copolymers. *Macromolecules*, 45(1):401–409, 2012.

[52] Peter J Lu and David A Weitz. Colloidal particles: crystals, glasses, and gels. *Annual Review of Condensed Matter Physics*, 4(1):217–233, 2013.

[53] Marguerite Leang, Frederique Giorgiutti-Dauphine, Lay-Theng Lee, and Ludovic Pauchard. Crack opening: from colloidal systems to paintings. *Soft Matter*, 13(34):5802–5808, 2017.

[54] Patrick Dietemann, Wibke Neugebauer, Luise Lutz, Cedric Beil, Irene Fiedler, and Ursula Baumer. A colloidal description of tempera and oil paints, based on a case study of arnold böcklin's painting villa am meer ii (1865). *e-PreservationScience*, 11:29–46, 2014.

[55] Tharwat F Tadros. Colloid aspects of cosmetic formulations with particular reference to polymeric surfactants. *Colloids in Cosmetics and Personal Care*, 4:1–34, 2008.

[56] Qun Wang, Limin Wang, Michael S Detamore, and Cory Berkland. Biodegradable colloidal gels as moldable tissue engineering scaffolds. *Advanced Materials*, 20(2):236–239, 2008.

[57] Qun Wang, Jinxi Wang, Qinghua Lu, Michael Scott Detamore, and Cory Berkland. Injectable plga based colloidal gels for zero-order dexamethasone release in cranial defects. *Biomaterials*, 31(18):4980–4986, 2010.

[58] Qun Wang, Syed Jamal, Michael S Detamore, and Cory Berkland. Plga-chitosan/plga-alginate nanoparticle blends as biodegradable colloidal gels for seeding human umbilical cord mesenchymal stem cells. *Journal of Biomedical Materials Research Part A*, 96(3):520–527, 2011.

[59] Baojun Xie, Robert L Parkhill, William L Warren, and James E Smay. Direct writing of three-dimensional polymer scaffolds using colloidal gels. *Advanced Functional Materials*, 16(13):1685–1693, 2006.

[60] Mani Diba, Huanan Wang, Thomas E Kodger, Shima Parsa, and Sander CG Leeuwenburgh. Highly elastic and self-healing composite colloidal gels. *Advanced Materials*, 29(11):1604672, 2017.

[61] Nikolai Gaponik, Anne-Kristin Herrmann, and Alexander Eychmüller. Colloidal nanocrystal-based gels and aerogels: material aspects and application perspectives. *The Journal of Physical Chemistry Letters*, 3(1):8–17, 2012.

[62] Larry L Hench and Jon K West. The sol-gel process. *Chemical Reviews*, 90(1):33–72, 1990.

[63] Jennifer A Lewis. Colloidal processing of ceramics. *Journal of the American Ceramic Society*, 83(10):2341–2359, 2000.

[64] M Reiner. The deborah number. *Physics Today*, 17(1):62, 1964.

[65] Jason R Stokes and William J Frith. Rheology of gelling and yielding soft matter systems. *Soft Matter*, 4(6):1133–1140, 2008.

[66] J Murali Krishnan, Abhijit P Deshpande, and PB Sunil Kumar. *Rheology of complex fluids*. Springer, 2010.

[67] James Freeman Steffe. *Rheological methods in food process engineering*. Freeman press, 1996.

[68] Daniel Bonn, Jose Paredes, Morton Denn, Ludovic Berthier, Thibaut Divoux, and Sébastien Manneville. Yield stress materials in soft condensed matter. *Reviews of Modern Physics*, 89, 02 2015.

[69] A Keller. Introductory lecture. aspects of polymer gels. *Faraday Discussions*, 101:1–49, 1995.

[70] F Randriamasy. Les grandes expériences de jean perrin: les preuves expérimentales de la réalité moléculaire. *Revue du Palais de la Découverte. Numéro Spécial*, 20(197):18–29, 1992.

[71] Clemens Bechinger, Francesco Sciortino, and Primož Ziherl. *Physics of complex colloids*, volume 184. IOS Press, 2013.

[72] Agustín E González. Colloidal aggregation coupled with sedimentation: A comprehensive overview. In *Advances in Colloid Science*. InTech, 2016.

[73] Wilson Poon. Colloids as big atoms. *Science*, 304(5672):830–831, 2004.

[74] Peter N Pusey and W Van Megen. Phase behaviour of concentrated suspensions of nearly hard colloidal spheres. *Nature*, 320(6060):340, 1986.

[75] Dirk GAL Aarts, Matthias Schmidt, and Henk NW Lekkerkerker. Direct visual observation of thermal capillary waves. *Science*, 304(5672):847–850, 2004.

[76] Stefan Auer and Daan Frenkel. Prediction of absolute crystal-nucleation rate in hard-sphere colloids. *Nature*, 409(6823):1020, 2001.

[77] Eric R Weeks, John C Crocker, Andrew C Levitt, Andrew Schofield, and David A Weitz. Three-dimensional direct imaging of structural relaxation near the colloidal glass transition. *Science*, 287(5453):627–631, 2000.

[78] Veronique Trappe and Peter Sandkühler. Colloidal gels—low-density disordered solid-like states. *Current Opinion in Colloid & Interface Science*, 8(6):494–500, 2004.

[79] Eric Dickinson. Structure and rheology of colloidal particle gels: Insight from computer simulation. *Advances in colloid and interface science*, 199:114–127, 2013.

[80] Valerie J Anderson and Henk NW Lekkerkerker. Insights into phase transition kinetics from colloid science. *Nature*, 416(6883):811, 2002.

[81] TA Martin, Joost HJ ávan Opheusden, et al. Brownian dynamics simulation of particle gel formation: from argon to yoghurt. *Faraday Discussions*, 101:51–64, 1995.

[82] Martin TA Bos and Joost HJ van Opheusden. Brownian dynamics simulation of gelation and aging in interacting colloidal systems. *Physical Review E*, 53(5):5044, 1996.

[83] M. Rottereau, J. C. Gimel, T. Nicolai, and D. Durand. Monte carlo simulation of particle aggregation and gelation: Ii. pair correlation function and structure factor. *The European Physical Journal E*, 15(2):141–148, 2004.

[84] M. Rottereau, J. C. Gimel, T. Nicolai, and D. Durand. Monte carlo simulation of particle aggregation and gelation: I. growth, structure and size distribution of the clusters. *The European Physical Journal E*, 15(2):133–140, 2004.
[85] Luca Cipelletti, S. Manley, R. C. Ball, and D. A. Weitz. Universal aging features in the restructuring of fractal colloidal gels. *Physical Review Letters*, 84:2275–2278, Mar 2000.
[86] MY Lin, HM Lindsay, DA Weitz, RC Ball, RCBR Klein, and Paul Meakin. Universality in colloid aggregation. *Nature*, 339(3), 1989.
[87] Paul Meakin. Formation of fractal clusters and networks by irreversible diffusion-limited aggregation. *Physical Review Letters*, 51:1119–1122, Sep 1983.
[88] Peter J. Lu, Emanuela Zaccarelli, Fabio Ciulla, Andrew B. Schofield, Francesco Sciortino, and David A. Weitz. Gelation of particles with short-range attraction. *Nature*, 453(7194):499–503, 2008.
[89] E Del Gado. Aggregation of model gels with directional interactions. *Journal of Physics: Condensed Matter*, 22(10):104117, 2010.
[90] G. Foffi, C. De Michele, F. Sciortino, and P. Tartaglia. Scaling of dynamics with the range of interaction in short-range attractive colloids. *Physical Review Letters*, 94:078301, Feb 2005.
[91] Frédéric Cardinaux, Thomas Gibaud, Anna Stradner, and Peter Schurtenberger. Interplay between spinodal decomposition and glass formation in proteins exhibiting short-range attractions. *Physical Review Letters*, 99:118301, Sep 2007.
[92] W C K Poon. The physics of a model colloid–polymer mixture. *Journal of Physics: Condensed Matter*, 14(33):R859, 2002.
[93] Emanuela Zaccarelli, Peter J Lu, Fabio Ciulla, David A Weitz, and Francesco Sciortino. Gelation as arrested phase separation in short-ranged attractive colloid–polymer mixtures. *Journal of Physics: Condensed Matter*, 20(49):494242, 2008.
[94] S. Manley, H. M. Wyss, K. Miyazaki, J. C. Conrad, V. Trappe, L. J. Kaufman, D. R. Reichman, and D. A. Weitz. Glasslike arrest in spinodal decomposition as a route to colloidal gelation. *Physical Review Letters*, 95:238302, Dec 2005.
[95] Emily R Russell, Joris Sprakel, Thomas E Kodger, and David A Weitz. Colloidal gelation of oppositely charged particles. *Soft Matter*, 8(33):8697–8703, 2012.
[96] Lorenzo Di Michele, Francesco Varrato, Jurij Kotar, Simon H Nathan, Giuseppe Foffi, and Erika Eiser. Multistep kinetic self-assembly of dna-coated colloids. *Nature Communications*, 4:2007, 2013.
[97] Mykolas Zupkauskas, Yang Lan, Darshana Joshi, Z Ruff, and E Eiser. Optically transparent dense colloidal gels. *Chemical Science*, 8(8):5559–5566, 2017.
[98] John P Pantina and Eric M Furst. Elasticity and critical bending moment of model colloidal aggregates. *Physical Review Letters*, 94(13):138301, 2005.
[99] Eduardo Sanz, Kathryn A White, Paul S Clegg, and Michael E Cates. Colloidal gels assembled via a temporary interfacial scaffold. *Physical Review Letters*, 103(25):255502, 2009.
[100] Richard AL Jones. *Soft condensed matter*, volume 6. Oxford University Press, 2002.
[101] Henk NW Lekkerkerker and Remco Tuinier. *Colloids and the depletion interaction*, volume 833. Springer, 2011.
[102] William Bailey Russel, WB Russel, Dudley A Saville, and William Raymond Schowalter. *Colloidal dispersions*. Cambridge University Press, 1991.
[103] Sho Asakura and Fumio Oosawa. On interaction between two bodies immersed in a solution of macromolecules. *The Journal of Chemical Physics*, 22(7):1255–1256, 1954.
[104] Sho Asakura and Fumio Oosawa. Interaction between particles suspended in solutions of macromolecules. *Journal of Polymer Science*, 33(126):183–192, 1958.
[105] A Vrij. Polymers at interfaces and the interactions in colloidal dispersions. *Pure and Applied Chemistry*, 48(4):471–483, 1976.
[106] JF Joanny, L Leibler, and PG De Gennes. Effects of polymer solutions on colloid stability. *Journal of Polymer Science: Polymer Physics Edition*, 17(6):1073–1084, 1979.
[107] Alice P Gast, Carol K Hall, and William B Russel. Phase separations induced in aqueous colloidal suspensions by dissolved polymer. *Faraday Discussions of the Chemical Society*,

76:189–201, 1983.
[108] HNW Lekkerkerker, WC-K Poon, PN Pusey, A Stroobants, and PB 0 Warren. Phase behaviour of colloid+ polymer mixtures. *EPL (Europhysics Letters)*, 20(6):559, 1992.
[109] Vikram Prasad. *Weakly interacting colloid polymer mixtures*. Citeseer, 2002.
[110] Jade Taffs, Alex Malins, Stephen R Williams, and C Patrick Royall. A structural comparison of models of colloid–polymer mixtures. *Journal of Physics: Condensed Matter*, 22(10):104119, 2010.
[111] C. Patrick Royall, Jens Eggers, Akira Furukawa, and Hajime Tanaka. Probing colloidal gels at multiple length scales: The role of hydrodynamics. *Physical Review Letters*, 114:258302, Jun 2015.
[112] SMA Cruz and JMC Marques. A detailed study on the low-energy structures of charged colloidal clusters. *The Journal of Physical Chemistry B*, 120(13):3455–3466, 2016.
[113] Lilian C Johnson, Benjamin J Landrum, and Roseanna N Zia. Yield of reversible colloidal gels during flow start-up: release from kinetic arrest. *Soft Matter*, 14(24):5048–5068, 2018.
[114] Poornima Padmanabhan and Roseanna Zia. Gravitational collapse of colloidal gels: non-equilibrium phase separation driven by osmotic pressure. *Soft Matter*, 14(17):3265–3287, 2018.
[115] Kolattukudy P Santo and Aleksey Vishnyakov. Reversible aggregation of particles with short oligomeric sidechains at the surface studied with langevin dynamics. *Colloids and Surfaces A: Physicochemical and Engineering Aspects*, 586:124143, 2020.
[116] Benjamin J Landrum, William B Russel, and Roseanna N Zia. Delayed yield in colloidal gels: Creep, flow, and re-entrant solid regimes. *Journal of Rheology*, 60(4):783–807, 2016.
[117] Luca Cipelletti, Laurence Ramos, Suliana Manley, Estelle Pitard, David A Weitz, Eugene E Pashkovski, and Marie Johansson. Universal non-diffusive slow dynamics in aging soft matter. *Faraday Discussions*, 123:237–251, 2003.
[118] Rodolphe JM d'Arjuzon, William Frith, and John R Melrose. Brownian dynamics simulations of aging colloidal gels. *Physical Review E*, 67(6):061404, 2003.
[119] Hugo Bissig, Sara Romer, Luca Cipelletti, Veronique Trappe, and Peter Schurtenberger. Intermittent dynamics and hyper-aging in dense colloidal gels. *PhysChemComm*, 6(5):21–23, 2003.
[120] Qimeng Wu, Melle TJJM Punter, Thomas E Kodger, Luben Arnaudov, Bela M Mulder, Simeon Stoyanov, and Jasper Van Der Gucht. Gravity-driven syneresis in model low-fat mayonnaise. *Soft Matter*, 15(46):9474–9481, 2019.
[121] T Van Vliet, HJM Van Dijk, P Zoon, and P Walstra. Relation between syneresis and rheological properties of particle gels. *Colloid and Polymer Science*, 269(6):620–627, 1991.
[122] Engelbert Tijskens and Josse De Baerdemaeker. Mathematical modelling of syneresis of cheese curd. *Mathematics and Computers in Simulation*, 65(1-2):165–175, 2004.
[123] M Mellema, P Walstra, JHJ Van Opheusden, and T Van Vliet. Effects of structural rearrangements on the rheology of rennet-induced casein particle gels. *Advances in Colloid and Interface Science*, 98(1):25–50, 2002.
[124] Stefan Nöbel, Konrad Weidendorfer, and Jörg Hinrichs. Apparent voluminosity of casein micelles determined by rheometry. *Journal of Colloid and Interface Science*, 386(1):174–180, 2012.
[125] Soumaya El Bouchikhi, Philippe Pagès, Yassir El Alaoui, Azeddine Ibrahimi, and Yahya Bensouda. Syneresis investigations of lacto-fermented sodium caseinate in a mixed model system. *BMC Biotechnology*, 19(1):57, 2019.
[126] Somayeh Heydari, Atefeh Amiri-Rigi, Mohammad Reza Ehsani, Mohammad Amin Mohammadifar, Nasim Khorshidian, Mohammad Reza Koushki, and Amir Mohammad Mortazavian. Rheological behaviour, sensory properties and syneresis of probiotic yoghurt supplemented with various prebiotics. *International Journal of Dairy Technology*, 71:175–184, 2018.
[127] Thibaut Divoux, Bosi Mao, and Patrick Snabre. Syneresis and delayed detachment in agar plates. *Soft Matter*, 11(18):3677–3685, 2015.

[128] Suliana Manley, JM Skotheim, L Mahadevan, and DAVID A Weitz. Gravitational collapse of colloidal gels. *Physical Review Letters*, 94(21):218302, 2005.

[129] Rim Harich, TW Blythe, Michiel Hermes, Emanuela Zaccarelli, AJ Sederman, Lynn F Gladden, and Wilson CK Poon. Gravitational collapse of depletion-induced colloidal gels. *Soft Matter*, 12(19):4300–4308, 2016.

[130] Paul Bartlett, Lisa J Teece, and Malcolm A Faers. Sudden collapse of a colloidal gel. *Physical Review E*, 85(2):021404, 2012.

[131] Malcolm A Faers, Tahsin H Choudhury, Bobby Lau, Kevin McAllister, and Paul F Luckham. Syneresis and rheology of weak colloidal particle gels. *Colloids and Surfaces A: Physicochemical and Engineering Aspects*, 288(1-3):170–179, 2006.

[132] Esmaeel Moghimi, Alan R Jacob, Nick Koumakis, and George Petekidis. Colloidal gels tuned by oscillatory shear. *Soft Matter*, 13(12):2371–2383, 2017.

[133] Nick Koumakis, Esmaeel Moghimi, Rut Besseling, Wilson CK Poon, John F Brady, and George Petekidis. Tuning colloidal gels by shear. *Soft Matter*, 11(23):4640–4648, 2015.

[134] N Koumakis and G Petekidis. Two step yielding in attractive colloids: transition from gels to attractive glasses. *Soft Matter*, 7(6):2456–2470, 2011.

[135] Jacinta C Conrad and Jennifer A Lewis. Structure of colloidal gels during microchannel flow. *Langmuir*, 24(15):7628–7634, 2008.

[136] Zsigmond Varga, Jennifer L Hofmann, and James W Swan. Modelling a hydrodynamic instability in freely settling colloidal gels. *Journal of Fluid Mechanics*, 856:1014–1044, 2018.

[137] Robert Brown. Xxvii. a brief account of microscopical observations made in the months of june, july and august 1827, on the particles contained in the pollen of plants; and on the general existence of active molecules in organic and inorganic bodies. *The Philosophical Magazine*, 4(21):161–173, 1828.

[138] Marc D Haw. Colloidal suspensions, brownian motion, molecular reality: a short history. *Journal of Physics: Condensed Matter*, 14(33):7769, 2002.

[139] Albert Einstein. Über die von der molekularkinetischen theorie der wärme geforderte bewegung von in ruhenden flüssigkeiten suspendierten teilchen. *Annalen der Physik*, 322(8):549–560, 1905.

[140] Jean Perrin. Mouvement brownien et réalité moléculaire. In *Annales de Chimie et de Physique*, volume 18, pages 5–104, 1909.

[141] A Brongniart. *Annales des Sciences Naturelles*, 12(41), 1827.

[142] Peter W Van der Pas. The discovery of the brownian motion. *Scientiarum Historia: Tijdschrift voor de Geschiedenis van de Wetenschappen en de Geneeskunde*, 13(1):27–35, 1971.

[143] Desmond J Higham. An algorithmic introduction to numerical simulation of stochastic differential equations. *SIAM review*, 43(3):525–546, 2001.

[144] William Sutherland. Lxxv. a dynamical theory of diffusion for non-electrolytes and the molecular mass of albumin. *The London, Edinburgh, and Dublin Philosophical Magazine and Journal of Science*, 9(54):781–785, 1905.

[145] Roger Eckhardt. Stan ulam, john von neumann, and the monte carlo method. *Los Alamos Science*, 15(131-136):30, 1987.

[146] Stanislaw Ulam, RD Richtmyer, and J Von Neumann. Statistical methods in neutron diffusion. *LAMS-551, Los Alamos National Laboratory*, pages 1–22, 1947.

[147] N Metropolis. Monte carlo method. *From Cardinals to Chaos: Reflection on the Life and Legacy of Stanislaw Ulam*, page 125, 1989.

[148] Nicholas Metropolis, Arianna W Rosenbluth, Marshall N Rosenbluth, Augusta H Teller, and Edward Teller. Equation of state calculations by fast computing machines. *The Journal of Chemical Physics*, 21(6):1087–1092, 1953.

[149] Gary D Doolen and John Hendricks. Monte carlo at work. *Los Alamos Science, Special Issue Dedicated to S. Ulam*, pages 142–143, 1987.

Strand plasticity governs fatigue in colloidal gels

2

Repeated loading of a solid leads to microstructural damage that ultimately results in catastrophic material failure. While posing a major threat to the stability of virtually all materials, the microscopic origins of fatigue, especially for soft solids, remain elusive. Here we explore fatigue in colloidal gels as prototypical inhomogeneous soft solids by combining experiments and computer simulations. Our results reveal how mechanical loading leads to irreversible strand stretching, which builds slack into the network that softens the solid at small strains and causes strain hardening at larger deformations. We thus find that microscopic plasticity governs fatigue at much larger scales. This gives rise to a new picture of fatigue in soft thermal solids and calls for new theoretical descriptions of soft gel mechanics in which local plasticity is taken into account.

Jan Maarten van Doorn[1*], Joanne E. Verweij[1*], Joris Sprakel & Jasper van der Gucht[1]

"Strand plasticity governs fatigue in colloidal gels"
Physical Review Letters , **120 (20)** , 208005 (2018)

[*] *These authors contributed equally.*
[1] *Physical Chemistry and Soft Matter, Wageningen University, Wageningen, 6708 WE, The Netherlands.*

Introduction

The application of repeated load to a solid material can lead to the erosion of its microstructure, in a process that is known as fatigue. While the initial stages of this process often go unnoticed, the gradual accumulation of damage that results can ultimately lead to the sudden and catastrophic failure of the material. Understanding the microscopic origins of fatigue is therefore crucial for the reliable prediction of a material's lifetime and for the development of strategies to improve mechanical stability. In materials such as steel and concrete, fatigue is characterized by the accumulation and growth of small micro-cracks [1, 2]. However, the mechanisms of fatigue in disordered soft materials are much less understood. A prototypical class of soft heterogeneous solids is comprised of colloidal gels. These are non-equilibrium structures consisting of aggregated colloidal particles that form a sample-spanning network [3].

The arrested dynamics of the aggregated particles lead to solid-like behaviour, with elastic properties that are determined by the structure and connectivity of the network [4, 5]. When subjected to a large enough stress, colloidal gels will eventually fluidize or fracture, often after a latent period of apparent stability [6–12]. The microstructural changes responsible for this delayed failure have been attributed to the brittle-like rupture of network strands due to force-activated breaking of interparticle bonds [13–15]. Such models assume that no restructuring of the network due to plastic particle rearrangements takes place. Yet, it is known that such rearrangements do occur [16, 17], even for colloidal gels in rest [18], where they lead to aging, coarsening, and slow relaxation of internal stresses [19–21]. While it is known that under large deformation aggregates break into smaller clusters [22], the response of aggregated structures to repeated small deformations remains unclear. To establish a link between the stability of colloidal gels and their microstructure, it is therefore needed to understand the role of plasticity in gel failure and fatigue.

In this Chapter, we report fatigue measurements on model colloidal gels subjected to cyclic loading. By combining experiments and computer simulations, we show that the gradual weakening that occurs in these gels is due to plastic deformations within individual gel strands. Our results thus shed new light on the mechanism of damage accumulation in colloidal gels, and suggest that the current models for colloidal gel failure must be revised to take this plastic softening into account.

Results and discussion

We investigate colloidal gels consisting of monodisperse polystyrene particles synthesized as described in Ref. [23], with a volume fraction $\phi = 0.18$. The particles have a diameter $a = 90$ nm as determined by dynamic light scattering. Attraction is induced by coating the particles with a thermo-responsive surfactant layer of approximately 8 nm thickness, as synthesized in Ref. [24]. To screen electrostatic repulsion between the particles, 100 mM NaCl is added to all samples. Rheological measurements are performed with a stress-controlled rheometer (MCR-501, Anton Paar) with a concentric cylinder geometry (CC10/Ti). The gels are formed in situ by heating the samples to 45°C, above the critical aggregation temperature of the surfactant, which results in gels with thick strands, each composed of many particles in its cross-section, in which it is established that significant rearrangements occur [24]. To minimize initial transient effects, samples are equilibrated for 1h before initiating measurements. Fatigue in the gels is studied by cyclically deforming the samples with a saw-tooth strain profile (Inset Fig. 2.1). After 14 cycles at the same strain amplitude γ_{max}, we allow the sample to rest for 120 s, before starting a new set of deformation cycles at a higher strain amplitude, with increment $\Delta\gamma_{\text{max}} = 0.005$.

For the smallest amplitude the stress-strain curve exhibits a linear elastic response (Fig. 2.1). For larger strain amplitudes, however, the stress increases non-linearly with increasing strain and shows a hysteresis loop, which indicates dissipative losses during the deformation cycle [25] (see also Fig. A2.9). The first cycle for every strain amplitude differs qualitatively from the subsequent cycles: with increasing strain, the stress increases strongly, until a threshold value of approximately 470 Pa is reached, after which it levels off, indicating that the material undergoes plastic flow at this stress level. For every subsequent cycle, the observed stress is lower than that in the first cycle, signalling a progressive, irreversible weakening of the material. The stress-strain curve then gradually approaches a limit cycle, with an enclosed area that reflects the viscoelastic dissipation in the network due to solvent flow or reversible particle rearrangements. Note that the viscous contribution to the stress is negative in the unloading branch of the cycle, leading to a negative overall stress as the strain returns to zero.

Because the timescale at which plastic rearrangements take place can be relatively long for these strongly aggregated particles, we expect the amount of plasticity to depend on the loading rate. Indeed, when we increase $\dot{\gamma}$ by a factor of 10, to 10^{-1} s^{-1}, we observe a much more elastic response, with the onset of non-linear plastic behaviour shifted to much larger strains and stresses (Fig. 2.2a).

To analyze the nature of the observed plasticity in colloidal gels in

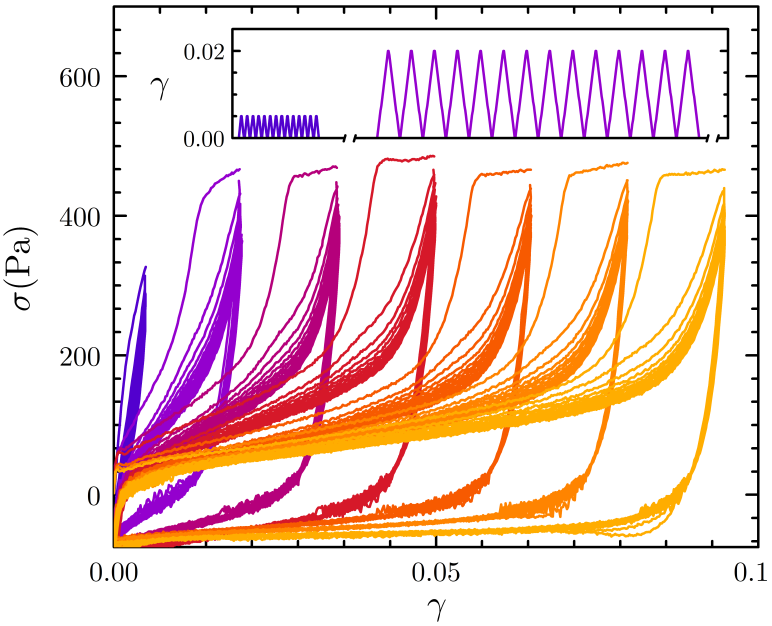

Figure 2.1 – Stress-strain curves as a result of saw-tooth strain cycles shown in the inset (only first two sets are shown) with $\dot{\gamma}$=10^{-2} s^{-1}. From blue to yellow: γ_{max} = 0.005, 0.02, 0.035, 0.05, 0.065, 0.08, 0.095 (note that only a selection of the sets is shown).

more detail, we first disentangle the elastic and viscous contributions to the mechanical response, by averaging the loading and unloading curve for each cycle [26]. This averages out the viscous contribution to the stress, so that only the elastic stress σ_{el} remains (Fig. 2.2b). For the smallest strain amplitude, the stress-strain response is linear; however, at higher strains, when the gels have undergone plastic deformation, the curves become strongly non-linear. The shapes of the non-linear response of all cycles are very similar.

After an initial linear response, characterized by a linear modulus G_0, the gels show pronounced strain hardening: at a characteristic strain amplitude γ^*, there is a sharp upturn of the stress. The linear modulus that characterizes the initial slope of the stress-strain curves decreases with increasing strain amplitude (Fig. 2.2c), signaling the progressive weakening of the gels resulting from the gradual erosion of the network structure during the fatigue cycles. We obtain γ^* by superimposing the different stress-strain curves for both strain rates by plotting the normalized stress, σ_{el}/σ^*, where $\sigma^* = G_0\gamma^*$, as a function of the rescaled strain γ/γ^* (Fig. 2.2d, Fig. A2.9). The excellent collapse indicates that the physical mechanism that underlies the mechanical response of the gels remains the same during the fatigue cycles. We find a linear increase of γ^* with increasing maximum strain amplitude (inset Fig. 2.2c), indicating that the strain hardening response is delayed by the fatigue process.

While our data demonstrate the importance of plasticity for fatigue in col-

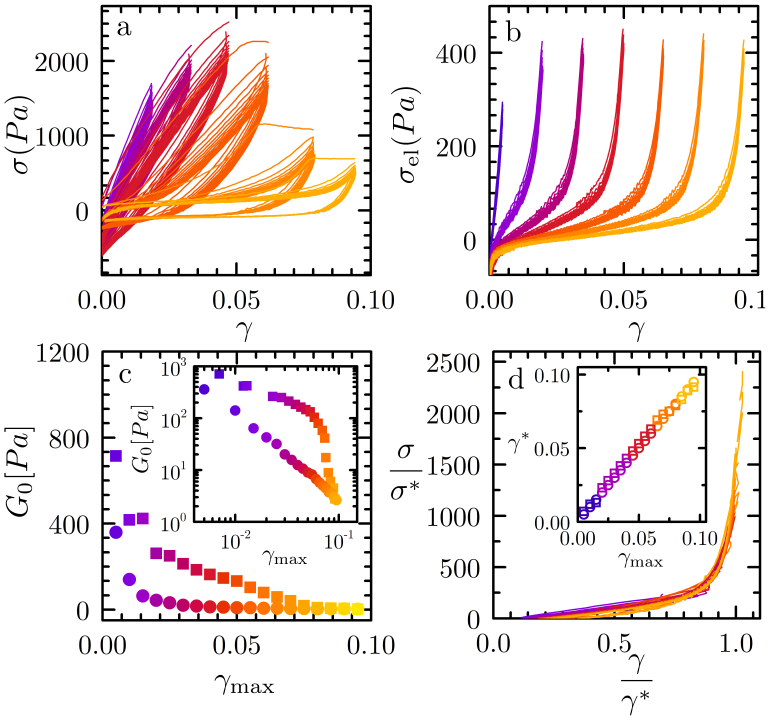

Figure 2.2 – a) Stress-strain curves for $\dot{\gamma} = 10^{-1}$ s^{-1}, from blue to yellow: γ_{max} = 0.005, 0.02, 0.035, 0.05, 0.065, 0.08, 0.095. b) Elastic midlines for curves in Fig. 2.1. c) The initial modulus as function of γ_{max} for $\dot{\gamma}$=10^{-1} s^{-1} (squares) and $\dot{\gamma}$=10^{-2} s^{-1} (circles). The inset shows the same data on a double-logarithmic scale. d) Collapse of every second elastic midline for both strain rates. The inset shows the dependence of γ^* on γ_{max} for $\dot{\gamma}$=10^{-1} s^{-1} (squares) and $\dot{\gamma}$=10^{-2} s^{-1} (circles).

loidal gels, the microscopic nature of this plastic deformation remains to be uncovered. Given that colloidal gels are networks of connected strands consisting of aggregated particles, the observed weakening must be caused either by the rupture of gel strands, leading to a decrease in network connectivity, or by softening of the gel strands, leading to a lower effective spring constant of the strands. To identify which of these scenarios is the dominant one, we need detailed information at the single strand level. Since this is extremely difficult to obtain experimentally for our system, we perform Brownian Dynamics computer simulations on single gel strands (Fig. 2.3). The strands are composed of 256 particles of diameter a interacting through a Morse potential [27], with an interaction strength $\epsilon = 10\ k_BT$ and interaction range parameter $\rho_0 = 33$, which corresponds to a well width of approximately $\Delta = 0.09\,a$, similar to the experimental system (Fig. A2.1). Following the experimental protocol, the gel strands are deformed cyclically with a saw-tooth strain profile (see appendix for further details about the simulation method). To connect our simulation results to the experimental findings, we calculate the force needed to deform the strand as a function of the strain [1]. The

[1]The force f on the simulation walls is related to the stress measured in the experiment as $\sigma \approx \frac{f}{\xi^2}$, with ξ the mesh size of the network.

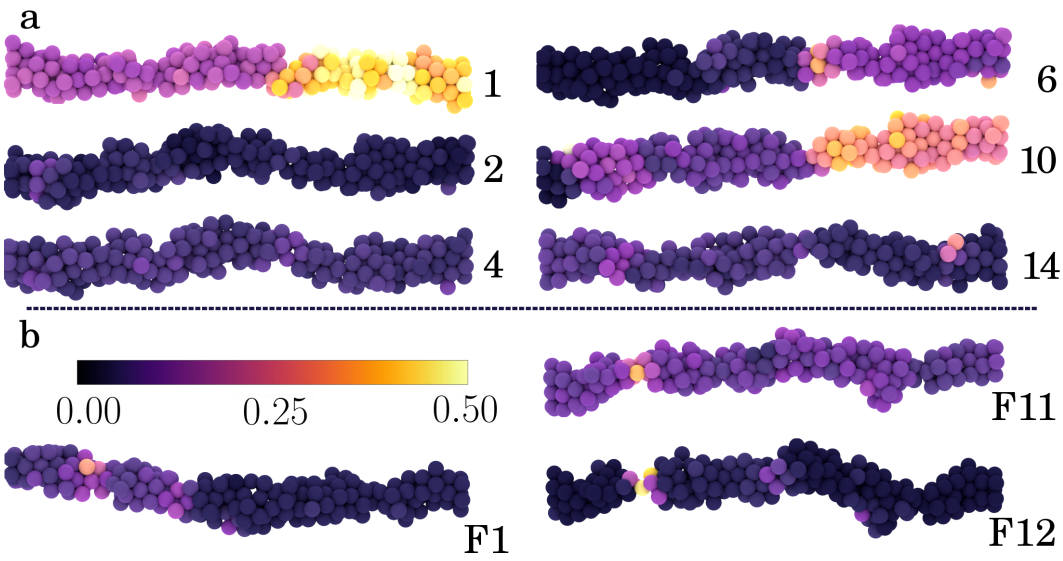

Figure 2.3 – (a) Visual representation of the non-cumulative average plastic deformation per particle in oscillation cycles 1,2,4,6,10 and 14 of a single gel strand ($\gamma_{max} = 0.04$, data Fig. A2.2). The color bar indicates the non-cumulative plastic deformation m_i per particle in each cycle from low (purple) to high (yellow). The cumulative plastic deformation of this gel strand is shown in Fig. A2.8. (b) Plastic deformation in a gel strand after the first cycle (F1), before fracture (F11) and after fracture (F12).

force-strain curves for non-fractured gel strands show features that are very similar to the macroscopic curves measured experimentally (Fig. 2.4a). Like in the experimental curves, we find that the first force-strain curve for each strain amplitude differs qualitatively from the subsequent cycles, showing a plateau above a critical force that indicates plastic deformation within the gel strand.

We use a similar procedure to rescale the force-strain curves as in Fig. 2.2d. Again, we average the force in the loading and unloading curve and plot the rescaled elastic force f_{el}/f^*, with $f^* = k\gamma^*$ the scaled stiffness of the strand in the linear regime as a function of the rescaled strain γ/γ^*. This yields a curve that shows similar features to the experimental one (Fig. 2.4b), with a linear response regime, followed by a strain-hardening response at higher strains. The linear spring constant of the gel strands k decreases in a similar fashion with the strain amplitude γ_{max} as the elastic modulus in the experiments (Fig. 2.4c). Furthermore, the onset of strain hardening shifts to higher strains with increasing strain amplitude (Fig. 2.4d), also in agreement with experiments (inset Fig. 2.2c). Since broken strands have been excluded from the analysis, the observed weakening in the simulated force-strain curves can be attributed completely to plastic rearrangements within the strands. This suggests that also the weakening observed at the macroscopic scale in our

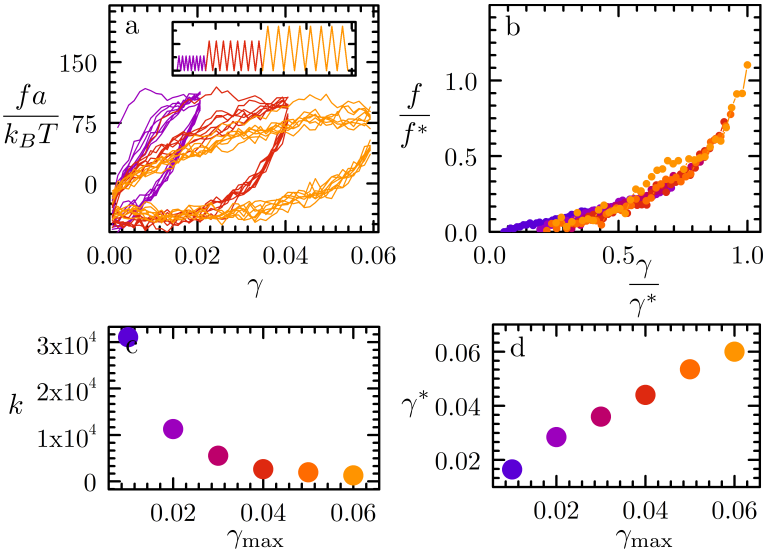

Figure 2.4 – (a) Force-strain curves for BD simulations of 24 (8x3) oscillations of a single gel strand at strain amplitudes (purple to orange) $\gamma_{max} = 0.02$, 0.04 and 0.06. (b) Collapse of the average force-strain curves (positive parts of the loading and unloading curve) of the 4^{th} oscillation cycle scaled by γ^* on the x-axis and $k \cdot \gamma^*$ on the y-axis. Data is obtained from Fig. A2.2. (c) Spring constant k (in units $k_B T a^{-1}$) as a function of γ_{max}. (d) γ^* as a function of γ_{max}.

fatigue experiments can be explained by plastic deformation and softening in individual gel strands, without the need to invoke rupture of strands.

To verify that this finding is not specific to the geometry of the simulated gel strands, we have carried out simulations for strands of different length and width and for larger gel networks consisting of many interconnected gel strands. In all cases, the force-strain loops show similar features to the curves in Fig. 2.4a (see Fig. A2.7 and Chapter 3), which affirms that gel strand plasticity is a mechanism for fatigue in a wide class of colloidal gels, irrespective of the precise structure of the gel strands.

To unravel the microscopic mechanism that underlies the plastic deformation of the gel strands, we analyze the rearrangements of individual particles and quantify the average plastic strain for each particle in an oscillation c_n as

$$m_i(c_n) = \frac{1}{\mathcal{N}_i a^2} \sum_{j=1}^{\mathcal{N}_i} \langle |\boldsymbol{r}_{ij}(0) - \boldsymbol{r}_{ij}(t)|^2 \rangle \tag{2.1}$$

where $\boldsymbol{r}_{ij}(0)$ and $\boldsymbol{r}_{ij}(t)$ denote the separation vector between particle i and neighbouring particles j at the start of the cycle and after a time t, respectively, $\mathcal{N}_i$ is the number of nearest neighbours of particle i. The average is taken over the entire oscillation.

During the strain cycles, the amount of plastic strain gradually increases, with most of the plastic rearrangements occurring during the first cycle. For larger strain amplitudes, the amount of plastic strain is also larger (Fig. A2.4). These irreversible particle rearrangements and the associated rupture of inter-particle bonds are responsible for the large energy dissipation in the

first strain cycles. As the gel strands are several particle diameters wide (Fig. 2.3), the breaking of a single bond does not immediately lead to rupture of the whole strand [13]. The overall integrity of the strand is maintained by adjacent bonds and due to thermal fluctuations, new bonds can form [11, 21, 26]. This provides a mechanism for plastic deformation of the gel strands.

Visual inspection of computer-rendered images of the simulated strands suggest that the plastic rearrangements of particles result in irreversible lengthening of the strands after deformation, leading to the build-up of slack in the strands and buckling during unloading (Fig. 2.3a). The linear increase of γ^* with increasing γ_{max} (inset Fig. 2.2a and 2.4d) furthermore suggests that this slack is proportional to the applied extension. During the next cycle the slack induced by previous cycles is pulled out first, which results in little resistance and explains the initial soft linear elastic response of the gels. When the strands are pulled taut, the resistance to further stretching increases strongly as the strand entropy vanishes and the physical bonds between the particles become perturbed. This results in the observed strain hardening in our colloidal gels. We note that these phenomena are reminiscent of observations made for networks of biopolymer bundles [26].

Interestingly, the plastic rearrangements do not occur homogeneously in the gel strand, but are strongly localized to specific regions (Fig. 3). This leads to the formation of thicker and thinner regions in the gel strand, reminiscent of the Rayleigh-Plateau instability in liquid jets, which highlights the arrested liquid state of colloidal gels [28]. This is further corroborated by looking at the average number of bonds per particle, which gradually increases during the oscillations (Fig. A2.4), suggesting that fatigue in colloidal gels is reminiscent of activated aging, in which the non-equilibrium gel structure tends to coarsen by increasing the number of bonds [29].

At high strains, the localization of plastic deformation ultimately leads to rupture of the gel strand at the weakest spot, i.e. at a local necking region (Fig. 3b). The percentage of broken strands increases with increasing strain amplitude and reaches about 65 % for a strain of 0.06 (Fig. A2.6). As the strands become longer and thinner, rupture occurs more frequently, but in all cases it is preceded by significant plastic deformation within the strands (see Chapter 3). Since our analysis focuses on the microscopic plastic events within strands, preceding their rupture, the role of strand rupturing for the mechanical stability of the gel as a whole remains to be understood.

To investigate the effect of the deformation rate, we also deform the gel strands at higher strain rates. Increasing the strain rate by a factor 100 leads to a considerably higher number of ruptured strands (Fig. A2.6). From the average plastic deformation per oscillation cycle (Fig. A2.5) as a function of increasing strain rate we observe a clear decline in the plasticity of the gel strands. This data suggest that colloidal gels with hardly any options to deform plastically will rupture in a brittle fashion. Macroscopically, the

extended linear regime in Figure 2.2a signals the onset of a transition to brittle failure. This is supported by the fact that G_0 decreases very rapidly at high γ^* for $\dot{\gamma} = 10^{-1}$ s^{-1} , suggesting that a larger part of the damage is caused by brittle fracture (inset Fig 2.2c).

Our results highlight how fatigue in colloidal gels results from plasticity at much smaller scales. This feature results from the strongly hierarchical and multiscale structure of networks of colloidal particles. To date, strand plasticity has been overlooked in describing the mechanics of colloidal gels but has also received little attention as a possible mechanism of fatigue in a wider variety of heterogeneous solids, while our data clearly indicate its pivotal role in deciding the material's fate under repeated loading. Strand stretching and the build-up of slack has also been identified as a mechanism for strain softening in networks of biological fibers [26]. This raises the question whether localized plasticity, which remains obscured in macroscopic mechanical testing, may have a more universal role in the fatigue mechanisms of a wider class of inhomogeneous soft solids with a hierarchical microstructure. If so, a universal description of these effects could have pronounced implications for the predictability of the non-linear mechanical response of soft materials, which remains an open challenge in the field. Finally, while our work has focused on fatigue induced by external loading, other failure mechanisms driven by internal stresses are known to exist for these inhomogeneous thermal solids, such as ageing and syneresis [19–21]. The plasticity we describe here results from the rearrangement of particles by thermally-activated debonding [18], in which the mechanical stress imposes a directional bias that leads to irreversible strand stretching. Based on our observations here, we hypothesize that internal stress can give rise to similar effects, where e.g. contractile internal stresses could bias rearrangements that lead to isotropic condensation of the structure, ultimately resulting in syneresis. While this remains unexplored to-date, it could open the way to a universal description of the failure of these non-equilibrium solids.

Acknowledgements

This work was carried out in collaboration with Jan Maarten van Doorn. Jan Maarten performed the rheology fatigue experiments in this chapter.

Bibliography

[1] M.K. Lee and B.I.G. Barr. An overview of the fatigue behaviour of plain and fibre reinforced concrete. *Cement and Concrete Composites*, 26(4):299 – 305, 2004.

[2] Mirko Klesnil and Petr Lukáš. *Fatigue of metallic materials*, volume 71. Elsevier, 1992.

[3] Veronique Trappe, V Prasad, Luca Cipelletti, PN Segre, and David A Weitz. Jamming phase diagram for attractive particles. *Nature*, 411(6839):772–775, 2001.
[4] A. H. Krall and D. A. Weitz. Internal Dynamics and Elasticity of Fractal Colloidal Gels. *Physical Review Letters*, 80(4):778–781, jan 1998.
[5] C. J. Rueb and C. F. Zukoski. Viscoelastic properties of colloidal gels. *Journal of Rheology*, 41(2):197–218, 1997.
[6] V. Gopalakrishnan and C.F. Zukoski. Delayed flow in thermo-reversible colloidal gels. *Journal of Rheology*, 51:623, 2007.
[7] Mehdi Bouzid and Emanuela Del Gado. Network topology in soft gels: Hardening and softening materials. *Langmuir*, 34(3):773–781, 2018.
[8] P. Bartlett, L.J. Teece, and M.A. Faers. Sudden collapse of a colloidal gel. *Physical Review E*, 85:021404, 2012.
[9] Thomas Gibaud, Christophe Perge, Stefan B. Lindström, Nicolas Taberlet, and Sébastien Manneville. Multiple yielding processes in a colloidal gel under large amplitude oscillatory stress. *Soft Matter*, 12:1701–1712, 2016.
[10] J. Kim, D. Merger, M. Wilhelm, and M.E. Helgeson. Microstructure and nonlinear signatures of yielding in a heterogeneous colloidal gel under large amplitude oscillatory shear. *Journal of Rheology*, 58:1359, 2014.
[11] Joris Sprakel, Stefan B. Lindström, Thomas E. Kodger, and David A. Weitz. Stress enhancement in the delayed yielding of colloidal gels. *Physical Review Letters*, 106:248303, Jun 2011.
[12] M. Leocmach, C Perge, T. Divoux, and S. Manneville. Creep and Fracture of a Protein Gel under Stress. *Physical Review Letters*, 113:038303, 2014.
[13] Stefan B. Lindström, Thomas E. Kodger, Joris Sprakel, and David A. Weitz. Structures, stresses, and fluctuations in the delayed failure of colloidal gels. *Soft Matter*, 8:3657–3664, 2012.
[14] J. Colombo and E. Del Gado. Stress localization, stiffening, and yielding in a model colloidal gel. *Journal of Rheology*, 58:1089, 2014.
[15] B. Saint-Michel, T. Gibaud, and S. Manneville. Predicting and assessing rupture in protein gels under oscillatory shear. *Soft Matter*, 13:2643, 2017.
[16] B.J. Landrum, W.B. Russell, and R.N. Zia. Delayed yield in colloidal gels: Creep, flow, and re-entrant solid regimes. *Journal of Rheology*, 60:783–807, 2016.
[17] Saikat Roy and Mahesh S Tirumkudulu. Yielding in a strongly aggregated colloidal gel. part i: 2d simulations. *Journal of Rheology*, 60(4):559–574, 2016.
[18] Jan Maarten van Doorn, Jochem Bronkhorst, Ruben Higler, Ties van de Laar, and Joris Sprakel. Linking particle dynamics to local connectivity in colloidal gels. *Physical Review Letters*, 118:188001, May 2017.
[19] Luca Cipelletti, S. Manley, R. C. Ball, and D. A. Weitz. Universal aging features in the restructuring of fractal colloidal gels. *Physical Review Letters*, 84:2275–2278, Mar 2000.
[20] Ajay Singh Negi and Chinedum O. Osuji. Dynamics of internal stresses and scaling of strain recovery in an aging colloidal gel. *Physical Review E*, 80:010404, Jul 2009.
[21] Jader Colombo, Asaph Widmer-Cooper, and Emanuela Del Gado. Microscopic picture of cooperative processes in restructuring gel networks. *Physical Review Letters*, 110:198301, May 2013.
[22] Alessio Zaccone, Hua Wu, Daniele Gentili, and Massimo Morbidelli. Theory of activated-rate processes under shear with application to shear-induced aggregation of colloids. *Physical Review E*, 80:051404, Nov 2009.
[23] Jeroen Appel, Niek de Lange, Hanne M. van der Kooij, Ties van de Laar, Jan Bart ten Hove, Thomas E. Kodger, and Joris Sprakel. Temperature Controlled Sequential Gelation in Composite Microgel Suspensions. *Particle & Particle Systems Characterization*, 32(7):764–770, jul 2015.
[24] Thomas E. Kodger and Joris Sprakel. Thermosensitive Molecular, Colloidal, and Bulk Interactions Using a Simple Surfactant. *Advanced Functional Materials*, 23(4):475–482, jan 2013.
[25] M. Laurati, S. U. Egelhaaf, and G. Petekidis. Plastic rearrangements in colloidal gels in-

vestigated by laos and ls-echo. *Journal of Rheology*, 58(5):1395–1417, 2014.
[26] Stefan Münster, Louise M Jawerth, Beverly A Leslie, Jeffrey I Weitz, Ben Fabry, and David A Weitz. Strain history dependence of the nonlinear stress response of fibrin and collagen networks. *Proceedings of the National Academy of Sciences of the United States of America*, 110(30):12197–202, jul 2013.
[27] C. Patrick Royall, Jens Eggers, Akira Furukawa, and Hajime Tanaka. Probing colloidal gels at multiple length scales: The role of hydrodynamics. *Physical Review Letters*, 114:258302, Jun 2015.
[28] Peter J Lu, Emanuela Zaccarelli, Fabio Ciulla, Andrew B Schofield, Francesco Sciortino, and David A Weitz. Gelation of particles with short-range attraction. *Nature*, 453(7194):499–503, 2008.
[29] Esmaeel Moghimi, Alan R. Jacob, Nick Koumakis, and George Petekidis. Colloidal gels tuned by oscillatory shear. *Soft Matter*, 13:2371–2383, 2017.
[30] Jun Dong Park, Kyung Hyun Ahn, and Seung Jong Lee. Structural change and dynamics of colloidal gels under oscillatory shear flow. *Soft Matter*, 11:9262–9272, 2015.

Appendix

I. Simulation details

Multiple strain amplitudes

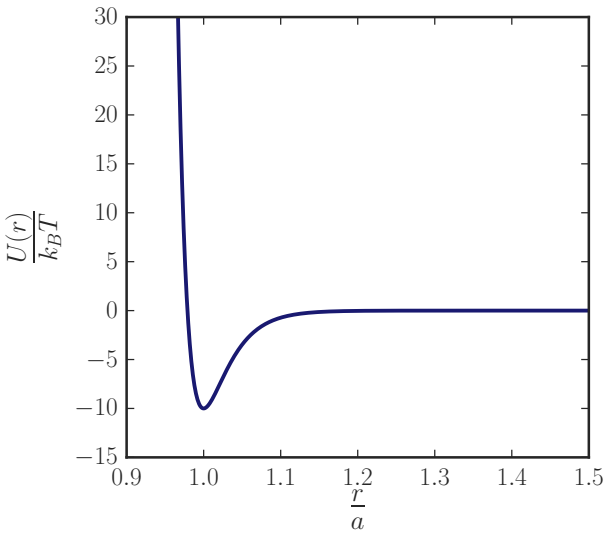

Figure A2.1 – Morse potential with interaction range parameter $\rho_0 = 33$ and interaction strength $\beta\epsilon = 10$. The cutoff of the potential is set to 1.5.

Brownian Dynamics (BD) simulations were performed to study the effect of repeated deformation on the microscopic scale only. We consider a gel strand

with 256 particles which interact through the Morse potential [27]:

$$\beta U(r) = \beta\epsilon \, \exp(\rho_0[a-r]) \, (\exp[\rho_0(a-r)] - 2) \tag{2.2}$$

with $\beta = 1/k_B T$, $\rho_0 = 33$, energy scale $\beta\epsilon = 10$ and particle diameter $a = 2r_a$ (see Fig. A2.1). The parameter ρ_0 determines the width of the potential, which becomes approximately $\Delta = 0.09\, a$ for $\rho_0 = 33$ [2]. In this way it matches the experimental interaction range, which is known to be around 8 nm for the thermo-responsive surfactant that coats the particles ($r_p = 45$ nm) [24].

The motion of a particle i with position $\boldsymbol{r}_i$ is obtained by solving the overdamped Langevin equation:

$$\dot{\boldsymbol{r}}_i(t) = \beta D_0[-\nabla_i U(t)] + \sqrt{2D_0}\boldsymbol{\xi}_i(t) \tag{2.3}$$

where $\boldsymbol{\xi}_i(t)$ is random white noise, sampled with zero mean and unit variance, to model the thermal fluctuations of the particles. $D_0 = k_B T/\zeta_f$ is the short-time diffusion coefficient with ζ_f the friction coefficient, set to unity. The time step δt for the numerical integration is set to $\delta t = 1 \times 10^{-6}\ \tau_B$. We express the unit of time in terms of the short-time self-diffusion $\tau_B = a^2/D_0$.

Individual strands are formed between two attractive walls, with a particle-wall interaction given also by Eq. 2.2 (with $\rho_0 = 33$, $\beta\epsilon = 10$). We use periodic boundary conditions in the y and z direction. We place particles initially in a face centered cubic (fcc) lattice in a 4 x 4 (height x width) arrangement (N = 256). The system is then equilibrated for 568 τ_B, which leads to aggregation of the particles and the formation of a gel strand between the two walls [3]. During equilibration, the particle positions are randomized, leading to a different internal strand structure for each simulation. (Note that the distances between the particles in the initial configuration are larger than the range of the potential.)

Similarly to the experiment, the single gel strand in the BD simulations is cyclically deformed with a sawtooth strain profile (Inset Fig. 2.1). One of the walls is moved outward, leading to an expansion at a fixed strain rate $\dot{\gamma} = 0.00284\ \tau_B^{-1}$. Note that this strain rate is comparable to a strain rate of $\dot{\gamma} = 1.7\ \mathrm{s}^{-1}$ in the experiment. After 8 successive oscillations the strain amplitude is increased from $\gamma = 0.02$ to $\gamma = 0.04$ and $\gamma = 0.06$ respectively.

[2] Here, Δ is determined by taking the end of the well at 10% of the original well-depth (1 $k_B T$). To determine the fraction of broken inter-particle bonds χ_n, the number of bonds per particle N_b and the irreversible displacements of particles m, the cut-off between the particles' center-to-center distance is set to 1.16 (1% of the original well-depth). The visual representations in Fig. 2.3 and Fig. A2.8 are made with a cut-off of 1.5

[3] Varying the equilibration time doesn't influence the obtained force-strain curves. However, for too short equilibration times the average number of bonds is still substantially increasing in the zero measurement; see Fig. A2.2 and A2.3 for the zero measurement (blue curve, $\gamma = 0$) of these simulations.

More than 65 % of the gel strands break after 24 oscillatory expansions at successive strain amplitudes of $\gamma = 0.02, 0.04$ and 0.06.

We note that the fracture of individual strands is highly ductile and occurs by strong necking. Moreover, fracture only occurs when a single bond connects the two halves. In all simulations a percentage of the strands is fractured (either by detaching from the wall or by breaking into clusters, see Fig. A2.6). To focus on plastic mechanisms, data of broken strands is excluded in further analysis. Each strain amplitude contains data of at least 30 statistically different gel strands.

Single strain amplitudes

For single strain amplitudes, simulations are performed exactly as described above, however, in this case we do not impose a higher strain after a certain amount of cycles. Data is shown both for expansion (Fig. A2.2) and compression (Fig. A2.3) of single gel strands. In the latter case the distance between the walls is first decreased, leading to compression of the gel strand, after which the walls are brought back to their original position. We impose 14 oscillations in total for strain amplitudes $\gamma = 0.02$, 0.04 and 0.06. The fourth oscillation for these strain amplitudes (expansion) is used to re-scale the force-strain curves as shown in Fig. 4b of this Chapter.

At higher strain amplitudes, compression favours the increase in number of bonds compared to expansion. Both the amount of dissipated energy and the fraction of inter-particle bonds that break per oscillation cycle is lower for compression, i.e. compression enhances the reformation of inter-particle bonds over expansion.

II. Analysis

Bond rearrangements

To quantify bond rearrangements, we calculate the average fraction of inter-particle bonds that is broken per oscillation cycle:

$$\chi_n(c_n) = \frac{\langle n_i(c_n) - n_i(c_n + 1)\rangle_p}{N_b(c_n)}, \tag{2.4}$$

where $n_i(c_n)$ is the number of nearest neighbours of particle i at the start of a certain oscillation, $n_i(c_n + 1)$ is the number of these neighbours that remain at the end of this oscillation and the average is taken over all particles p in the strand. The number of broken inter-particle bonds is normalized by the average number of bonds per particle N_b. We find that the number of broken bonds is highest in the first deformation cycle and decreases gradually

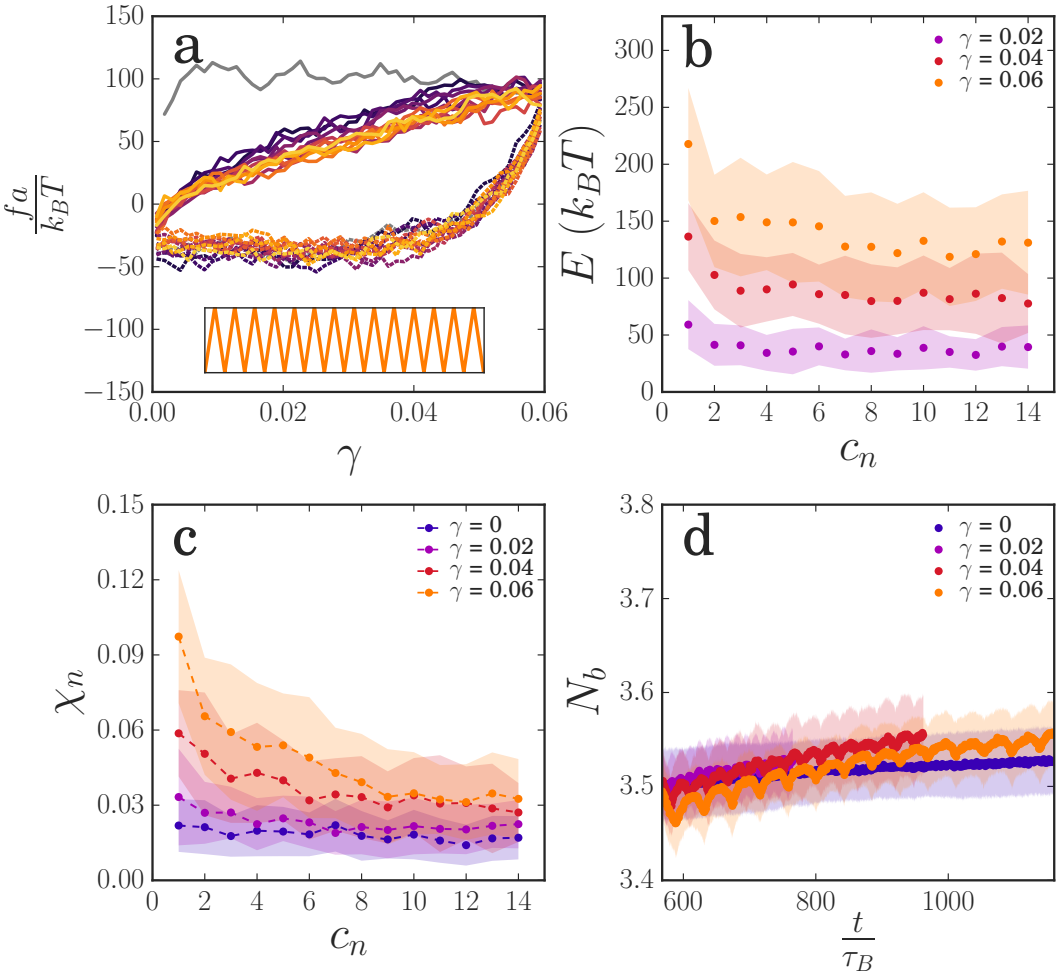

Figure A2.2 – (a) Force-strain curve for BD simulations upon 14 oscillatory *expansions* of a single gel strand at strain amplitude $\gamma_{max} = 0.06$. The strain profile is shown in the inset. The loading branch of each cycle is indicated with a solid line. The dotted line indicates the unloading branch. The different oscillations (1-14) are plotted from purple to yellow. To highlight the first oscillation cycle this one is plotted in gray. (b) Dissipated energy in each oscillation number c_n for strain amplitudes $\gamma_{max} = 0.02$, 0.04 and 0.06 obtained through integration of the force-strain curves. (c) The fraction of bonds that break per oscillation. The dotted line is drawn to guide the eye. (d) Average number of bonds in time. The shaded areas indicate the standard deviation.

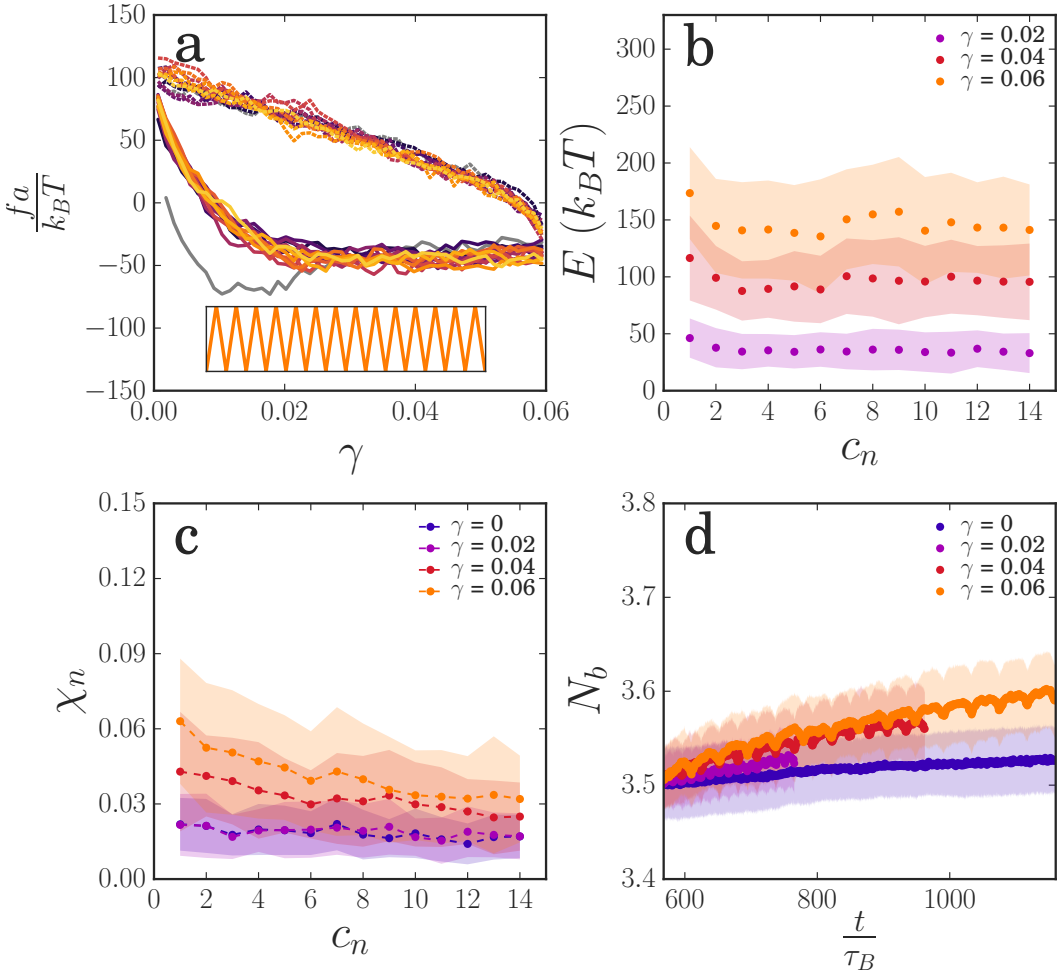

Figure A2.3 – Data of BD simulations upon 14 oscillatory *compressions*. See Fig. A2.2 for the explanation of each subplot.

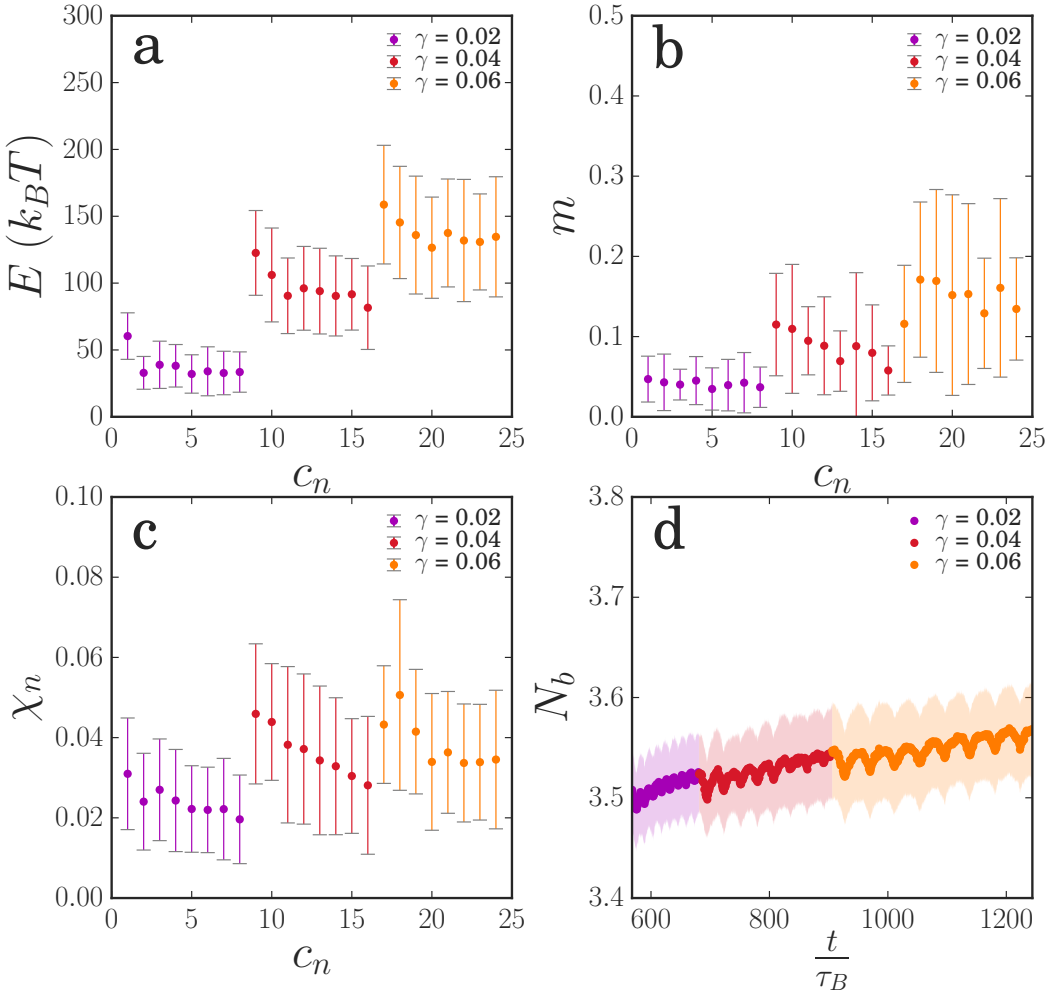

Figure A2.4 – (a) Dissipated energy per oscillation for strain amplitudes γ_{max} = 0.02, 0.04 and 0.06, obtained by integration of the force-strain curves (Fig. 2.4). (b) Average plastic deformation per oscillation (Eq. 2.1). (c) The fraction of broken bonds per oscillation. (d) Number of bonds in time. The shaded area indicates the standard deviation.

(Fig. A2.4c). As described in the main text, the average number of bonds per particle in the gel strand N_b increases in time (Fig. A2.4d) [30]. Repeated oscillatory deformation hence is reminiscent to activated aging, in which the non-equilibrium gel structure tends to coarsen to increase the number of bonds in the network.

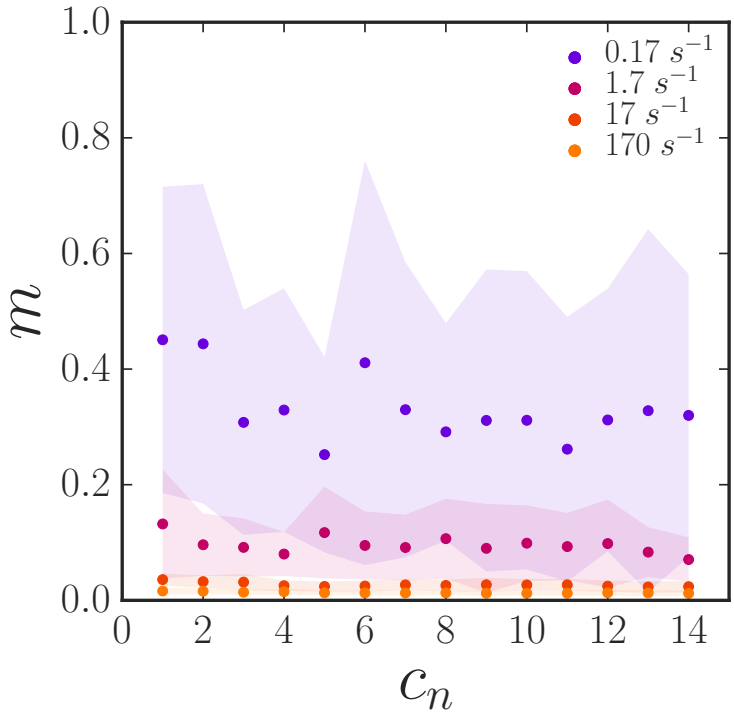

Figure A2.5 – Average plastic deformation per oscillation cycle as a function of the strain rate $\dot{\gamma}$.

Broken gel strands

Gel strands that break during the simulation are not included in further analysis. Statistics of the broken strands (Fig. A2.6) shows the percentage of strands that detach from the wall or break into clusters. The number of gel strands that break upon expansion is higher compared to compression. Yet, for expansion the majority of the strands break into clusters whereas for compression the effect of breaking at the wall or into clusters is more evenly distributed. Deformation of gel strands at different strain rates $\dot{\gamma}$ only shows different breakage statistics at a strain rate of 170 s^{-1}. Here, the amount of broken strands increases drastically and strands start to break profoundly at the wall instead of breaking into clusters. This indicates that the amount of

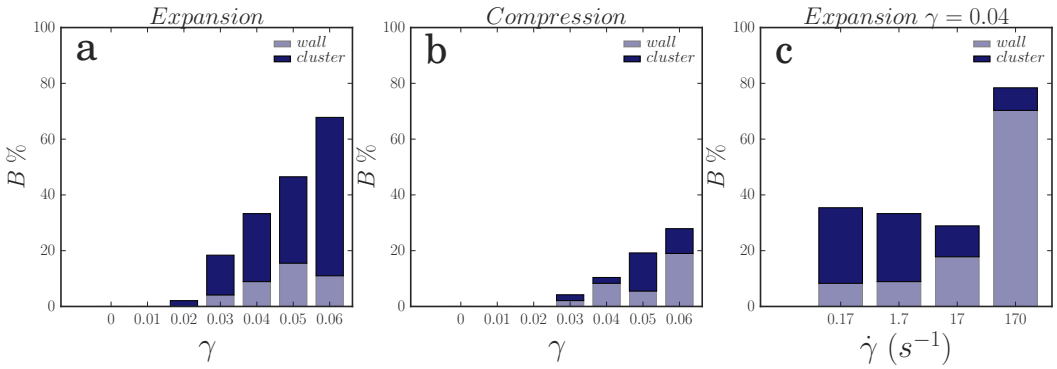

Figure A2.6 – Breakage percentage (B %) for (a) expansion and (b) compression of gel strands at strain amplitudes γ = 0.01 - 0.06. (c) Breakage statistics of gel strands that are deformed with strain rates $\dot{\gamma}$ = 0.17, 1.7, 17 and 170 s^{-1} respectively (expansion, γ_{max} = 0.04).

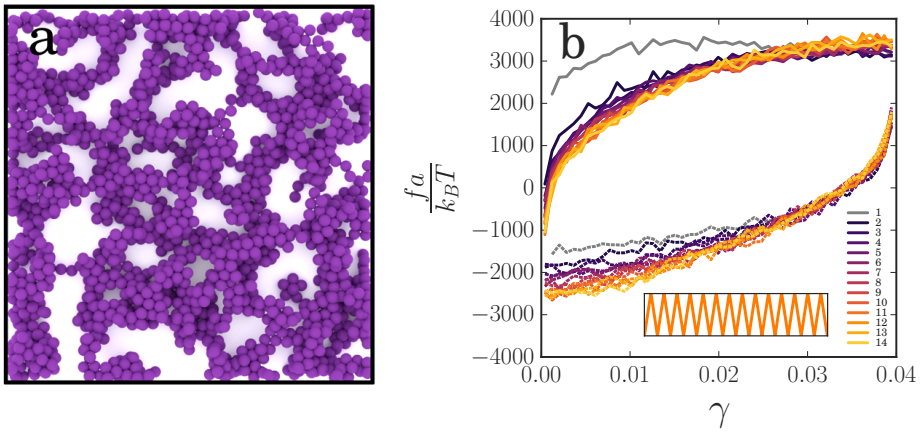

Figure A2.7 – a) Small slab (N=1880) of a large 3D colloidal gel (N=13500) at volume fraction $\phi = 0.2$. b) Force-strain curves upon 14 oscillatory expansions of a large gel (γ_{max} = 0.04).

broken gel strands is not affected by the strain rate used in the simulations (1.7 s^{-1}).

III. Comparing a single gel strand with a network of strands

Deformation of a large 3D gel ($N = 13500$, $\phi = 0.2$) is performed in the same way as described for the single gel strands. The gel is formed between two attractive walls, starting from a random particle configuration, and equi-

librated for 11 τ_B. Expansion is performed by moving both walls outward. To make simulations feasible, the strain rate is increased to $\dot{\gamma} = 0.0284\,\tau_B^{-1}$. This is comparable to an experimental strain rate of $\dot{\gamma} = 17\,s^{-1}$. The results are averaged over ten independent runs.

The obtained network structure (Fig. A2.7a) is highly heterogeneous. To get a clear picture we only show a small slab of the total gel. In Fig. A2.7b the force-strain curve of the large gel is shown. Similar to the single gel strands we see irreversible weakening of the network structure, by plastic rearrangements during the first deformation cycle. This confirms that simulations on single gel strands are representative for a large colloidal gel network.

VI. Additional data

Fig A2.8 contains the same data as shown in Fig 2.3 of this Chapter. Yet, here the plasticity is plotted in a cumulative fashion. After each oscillation the particle positions are always compared to the configuration at the start of cycle 1. For the non-cumulative plasticity particle positions at the start of cycle 1 are compared with the start of cycle 2, the start of cycle 2 with the start of cycle 3 etc.

Fig. A2.9 contains additional experimental data.

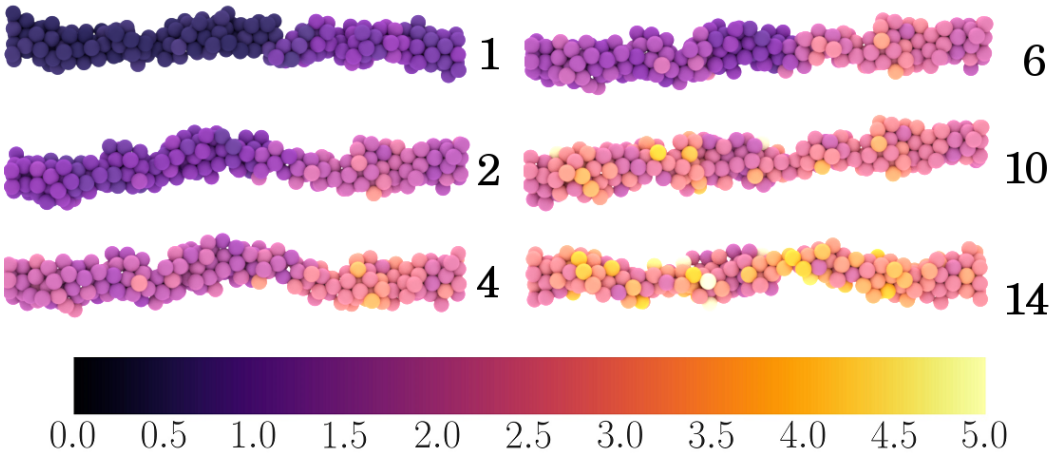

Figure A2.8 – Visual representation of the cumulative average plastic deformation in cycles 1,2,4,6,10 and 14 of a single gel strand ($\gamma_{max} = 0.04$). The color bar indicates the cumulative irreversible displacements of the particles from low (purple) to high (yellow).

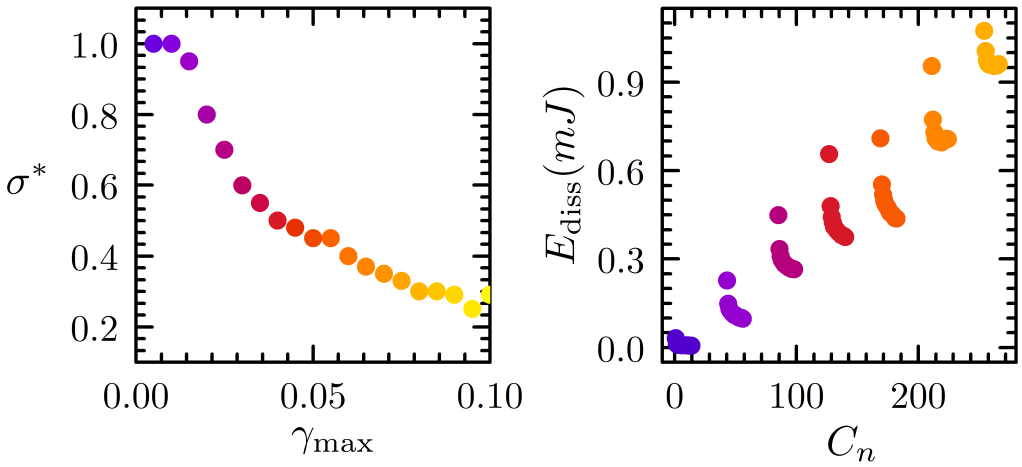

Figure A2.9 – (left) Characteristic stress σ^* (with $\sigma^* = G_0\gamma^*$) used to rescale experimental data presented in Fig. 2.2 as funtion of γ_{max}. Data points are color-coded to their respective γ_{max} value. (right) Dissipated energy for every cycle (c_n) shown in Fig. 2.1. The data points are color-coded to their respective γ_{max} value. The dissipated energy is highest in the first cycle for a given strain amplitude and then gradually decreases to a plateau value as the stress-strain curve approaches a limit cycle. This limiting dissipated energy reflects the viscoelastic dissipation in the network due to solvent flow through the network or to reversible rearrangements, while the additional dissipation in the firct cycle reflects the irreversible plastic deformation that occurs during loading of the gels.

Plasticity in colloidal gel strands

3

Colloidal gels are space-spanning networks of aggregated particles. The mechanical response of colloidal gels is governed, to a large extent, by the properties of the individual gel strands. To study how colloidal gels respond to repeated deformations, we perform Brownian Dynamics simulations on single strands of aggregated colloidal particles. While current models assume that gel failure is due to the brittle rupture of gel strands, our simulations show that gel strands undergo large plastic deformations prior to breaking. Rearrangement of particles within the strands leads to plastic lengthening and softening of the strands, which may ultimately lead to strand necking and ductile failure. This failure mechanism occurs irrespective of the thickness and length of the strands and the range and strength of the interaction potential. Rupture of gel strands is more likely for long and thin strands and when the well width of the interaction increases.

Joanne E. Verweij, Frans A.M. Leermakers, Joris Sprakel & Jasper van der Gucht[1]

"Plasticity in colloidal gel strands"
Soft Matter , **15 (32)** , 6447-6454 (2019)

[1] *Physical Chemistry and Soft Matter, Wageningen University, Wageningen, 6708 WE, The Netherlands.*

Introduction

Upon introducing an attractive interaction colloidal particles can aggregate and form a space-spanning network of dynamically arrested particles [1, 2]. Such a network, called a colloidal gel, behaves as an elastic solid that is able to withstand mechanical stress. Yet, when the applied stress exceeds the yield stress, the gel fluidizes and/or fractures and flows like a liquid [3–9]. This combination of properties makes colloidal gels interesting for a variety of applications, including food products, cosmetics, and scaffolds for tissue engineering [10–14].

The macroscopic properties of colloidal gels, such as their elasticity and yielding behaviour, are intimately linked to the structure and connectivity of the particle network at the microscale [15–17]. The main control parameters that determine the structure of a colloidal gel are the magnitude of the attraction strength between the particles [18–22], the particle volume fraction [18, 21, 22], and the shear history of the gel [23–25]. In the limit of very strong attraction and very low volume fraction, irreversible aggregation leads to the formation of dilute, diffusion-limited fractal gels [18]. In this regime, the mechanics and dynamics of the gel can be described using scaling approaches or by simulation models based on percolating networks of gel strands that ignore the internal structure of the strands [26–29]. However, when the attraction strength is only a few times the thermal energy k_BT, particle rearrangements can occur within the gel, leading to a much coarser gel structure formed by spinodal decomposition [19, 20]. The interplay between phase separation through spinodal decomposition and kinetic arrest then leads to very heterogeneous gels. As long as the volume fraction of particles is not too high (i.e. significantly below the colloidal glass transition), the microstructure of these gels consists of interconnected gel strands with a length and thickness that depends strongly on the interaction potential and the volume fraction [21, 22].

The linear elasticity of colloidal gels can be understood by considering the colloidal gel as a random network of gel strands, with an effective spring constant that depends on the thickness of the strands [30]. However, the non-linear response of colloidal gels remains much less clear. Fracture and yielding of colloidal gels have been attributed to the brittle-like rupture of individual gel strands due to force-activated breaking of inter-particle bonds [30, 31]. However, several authors have shown evidence that this picture may not be very accurate, and that failure of colloidal gels is preceded by significant plastic particle rearrangements [32–34]. In Chapter 2 we

have shown, using a combination of rheological experiments and computer simulations, that these plastic rearrangements within gel strands lead to irreversible strand stretching and build-up of excess length, or slack, rather than strand rupture. [35]

Our results also suggested that the rheological response of colloidal gel networks can be understood by considering the mechanical and dynamic properties of the individual gel strands, which form the basic structural units of the gel (at least, at moderate volume fractions). To relate rheology to the structure of the colloidal gel, it is therefore necessary to know how the response of a gel strand depends on its thickness and length and on the interaction potential between the particles. Here, we will study this relation using computer simulations of gel strands under repeated deformation.

Method

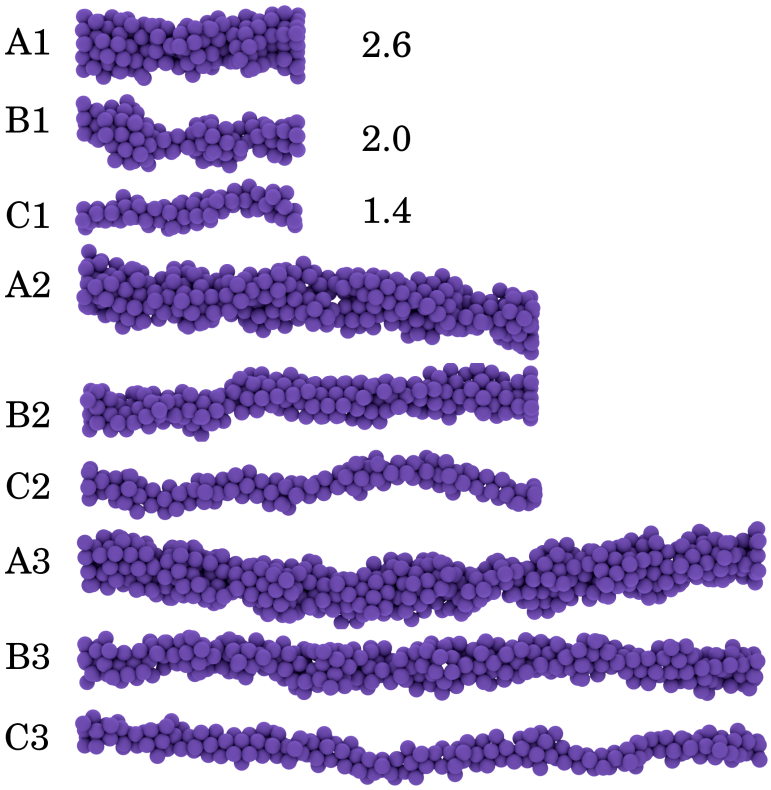

Figure 3.1 – Visual representation of A) thick, B) intermediate and C) thin strands before deformation. A_2, B_2 and C_2, show strands that are 2x longer compared to A_1, B_1 and C_1, whereas A_3, B_3 and A_3 are 3x longer compared to the shortest strands. The average thickness of the start configurations $\langle D_0 \rangle$ (expressed in particle diameters) is indicated next to the strands (see Eq. 3.4.

We perform Brownian Dynamics simulation to study the effect of repeated deformation on individual gel strands. We consider colloidal particles that interact through a Morse potential [36]:

$$\beta u(r) = \beta\epsilon \, \exp(\rho_0[a-r]) \, (\exp[\rho_0(a-r)] - 2) \tag{3.1}$$

with $\beta = 1/k_BT$, ϵ the depth of the energy minimum and a the particle diameter. The parameter ρ_0 specifies the width of the interaction [3]. The different potentials used in this Chapter are shown in Fig. A3.1.

The motion of a particle i with position $\boldsymbol{r}_i$ is obtained by solving the overdamped Langevin equation:

$$\dot{\boldsymbol{r}}_i(t) = \beta D_0[-\nabla_i U(t)] + \sqrt{2D_0}\boldsymbol{\xi}_i(t) \tag{3.2}$$

where $\boldsymbol{\xi}_i(t)$ is random white noise, sampled with zero mean and unit variance, to model the thermal fluctuations of the particles. $D_0 = k_BT/\zeta_f$ is the short-time diffusion coefficient with ζ_f the friction coefficient, set to unity. The time step δt for the numerical integration is set to $\delta t = 1 \times 10^{-6} \, \tau_B$, where $\tau_B = a^2/D_0$ is the Brownian time scale, which defines the unit of time in our simulations.

Gel strands are formed between two attractive flat walls. The parameters for the particle-wall interaction are the same as those for the particle-particle interactions, to make this interaction as inert as possible. The simulation box is periodic in the y- and z direction. The initial configuration of the gel strands is formed by placing a number of particles on a face centered cubic (fcc) lattice in a certain $H \times W \times L$, with H, W, and L the height, width, and length, respectively, expressed in numbers of particles. We consider nine types of gel strands that vary in thickness and length. For a thick gel strand, $H = W = 5$ particles (type A), for intermediate gel strands, $H = W = 4$ (type B), and for thin gel strands, $H = W = 3$ (type C). For each strand thickness, we consider three different lengths (specified as 1, 2, and 3), which gives the following number of particles for the different configurations: A_1 = 200, B_1 = 128, C_1 = 77, A_2 = 400, B_2 = 256, C_2 = 144, A_3 = 600, B_3 = 384 and C_3 = 216. The equilibration time before applying oscillatory deformation is set to t = 568 τ_B. As distances between particles in the initial configuration are larger than the range of the potential, particles aggregate randomly. Thus, the initial fcc lattice affects the approximate thickness of the gel strand but does not influence how particles are structured after equilibration. In Fig. 3.1 examples of these equilibrated gel strands are shown. The average thickness for each type of strand before deformation $\langle D_0 \rangle$ expressed in particle diameters equals 2.6, 2.0 and 1.4, respectively (see also Eq. 3.4).

[3] To determine the inter-particle bonds, we will consider all particles that are within a distance corresponding to 1% of the original well depth ($u(r) < 0.01\epsilon$) as bonded. When not mentioned otherwise, ρ_0 equals 33. This corresponds to a well-width of approximately $\Delta = 0.16 \, a$.

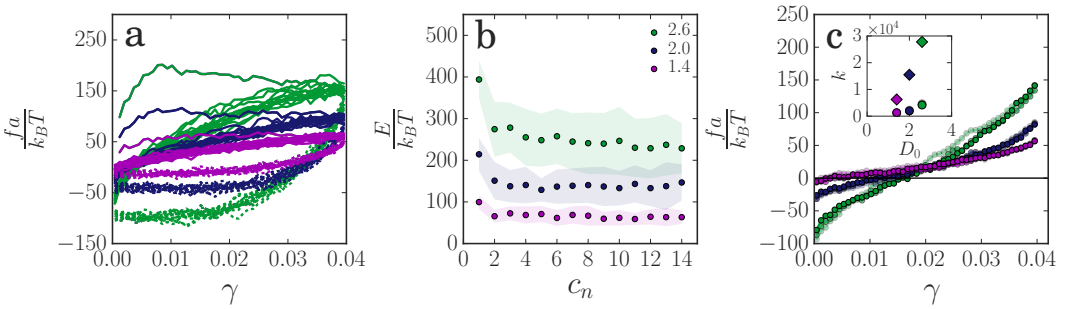

Figure 3.2 – (a) Force-strain curves upon 14 oscillatory expansions of gel strands of different diameter ($\gamma_{max} = 0.04$). The solid line indicates the loading- and the dotted line the unloading curve. (b) Dissipated energy per oscillation c_n, obtained by integration of the force-strain curves. The shaded area indicates the standard deviation. (a) and (b) contain data of the longest gel strands ($A_3 - C_3$) (c) Average elastic force of the $3^{th}, 4^{th}$ and 5^{th} oscillation cycle for gel strands of different diameter and length ($\gamma_{max} = 0.04$). The color gradient indicates the length of the strands from short (light) to long (dark). The inset shows the spring constant k (units $k_BT\ a^{-1}\ \gamma^{-1}$) for the different strands at a deformation of $\gamma_{max} = 0.04$ ($\circ$) and $\gamma_{max} = 0.005$ ($\diamond$).

After equilibration, the gel strand is deformed through 14 oscillations in which the distance between the two walls is varied in a cyclic manner by moving the position of the left wall outwards. This leads to a sawtooth strain profile with a maximum strain $\gamma_{max} = 0.04$ and a fixed strain rate $\dot{\gamma} = 0.00284\tau_B^{-1}$. Data for different amplitudes and strain rates are shown in the Appendix (Fig. A3.7 and A3.8). To make sure that observations are statistically relevant, each data point contains simulation data for at least 30 different gel strands. Here, we only consider strands that stay intact during the entire deformation.

Results and discussion

We cyclically deform the gel strands at constant strain rate and measure the resulting force f exerted on the walls. For strain cycles at small amplitude ($\gamma_{max} = 0.005$), the force increases linearly with deformation, with a spring constant that increases with the strand thickness (Fig. A3.2). However, for larger amplitude ($\gamma_{max} = 0.04$), the force-strain curves are highly non-linear for all gel strands and show a pronounced hysteresis loop (Fig. 3.2a), which indicates significant energy dissipation during the deformation cycles. The dissipated energy is highest in the first deformation cycle (Fig. 3.2b), which is found to differ qualitatively from the subsequent cycles: the force first increases with increasing strain until a threshold value is reached, after which it levels off. This plateau in the force indicates plastic

flow inside the gel strand due to irreversible particle rearrangements. The threshold force for plastic flow is proportional to the cross-section of the strands (Fig. A3.3a), and increases with increasing strain rate (Fig. A3.8), in agreement with models based on Kramers theory for force-activated dissociation of particle-particle bonds [37]. As we have shown previously [35], the plastic rearrangements are associated with the irreversible stretching of the gel strand and the build-up of slack. Here, slack is defined as excess length that is created due to lengthening of the strands. This softens the gel strand, so that in subsequent cycles the observed force is lower than in the first cycle. The force-strain curve then quickly reaches a limit cycle, with an enclosed area that accounts for the viscoelastic dissipation due to reversible particle rearrangements. The dissipated energy is highest for the thick gel strands and lowest for the thin strands (Fig. 3.2b). As shown in Fig. A3.3b, the dissipated energy is roughly proportional to the cross-section A of the strands, with each particle contributing 3-4$\%$ of the interaction energy ϵ to the energy dissipation. Increasing the strain amplitude from $\gamma_{max} = 0.04$ to $\gamma_{max} = 0.06$ (Fig. A3.7) results in a single particle contribution of 5-6$\%$ of ϵ to the dissipated energy. The total energy dissipation thus scales with the applied strain amplitude and with the interaction energy.

To analyze the softening of the gel strands in more detail, we disentangle the elastic and viscous contributions to the measured response by averaging the loading and unloading curve for each cycle [38]. This averages out the viscous contribution, so that only the elastic contribution remains. The resulting elastic force goes through zero at a finite strain (Fig. 3.2c), which reflects the increase in the rest length due to the expansion cycles. The relative increase in rest length is highest for the thick strands (approximately 1.7%) and smallest for the thin strands ($\sim 0.3\%$), indicating that thicker strands have more possibilities to deform plastically.

The plastic stretching of the gel strand leads to the build-up of slack. In subsequent deformation cycles, the slack induced in previous cycles is pulled out first, which results in little resistance and a strong decrease in the effective spring constant. Indeed, the effective spring constants measured after deforming the gel at a strain γ_{max} = 0.04 is significantly smaller than those measured in the linear deformation regime (γ_{max} = 0.005) (inset Fig. 3.2c). When the strain amplitude of the cycles becomes larger, the accumulated slack increases so that the effective spring constant decreases even further [35] (see Fig. A3.7). As expected, the spring constant increases with strand thickness and is approximately proportional to the cross-section of the the strands (Fig. A3.3c), indicating that each inter-particle bond contributes roughly equally to the spring constant.

As the rest length of the gel strands increases in the loading cycle, it must be compressed in the return cycle. This could lead to bending or buckling of the strand. To investigate this, we follow the contour of the gel strand during the deformation cycles. We do this by dividing the strand into equally sized

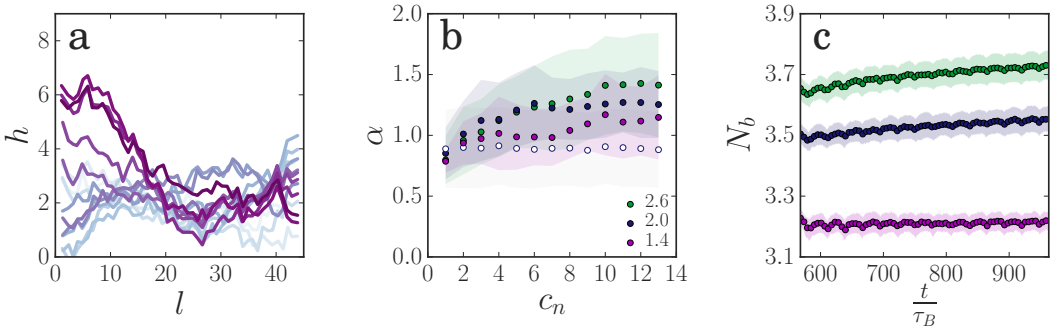

Figure 3.3 – (a) Projected 3D coordinates of a single gel strand (B_3, $\gamma_{max} = 0.04$) at the start of each oscillation (cycle number increases from light blue to dark purple). The height (h) and length (l) of the strand are both represented in dimensions of particle diameter a. (b) The deviation from a straight configuration α as function of oscillation cycle c_n (A_3 - C_3). Open markers represent an undeformed gel strand (zero measurement). (c) Average number of bonds per particle in time (A_2 - C_2).

bins (σ = 0.9) and calculating the average coordinates in each bin [39]. Since the ends of the strand are not fixed in our simulation, the strand fluctuates significantly, both during the deformation cycles and in rest (Fig. 3.3a). To analyze the shape of the strand and the amount of bending that occurs, we draw a line through the two ends of the strand and for each bin calculate the local distance of the gel strand contour to this straight line. The average distance over all bins α (Fig. 3.3b) is a measure for how much the shape of the gel strand deviates from a straight line, and indicates bending of the strand. For a gel strand that is not deformed, α does not change significantly, indicating that the shape of the gel strand remains more or less the same. However, when the gel strands are deformed α increases gradually with each deformation cycle, indicating that the strands must bend more to accommodate the increase in rest length. The increase in α is more pronounced for the thicker gel strands, which is in agreement with our observation that the thick strands show a larger increase in rest length upon deformation [4]. Thus, thick strands are more prone to plastically elongate and develop slack, thereby contributing more strongly to this unusual non-linear response.

The internal rearrangements in the gel strands lead to the breaking and reformation of inter-particle bonds. Surprisingly, the average number of bonds per particle N_b increases as the strands are deformed and become longer (Fig. 3.3c). This suggests that the applied deformation leads to accelerated aging and coarsening of the gel strand, driving it gradually into a more favorable state by forming more inter-particle bonds [25, 40]. A sim-

[4] Although a gel strand is also allowed to move up and down along the walls we do not see an increase of the length of line l in subsequent oscillations. Thus, parameter α is a good measure to describe strand lengthening as a consequence of buckling.

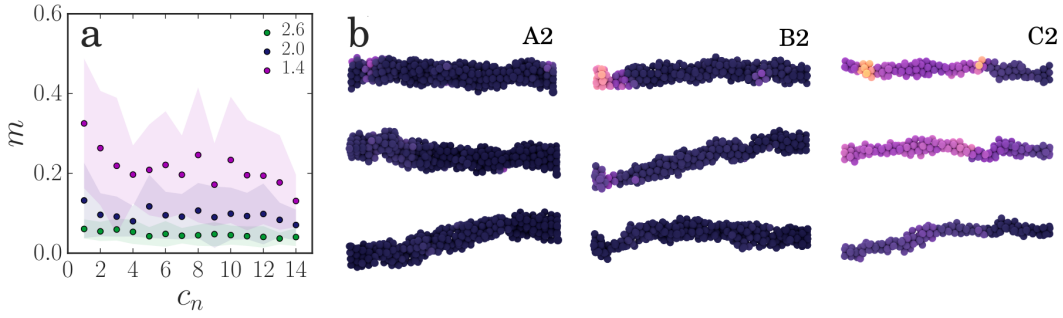

Figure 3.4 – (a) Average mobility of the particles per oscillation (for strand types A_2 - C_2). (b) Visual representation of particle displacements, highlighting the heterogeneity of the strain.

ilar strain-induced increase of the number of inter-particle bonds has been seen in computer simulations [41] and in experiments [24] on colloidal gel networks. We note that the strain-induced increase in the number of bonds is more pronounced and continues for a longer period as the gel strands get thicker (see also Fig. A3.6b where data for even thicker gel strands are shown). This is further confirmed by the dissipated energy per cycle, which takes much longer to reach a plateau for thicker strands (Fig. A3.6a). Again, this indicates that thick strands have more possibilities for local particle rearrangements and plastic deformation than thinner strands. The overall coarsening must imply that the deformation of the strands upon stretching occurs heterogeneously, so that thicker regions can form that are connected by thinner sections. This is reminiscent of the Rayleigh-Plateau instability in liquid jets (see Fig. 3.4b), and highlights the arrested liquid state of the colloidal gel. We further note that, even though the total number of bonds gradually increases, the force sustained by the strand does not increase. Our data suggests that this is because these newly formed bonds only stiffen the parts of the gel strand that are already strong, while the overall stiffness is determined mainly by the weak regions. A similar conclusion was obtained in recent computer simulations on large gel networks [41].

We can further quantify the heterogeneity of the internal rearrangements by considering the displacement for each particle during a deformation cycle c_n:

$$m_i(c_n) = \frac{1}{\mathcal{N}_i a^2} \sum_{j=1}^{\mathcal{N}_i} \langle \left| \boldsymbol{r}_{ij}(0) - \boldsymbol{r}_{ij}(t) \right|^2 \rangle_n \tag{3.3}$$

where $\boldsymbol{r}_{ij}(0)$ and $\boldsymbol{r}_{ij}(t)$ denote the separation vector between particle i and neighbouring particles j at the start of the cycle and after a time t, respectively, and $\mathcal{N}_i$ is the number of nearest neighbours of particle i. Here, the average is taken over the entire oscillation.

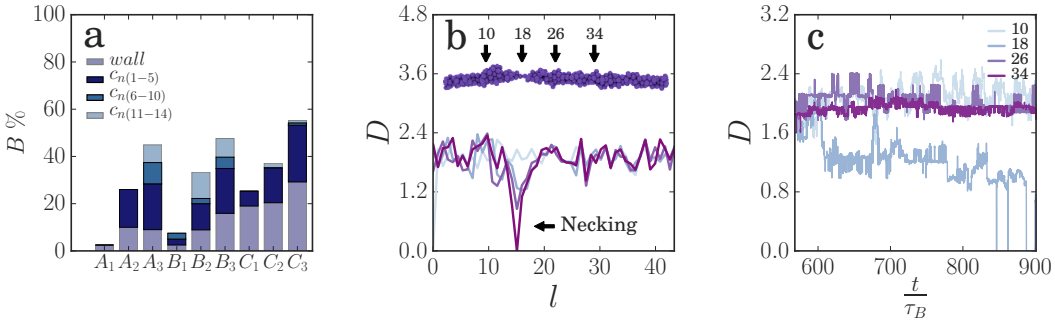

Figure 3.5 – (a) Breakage statistics for gel strands of different sizes ($\gamma = 0.04$), separated into strands that detach from the wall or break into clusters. To specify the moment of failure, breakage is categorized into oscillation cycle intervals. (b) Thickness D as a function of the length of a strand (B_3, $\langle D_{start} \rangle = 2.0$, $\gamma_{max} = 0.04$) plotted in time (568-928 τ_B, colored from light to dark) (c) Thickness D in time for different segments of the strand in plot (b).

As shown in Fig. 3.4, particles in thin strands on average rearrange over larger distances compared to particles in thick strands. Upon deformation, many particles in a thin strand participate in movement, whereas only a few particles in the thicker strands move. Note, that the displacements of the particles contain both the elastic and plastic contributions. From the rest length of the strands we know that thick strands lengthen more and have a higher plastic deformation. Here, we see that these plastic deformations are indeed very heterogeneous and strongly localized to certain regions in the gel strand. The same heterogeneity is seen in thin strands, but these strands are also largely elastically deformed. The strong strain localization leads to the formation of thin necks, where the strand will eventually rupture.

We also monitor strand rupture in our simulations and find that the percentage of broken gel strands increases strongly with increasing strand length and decreasing strand thickness (Fig. 3.5a). Long strands break more easily, because the probability that a weak spot forms during the deformation increases as strands get longer. Thin strands are held together by fewer interparticle bonds, making them more prone to breakage. For the longest gel strands, the moment of rupture appears to shift to longer times as the strands get thicker: most of the thin strands (C_3) rupture in the first cycles, while for the thicker strands (A_3) rupture occurs more frequently in the later cycles, probably because more plastic deformation is needed before a sufficiently weak spot is formed. For the shorter strands, we do not observe such a trend, but this could be due to poor statistics, as the number of broken strands is much smaller for short chains. The fraction of broken gel strands also increases strongly with increasing strain amplitude (Fig. A3.7), and with in-

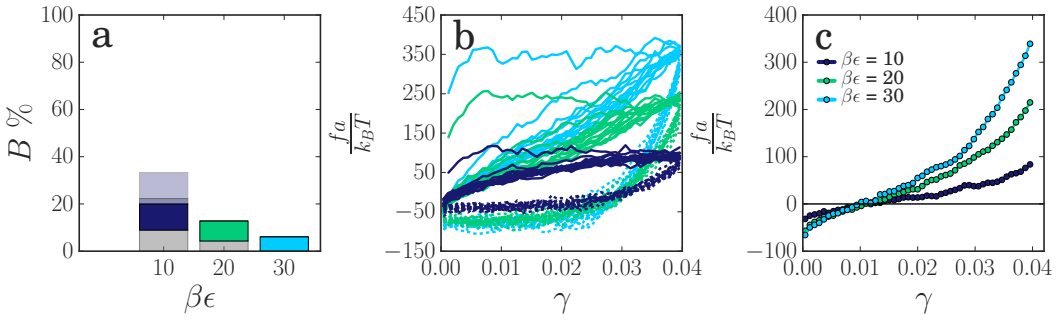

Figure 3.6 – (a) Breakage statistics for gel strands at different interaction energies. We distinguish breakage at the wall (gray) and breakage into clusters at oscillation cycles interval 1-5, 6-10 and 11-14 (dark till light) respectively. (b) Force-strain curves of 14 subsequent oscillatory deformations. (c) Average elastic force of the 3^{th}, 4^{th} and 5^{th} oscillation cycle.

creasing strain rate (Fig. A3.8), the latter indicating a transition to a more brittle response at higher rates due to fewer possibilities for plastic rearrangements [35]. In the breakage statistics we specifically show the amount of breakage at the walls. This breakage does not dominate. Only for thin gel strands we see that the connection with the wall becomes a weak spot. We note that failure at the walls of the container is also observed experimentally in the yielding of some colloidal gels [5, 6].

To follow the ductile deformation leading to strand rupture, we consider the local thickness of the gel strand by dividing the strand into a number of segments and calculating the root-mean square thickness in each segment [42]:

$$D(x) = \frac{1}{N_x r_a} \sum_{k=1}^{N_x} \sqrt{|\boldsymbol{r}_k(x) - \boldsymbol{r}_{mean}(x)|^2} \tag{3.4}$$

where $\boldsymbol{r}_{mean}$ is the average coordinate of the particles in a specific segment, $\boldsymbol{r}_k$ is the position of particle k in this segment (projected onto the xz-plane of the average coordinate), N_x equals the total number of particles per segment and r_a is the radius of the particles. We plot the local thickness along the gel strand for different times (Fig. 3.5b). Before the deformation cycles, the thickness is quite uniform along the strand. However, as the deformation cycles continue, a necking region arises locally. This necking region forms rather abruptly, as shown in Fig. 3.5c, where the thickness for a few locations along the gel strand (see arrows Fig. 3.5b) is plotted as a function of time. This rapid decrease in local thickness finally results in breakage of the gel strand.

The necking process leading to strand fracture raises the question whether strand rupture occurs at pre-existing defects in the gel strands,

formed during gel formation as suggested previously [30], or at random locations along the strand where plastic deformations happen to localize during deformation of the gel. In other words, is there a correlation between the thinnest region of the gel strand before deformation and the location where the strand finally breaks? To test this, we deform the initial configurations of 15 strands multiple times and monitor the initial thickness at the location where the strand is found to break. We find that the strand is indeed more likely to break at a thin region: the average initial thickness at the location of rupture, normalized by the average strand thickness, $\langle D_{break} \rangle / \langle D_0 \rangle$ is 0.74, 0.82 and 0.82 for the thick, intermediate, and thin strands, respectively. Thus, strain localization and subsequent strand rupture tend to occur predominantly in low density regions of gel strands.

In $46\ \%$ of the cases, thick strands break at the thinnest part D_{min} of the start configuration. For intermediate and thin strands, this is only $37\ \%$ and $18\ \%$, respectively. It can be concluded, therefore, that thick strands are more likely to break at a weak spot or defect in the original strand, while thin strands tend to break at more random locations. Previously, we noted that in thick strands only a few particles have large rearrangements at the weak spots. As a result, the initial structure of these strands is more likely to determine where failure will occur, in line with previous work [30].

Now that we have shown how the thickness and length of colloidal gel strands affect their mechanical and plastic response, we consider the effect of the interaction potential between the particles (for potentials see Fig. A3.1). Increasing the attraction strength between the particles makes the strands more resistant to rupture, as indicated by a lower percentage of broken strands (Fig. 3.6a). The force-strain relations for the different interaction energies show a similar plastic flow regime in the first deformation cycle, with a threshold force for plastic flow that increases approximately proportionally to the attraction strength (Fig. 3.6b). These findings are in agreement with theoretical models based on Kramers theory for force-activated bond rupture, which predict a rupture probability that decreases exponentially with the interaction strength and a threshold force that, for a given strain rate, is proportional to the effective spring constant and thus to the attraction strength ε [4, 37, 43]. From the elastic contribution to the force, we observe that the change in rest length induced by the deformation cycles does not depend on the attraction strength (Fig. 3.6c). This indicates that the mechanism by which colloidal gels weaken due to local plasticity does not depend on the strength of the interaction, even when this attraction strength is as large as 30 k_BT. This is further confirmed by the amount of particle displacements, which is nearly independent of the attraction strength (Fig. A3.4a), and the total dissipated energy in the cycles, which is proportional to the attraction strength (Fig. A3.4b). The spring constant of the strands after the deformation cycles increases with increasing attraction energy (Fig. 3.6c), and after rescaling with ϵ, we find that the elastic contribution to the force is

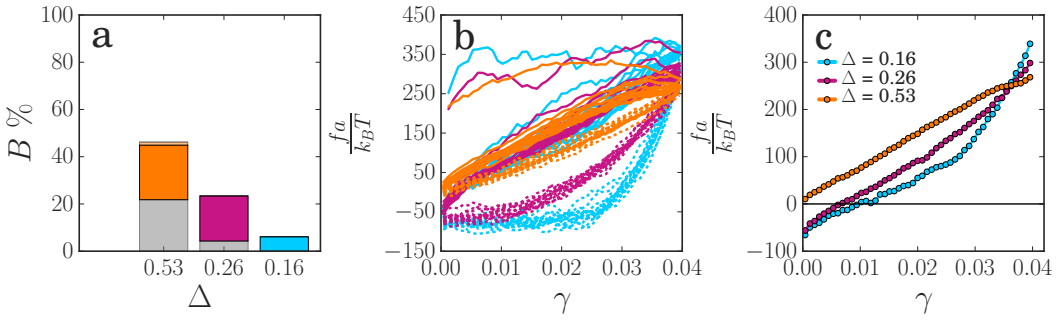

Figure 3.7 – (a) Breakage statistics for gel strands with different well widths $\Delta = 0.53$, 0.26 and 0.16 ($\beta\epsilon = 30$). (b) Force-strain curves of 14 subsequent oscillatory deformations. (c) Average elastic force of the $3^{th}, 4^{th}$ and 5^{th} oscillation cycle.

proportional to ϵ (Fig. A3.4c).

In addition to varying the strength of the interactions, we also change the range of the attraction by changing the range parameter ρ_0, giving well widths of approximately $\Delta = 0.528\ a, 0.264\ a$, and $0.160\ a$ (for $\rho_0 = 10, 20$, and 33 respectively) (see Fig. A3.1). This is an interesting property to vary as the range over which interactions are sticky influences the deformation of the strands. Note that for simulations of a full colloidal gel a given pair potential and volume fraction ϕ gives an average length and thickness distribution of the gel strands. Here, we try to uncouple these two, by looking at strands of a single length and thickness with different pair potentials. To a certain extent this gives some 'artificial' effects, as in real gels the potential width and network structure are coupled. Still, we can show some interesting observations.

We find that increasing the range of the attraction makes the strands more prone to rupture (Fig. 3.7a). However, note that due to a larger potential width strands are aged substantially more (see Fig. A3.5) and thus contain a higher number of weak spots.

The force-strain curves again look similar, showing a plastic flow regime in the first cycle. The threshold force for plastic deformation appears to be rather insensitive to the range of the attraction, while the amount of dissipated energy increases significantly as the attraction range decreases (Fig. A3.5), reflecting a higher number of broken bonds. When looking at the elastic component of the force-strain curve for the deformed strands (Fig. 3.7c), we find a much larger increase in rest length for the shorter-ranged attraction. We thus conclude that plastic deformation, leading to strand stretching and softening, is more pronounced in gels with a short-ranged attraction, while a gel with a higher well width only shows a linear deformation response at $\gamma_{max} = 0.04$.

Note also that the stiffness of the deformed gel strands, as indicated by

the slope of the force-strain curves in Fig. 3.7c, becomes almost independent of the attraction range. This might seem surprising, as the stiffness of a single bond is given by the second derivative of the potential, $k \sim \epsilon\rho_0^2 \sim \epsilon/\Delta^2$, so that one would expect the highest stiffness for the smallest well width. Yet, we know that for small Δ the strand is plastically deformed and softening occurs, resulting in a decrease of the spring constant in the linear regime. The effective resulting stiffness is set by the threshold force f^* where the plastic flow regime starts, $k_{eff} \approx f^*/\gamma_{max}$.

Conclusions

Our results highlight how failure and yielding of colloidal gels result from plasticity at the scale of individual gel strands. While previous models for colloidal gel rheology and failure were based on the brittle rupture of gel strands, we show that this rupture is preceded by significant plastic deformations that cause irreversible lengthening and softening of gel strands. We observe this mechanism of failure for strands of different length and thickness and for interaction potentials of different strength and range, suggesting that it should be relevant for a wide range of experimental colloidal systems. Recently, we showed experimental results that support this finding [35]. Our findings are also in agreement with earlier experiments that showed a two-step yielding in colloidal gels under shear [32]; here, the first yielding event was attributed to restructuring and effective lengthening of gel elements in the shear direction, while the second step was attributed to strand rupture. Our results underpin this hypothesis and provide a microscopic mechanism. Furthermore, our results indicate that the amount of plastic deformation that a gel can undergo before it ruptures is determined by the structure of the gel and by the interaction potential. Coarser gels, consisting of short and thick gel strands, will deform much more plastically than dilute gels with long and thin strands. Plasticity is also promoted by a large attraction strength and a short attraction range.

Our simulations have focused on single gel strands. While our recent results have shown that the macroscopic rheological properties of a colloidal gel can indeed be linked to the properties of the individual strands that constitute the gel [35], it remains an open question how the network topology influences the non-linear response. Combining our results for single strands with a full characterization of the network structure may be a first step towards a fully predictive model for colloidal gel rheology.

Bibliography

[1] Emanuela Zaccarelli. Colloidal gels: equilibrium and non-equilibrium routes. *Journal of Physics: Condensed Matter*, 19(32):323101, 2007.

[2] Veronique Trappe and Peter Sandkühler. Colloidal gels—low-density disordered solid-like states. *Current Opinion in Colloid & Interface Science*, 8(6):494 – 500, 2004.

[3] Benjamin J Landrum, William B Russel, and Roseanna N Zia. Delayed yield in colloidal gels: Creep, flow, and re-entrant solid regimes. *Journal of Rheology*, 60(4):783–807, 2016.

[4] Joris Sprakel, Stefan B Lindström, Thomas E Kodger, and David A Weitz. Stress enhancement in the delayed yielding of colloidal gels. *Physical Review Letters*, 106(24):248303, 2011.

[5] Thomas Gibaud, Damien Frelat, and Sébastien Manneville. Heterogeneous yielding dynamics in a colloidal gel. *Soft Matter*, 6(15):3482–3488, 2010.

[6] Thomas Gibaud, Christophe Perge, Stefan B Lindström, Nicolas Taberlet, and Sébastien Manneville. Multiple yielding processes in a colloidal gel under large amplitude oscillatory stress. *Soft Matter*, 12(6):1701–1712, 2016.

[7] Kasper Masschaele, Jan Fransaer, and Jan Vermant. Direct visualization of yielding in model two-dimensional colloidal gels subjected to shear flow. *Journal of Rheology*, 53(6):1437–1460, 2009.

[8] Vincent Grenard, Thibaut Divoux, Nicolas Taberlet, and Sébastien Manneville. Timescales in creep and yielding of attractive gels. *Soft Matter*, 10(10):1555–1571, 2014.

[9] Christophe Perge, Nicolas Taberlet, Thomas Gibaud, and Sébastien Manneville. Time dependence in large amplitude oscillatory shear: A rheo-ultrasonic study of fatigue dynamics in a colloidal gel. *Journal of Rheology*, 58(5):1331–1357, 2014.

[10] Mani Diba, Huanan Wang, Thomas E. Kodger, Shima Parsa, and Sander C. G. Leeuwenburgh. Highly elastic and self-healing composite colloidal gels. *Advanced Materials*, 29(11):1604672–n/a, 2017. 1604672.

[11] Raffaele Mezzenga, Peter Schurtenberger, Adam Burbidge, and Martin Michel. Understanding foods as soft materials. *Nature Materials*, 4:729–740, 2005.

[12] Chinmay Das, Massimo G. Noro, and Peter D. Olmsted. Lamellar and inverse micellar structures of skin lipids: Effect of templating. *Physical Review Letters*, 111:148101, Oct 2013.

[13] Kuen Yong Lee and David J. Mooney. Hydrogels for tissue engineering. *Chemical Reviews*, 101(7):1869–1880, 2001. PMID: 11710233.

[14] A. Zemel, I. B. Bischofs, and S. A. Safran. Active elasticity of gels with contractile cells. *Physical Review Letters*, 97:128103, Sep 2006.

[15] Lilian C Hsiao, Richmond S Newman, Sharon C Glotzer, and Michael J Solomon. Role of isostaticity and load-bearing microstructure in the elasticity of yielded colloidal gels. *Proceedings of the National Academy of Sciences*, 2012.

[16] A. D. Dinsmore, V. Prasad, I. Y. Wong, and D. A. Weitz. Microscopic structure and elasticity of weakly aggregated colloidal gels. *Physical Review Letters*, 96:185502, May 2006.

[17] Mehdi Bouzid, Jader Colombo, Lucas Vieira Barbosa, and Emanuela Del Gado. Elastically driven intermittent microscopic dynamics in soft solids. *Nature Communications*, 8, 2017.

[18] Samuel Griffiths, Francesco Turci, and C Patrick Royall. Local structure of percolating gels at very low volume fractions. *The Journal of Chemical Physics*, 146(1):014905, 2017.

[19] Benjamin J. Landrum, William B. Russel, and Roseanna N. Zia. Delayed yield in colloidal gels: Creep, flow, and re-entrant solid regimes. *Journal of Rheology*, 60(4):783–807, 2016.

[20] Peter J. Lu, Emanuela Zaccarelli, Fabio Ciulla, Andrew B. Schofield, Francesco Sciortino, and David A. Weitz. Gelation of particles with short-range attraction. *Nature*, 453(7194):499–503, 2008.

[21] A D Dinsmore and D A Weitz. Direct imaging of three-dimensional structure and topology of colloidal gels. *Journal of Physics: Condensed Matter*, 14(33):7581, 2002.

[22] V. Trappe, V. Prasad, Luca Cipelletti, P. N. Segre, and D. A. Weitz. Jamming phase diagram for attractive particles. *Nature*, 411(6839):772–775, 2001.

[23] Nick Koumakis, Esmaeel Moghimi, Rut Besseling, Wilson CK Poon, John F Brady, and George Petekidis. Tuning colloidal gels by shear. *Soft Matter*, 11(23):4640–4648, 2015.

[24] Ahmed Helal, Thibaut Divoux, and Gareth H McKinley. Simultaneous rheoelectric measurements of strongly conductive complex fluids. *Physical Review Applied*, 6(6):064004, 2016.

[25] Esmaeel Moghimi, Alan R Jacob, Nick Koumakis, and George Petekidis. Colloidal gels tuned by oscillatory shear. *Soft Matter*, 13(12):2371–2383, 2017.

[26] Yacov Kantor and Itzhak Webman. Elastic properties of random percolating systems. *Physical Review Letters*, 52(21):1891, 1984.

[27] Wei-Heng Shih, Wan Y Shih, Seong-Il Kim, Jun Liu, and Ilhan A Aksay. Scaling behavior of the elastic properties of colloidal gels. *Physical Review A*, 42(8):4772, 1990.

[28] AH Krall and DA Weitz. Internal dynamics and elasticity of fractal colloidal gels. *Physical Review Letters*, 80(4):778–781, JAN 26 1998.

[29] Emanuela Del Gado and Walter Kob. Network formation and relaxation dynamics in a new model for colloidal gelation. *Journal of Non-Newtonian Fluid Mechanics*, 149(1-3, SI):28–33, FEB 15 2008. International Workshop on Mesoscale and Multiscale Description of Complex Fluids, Prato, Italy, July 05-08, 2006.

[30] JC Conrad, HM Wyss, Véronique Trappe, Suliana Manley, K Miyazaki, LJ Kaufman, AB Schofield, David R Reichman, and DA Weitz. Arrested fluid-fluid phase separation in depletion systems: Implications of the characteristic length on gel formation and rheology. *Journal of Rheology*, 54(2):421–438, 2010.

[31] Stefan B. Lindström, Thomas E. Kodger, Joris Sprakel, and David A. Weitz. Structures, stresses, and fluctuations in the delayed failure of colloidal gels. *Soft Matter*, 8:3657–3664, 2012.

[32] Hubert K Chan and Ali Mohraz. Two-step yielding and directional strain-induced strengthening in dilute colloidal gels. *Physical Review E*, 85(4):041403, 2012.

[33] V Gopalakrishnan and CF Zukoski. Delayed flow in thermo-reversible colloidal gels. *Journal of Rheology*, 51(4):623–644, 2007.

[34] Stefano Aime, Laurence Ramos, and Luca Cipelletti. Microscopic dynamics and failure precursors of a gel under mechanical load. *Proceedings of the National Academy of Sciences of the United States of America*, 115(14):3587–3592, APR 3 2018.

[35] Jan Maarten van Doorn, Joanne E Verweij, Joris Sprakel, and Jasper van der Gucht. Strand plasticity governs fatigue in colloidal gels. *Physical Review Letters*, 120(20):208005, 2018.

[36] C. Patrick Royall, Jens Eggers, Akira Furukawa, and Hajime Tanaka. Probing colloidal gels at multiple length scales: The role of hydrodynamics. *Physical Review Letters*, 114:258302, Jun 2015.

[37] Paulina J. Skrzeszewska, Joris Sprakel, Frits A. de Wolf, Remco Fokkink, Martien A. Cohen Stuart, and Jasper van der Gucht. Fracture and Self-Healing in a Well-Defined Self-Assembled Polymer Network. *Macromolecules*, 43(7):3542–3548, APR 13 2010.

[38] Stefan Münster, Louise M Jawerth, Beverly A Leslie, Jeffrey I Weitz, Ben Fabry, and David A Weitz. Strain history dependence of the nonlinear stress response of fibrin and collagen networks. *Proceedings of the National Academy of Sciences of the United States of America*, 110(30):12197–202, jul 2013.

[39] F Gittes, B Mickey, J Nettleton, and J Howard. Flexural rigidity of microtubules and actin filaments measured from thermal fluctuations in shape. *The Journal of Cell Biology*, 120(4):923–934, 1993.

[40] Roseanna N. Zia, Benjamin J. Landrum, and William B. Russel. A micro-mechanical study of coarsening and rheology of colloidal gels: Cage building, cage hopping, and smoluchowski's ratchet. *Journal of Rheology*, 58(5):1121–1157, 2014.

[41] Jader Colombo and Emanuela Del Gado. Stress localization, stiffening, and yielding in a model colloidal gel. *Journal of Rheology*, 58(5):1089–1116, 2014.

[42] AU Grosberg and Aleksej Removič Hohlov. *Statistical physics of macromolecules; Transl. by: YA Atanov*. AIP press Woodbury (NY), 1994.

[43] Breanndan O Conchuir and Alessio Zaccone. Mechanism of flow-induced biomolecular and colloidal aggregate breakup. *Physical Review E*, 87(3):032310, 2013.

Appendix

On the next few pages the additional figures from the appendix can be found.

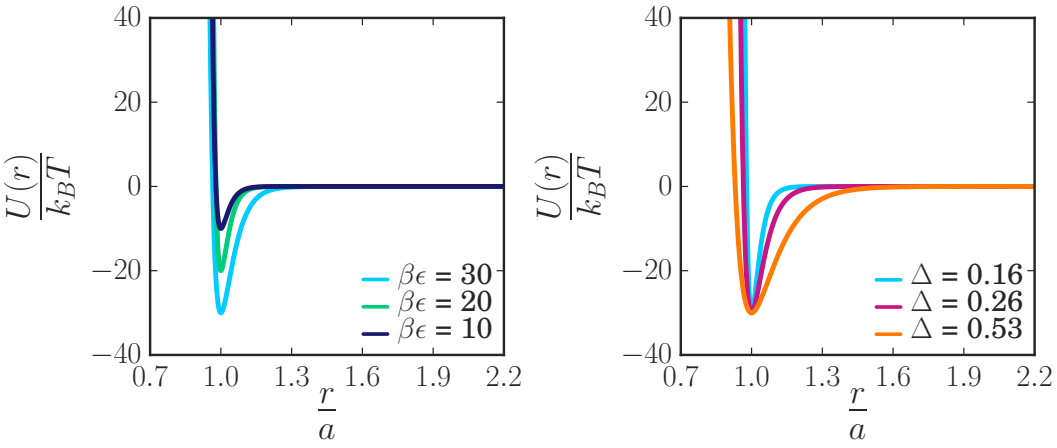

Figure A3.1 – (left) Morse potential with different depths of the potential, $\beta\epsilon = 10$, 20 and 30 respectively. (right) Morse potential ($\beta\epsilon = 30$) with different well widths corresponding to $\Delta = 0.16$, 0.26 and 0.53 a ($\rho_0 =$ 33, 20 and 10).

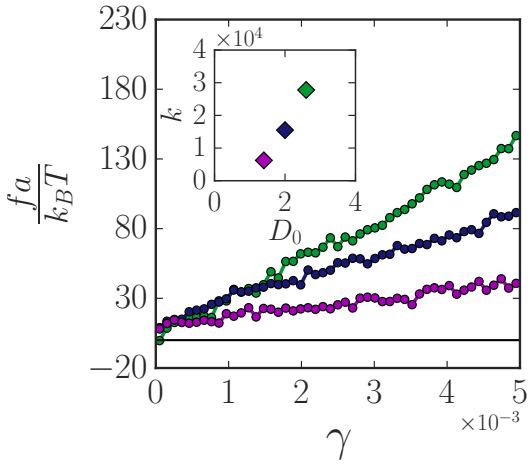

Figure A3.2 – Average elastic force of the $3^{th}, 4^{th}$ and 5^{th} oscillation cycle for gel strands of different diameter ($A_3, B_3, C_3, \gamma_{max} = 0.005$). The inset shows the spring constant k (units $k_BT\ a^{-1}\ \gamma^{-1}$) for the different strands at a deformation of $\gamma_{max} = 0.005$ ($\diamond$).

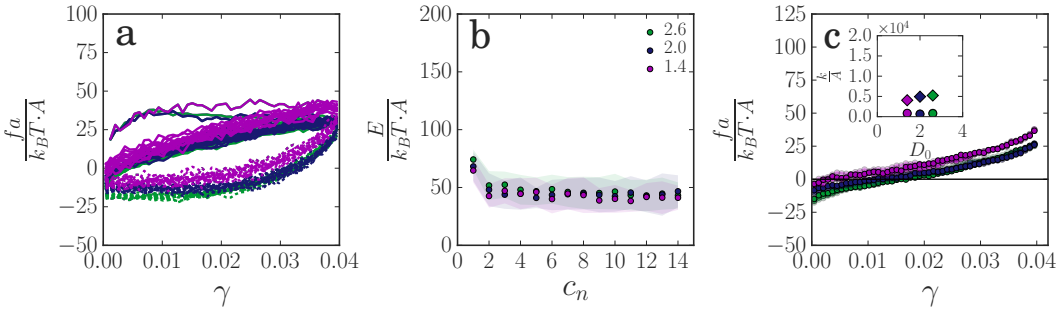

Figure A3.3 – All data is normalized by the cross-section $A = \pi \cdot (\frac{D_0}{2})^2$ of the strands. (a) Force-strain curves upon 14 oscillatory expansions of gel strands of different diameter ($\gamma_{max} = 0.04$). The solid line indicates the loading- and the dotted line the unloading curve. (b) Dissipated energy per oscillation c_n, obtained by integration of the force-strain curves. The shaded area indicates the standard deviation. (a) and (b) contain data of the longest gel strands ($A_3 - C_3$). (c) Average elastic force of the $3^{th}, 4^{th}$ and 5^{th} oscillation cycle for gel strands of different diameter and length ($\gamma_{max} = 0.04$). The color gradient indicates the length of the strands from short (light) to long (dark). The inset shows the spring constant k (units $k_BT\ a^{-1}\ \gamma^{-1}$) for the different strands at a deformation of $\gamma_{max} = 0.04$ ($\circ$) and $\gamma_{max} = 0.005$ ($\diamond$).

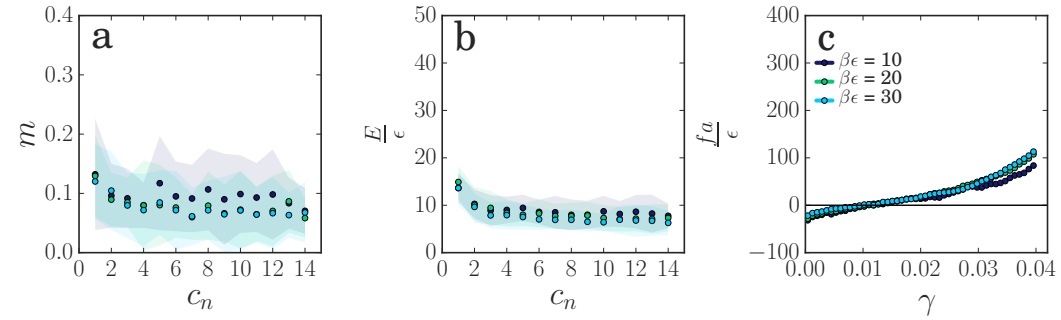

Figure A3.4 – $\gamma_{max} = 0.04$, gel strand B_2 (a) Average mobility of particles in successive oscillation cycles. (b) Dissipated energy per oscillation c_n , obtained by integration of the force-strain curves. The shaded area indicates the standard deviation. (c) Average elastic force of the $3^{th}, 4^{th}$ and 5^{th} oscillation cycle. Plot (b) and (c) are scaled by $\beta\epsilon$.

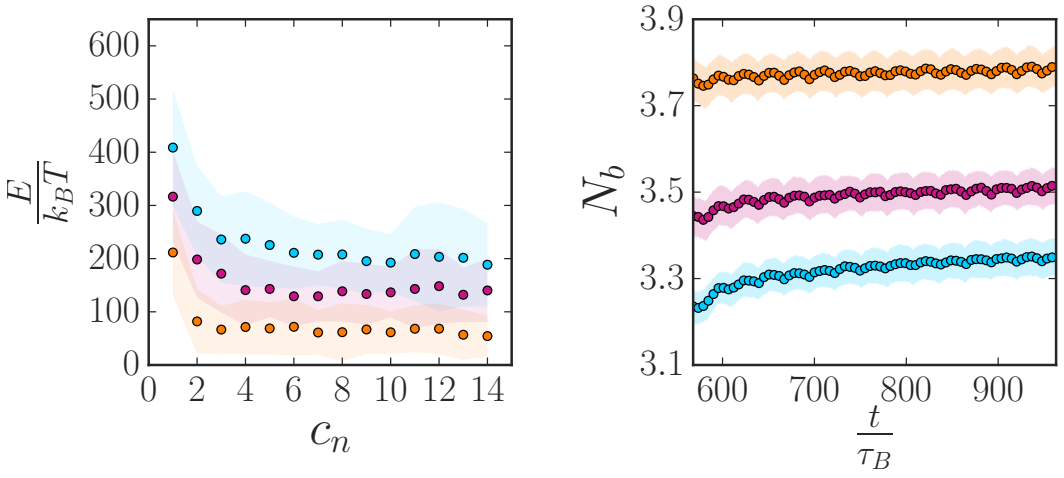

Figure A3.5 – $\gamma_{max} = 0.04$, gel strand B_2 (left) Dissipated energy per oscillation c_n, obtained by integration of the force-strain curves. The shaded area indicates the standard deviation. (right) Average number of bonds per particle in time. To compare the number of bonds of these strands we take the cut-off at the same position, 1.16 respectively.

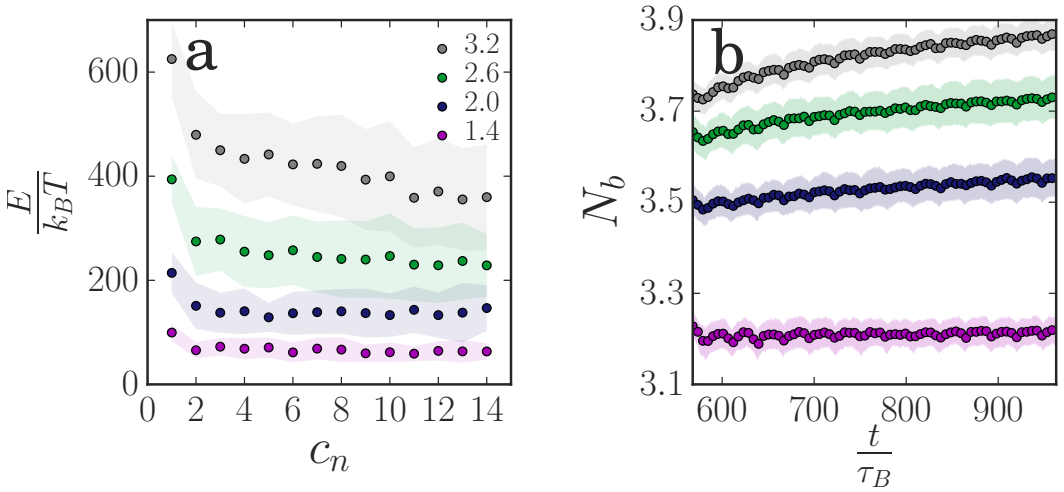

Figure A3.6 – strands $A_2 - C_2$ (a) Dissipated energy per oscillation cycle c_n (b) Average number of bonds per particle in time. In gray additional simulations -of even thicker strands- with a strand configuration of H = W = 6. The total number of particles in these strands is equal to $N = 864$.

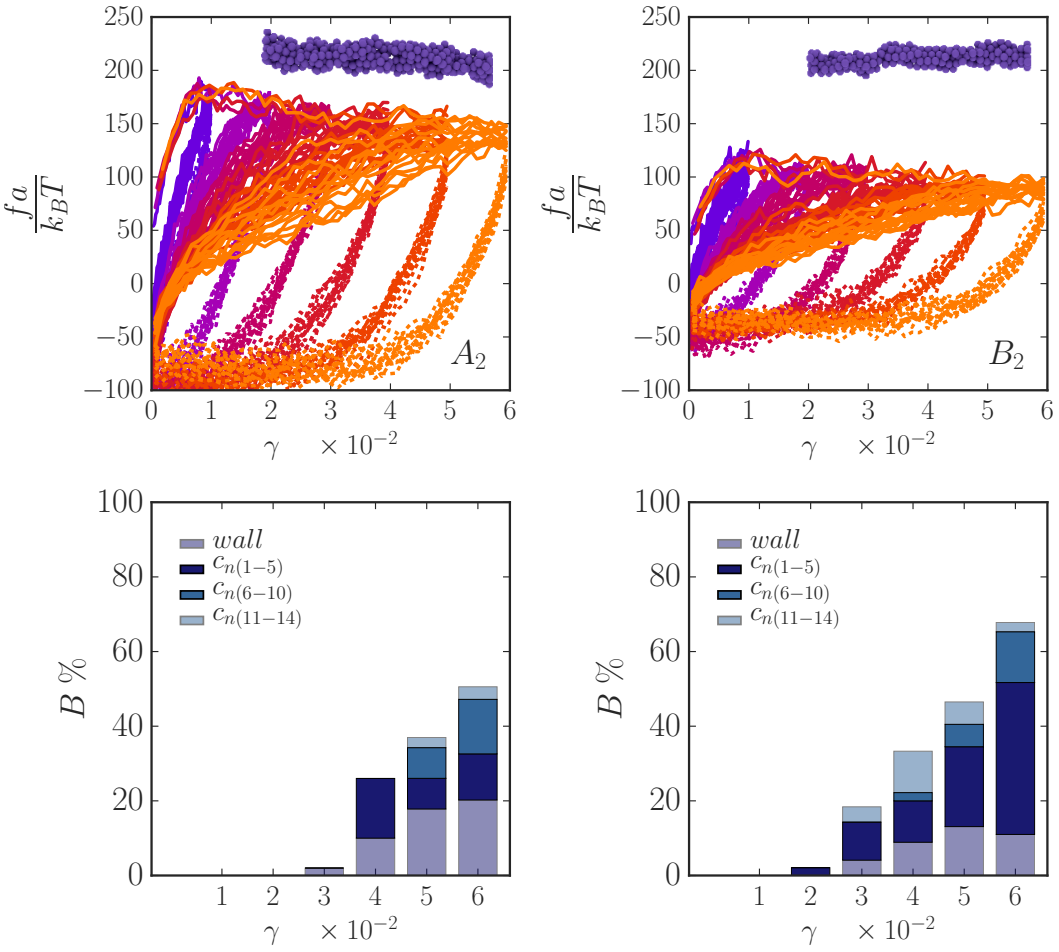

Figure A3.7 – (Top) Force-strain curves of 14 oscillatory expansions at a strain amplitude from $\gamma = 0.01$ (purple) till $\gamma = 0.06$ (orange) for strands with different aspect ratios (A_2 and B_2). (Bottom) Breakage statistics for oscillatory expansions at different strain amplitudes for strands A_2 and B_2

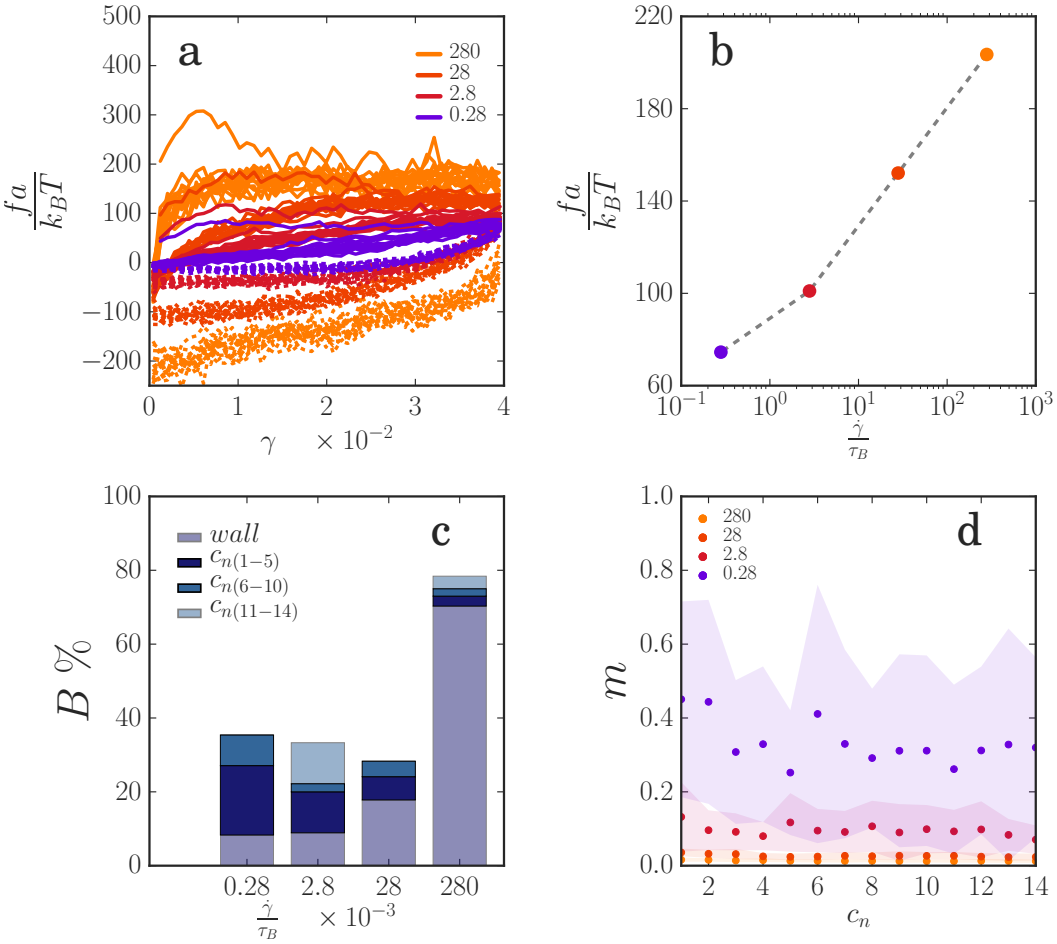

Figure A3.8 – (a) Force strain-curves upon 14 oscillatory expansions at different strain rates (b) The average plateau force of the first extension (between $\gamma = 0.01$ and 0.04) plotted versus strain rate. According to the force-activated Kramers model we expect the threshold force to scale logarithmic with the shear rate [37]. (c) Breakage statistics at different strain rates. (d) The mobility of particles in the strand as a function of the strain rate.

Simplifying structure: elucidating the network topology of colloidal gels

4

The mechanics of soft solids is determined by the network topology of the underlying rigid network. Yet, quantifying this heterogeneous structure is challenging. In this Chapter, we describe an algorithm that reduces a colloidal gel to a network consisting of nodes and strands, which allows us to map the complete topology of the gel – both in experiments and simulations. Colloidal gels are quantified based on the number and coordination of nodes and the number, length and thickness of the segments. This allows us to map the gel topology of gels with different morphologies. Remarkable topological resemblance is shown for experimental and simulated gels. The developed topological mapping algorithm opens up a wide range of possibilities to study colloidal network physics in more detail.

Joanne E. Verweij, Thomas E. Kodger, Frans A. M. Leermakers, Joris Sprakel & Jasper van der Gucht[1]

"Simplifying structure: elucidating the network topology of colloidal gels"
To be submitted (2020)

[1]*Physical Chemistry and Soft Matter, Wageningen University, Wageningen, 6708 WE, The Netherlands.*

Introduction

The linear and non-linear mechanics of soft materials depend on the structure of the underlying rigid network [1–3]. To optimize the softness, texture and stability of food products and tissue engineering scaffolds [4, 5] a more thorough understanding of the structure-function relationship of these materials is required. Here, the main challenge is to quantify the materials' complex, heterogeneous structure and to find the mechanical backbone of the network.

The prototype of heterogeneous elastic solids, with a complex network architecture, are colloidal gels. The non-equilibrium structure of these gels constitutes of aggregated particles which can form large percolating networks. Even at very low volume fraction ϕ, networks form due to short-ranged interactions between particles [6–8]. The obtained network topology varies based on the volume fraction and particle-particle attraction.

Experimentally, the structure of colloidal gels can be obtained from three-dimensional confocal microscopy images [6, 9–11]. Dinsmore et. al. quantitatively described the chains in the gel based on the number of bonds per particle, bond fractal dimension and number of flexible pivot points [1, 12]. Even though gels have been described based on properties of individual strands [1, 12–14], studies that take into account the full mechanical backbone of the network are still lacking.

In simulations, patchy models with particles having fixed sticky spots [15] and the DelGado-Kob model [16, 17] have allowed the investigation of the network topology of soft solids. Here, mainly dilute networks with 2- or 3-fold particle coordination have been investigated, based on the low-coordination number restrictions of these models. However, colloidal gels obtained in experiments or simulations often consist of a network with bulky strands [1, 18–24] and should be quantified as such. To this end, a method is needed to determine the mechanical backbone of the network.

For networks of biopolymers, it is well known that the coordination number of the network nodes plays a crucial role in the mechanical behaviour of the material [25, 26]. So far, a number of methods have been presented to study dense 3D biopolymer networks [27–29]. As these methods are based on filament recognition in microscopy images, they cannot be directly applied to particle gels. Attempts have been made to quantify the topology of colloidal gels directly from binarized microscopy images [30, 31]. However, this is not ideal when particle coordinates can be obtained from simulations and experiments. To obtain a full topological description of the

mechanical backbone of even the most complex colloidal gel architectures, we propose a method to determine the network topology of colloidal gels based on particle coordinates and their connectivity.

In this Chapter, we map the topology of colloidal gels with different morphologies, both in experiments and simulations. Colloidal gels are quantified based on the number and coordination of nodes, number of segments and segment lengths. In addition, overlaying the reduced network structure on top of the original data provides spatial information concerning the thickness of the individual segments. Notably, the topology of experimental and simulated gels show close resemblance. The topological mapping of colloidal gels opens up the possibility to study colloidal network physics in more detail. As an example we show the difference in particle dynamics between nodes and strands close to percolation.

Methods

Simulations - Colloidal Gels

The topology of colloidal gels is quantified from gel structures formed through Brownian Dynamics simulations (N = 32.000). The motion of a particle i with position $\boldsymbol{r}_i$ is obtained by solving the overdamped Langevin equation:

$$\dot{\boldsymbol{r}}_i(t) = \beta D_0[-\nabla_i U(t)] + \sqrt{2D_0}\boldsymbol{\xi}_i(t) \tag{4.1}$$

where $\boldsymbol{\xi}_i(t)$ is random white noise, sampled with zero mean and unit variance, to model the thermal fluctuations of the particles. $D_0 = k_B T/\zeta_f$ is the short-time diffusion coefficient with the friction coefficient ζ_f, set to unity. The time step δt for the numerical integration is set to $\delta t = 1 \times 10^{-6}\ \tau_B$. The unit of time is expressed in terms of the short-time self-diffusion $\tau_B = a^2/D_0$ with a the particle diameter.

Particle interactions are parametrized using the Morse potential [32]:

$$\beta u(r) = \beta\epsilon\ \exp(\rho_0[a-r])\ (\exp[\rho_0(a-r)] - 2) \tag{4.2}$$

with $\beta = 1/k_B T$ and energy scale $\beta\epsilon$. Parameter ρ_0 determines the width of the potential, which equals approximately $\Delta = 0.16\ a$ for $\rho_0 = 33$ [1].

The interaction strength between the particles is varied between $\beta\epsilon = 5$ and $\beta\epsilon = 40$, which is within the range of experimental attraction strengths for weak gels. The volume fraction ϕ is varied from $\phi = 0.05$ to $\phi = 0.25$. The equilibration time of the gel structures is set to $10\ \tau_B$. For every set of

[1] Here, Δ is determined by taking the end of the well at 1% of the original well-depth.

parameters, 10 independent simulations are performed to make sure that observations are statistically relevant.

To gain information about thermal fluctuations at nodes and strands, the mean square displacement of particles in the gel is determined at $t = 0.06\,\tau_B$. Particles within a cutoff of 1.4 a from the node position are considered to belong to a node.

Simulations - Test Data

Gels are highly complex and heterogeneous structures. To test the the topological mapping algorithm on a simple structure, a raster is constructed using Monte Carlo (MC) simulations in the canonical ensemble (NVT). In this raster particles are attracted to specific lines on a regular grid. In this way, a structure is obtained which can be easily quantified. The interaction between line l of this raster and particle i is described by a square-well potential:

$$u^{\text{sw}}(r_l) = \begin{cases} \epsilon & 0 \leq r_l \leq \Delta \\ 0 & r_l > \Delta \end{cases} \tag{4.3}$$

where r_l is the distance between the line and the center of the particle, ϵ denotes the interaction energy (set to $-40\,k_BT$) and Δ is the interaction range (set to 1.5 particle diameter a). A small hard-sphere square-well interaction is present between the spheres ($\epsilon = -2\,k_BT$, $\Delta = 1.1\,a$).

Simulations were performed for 1.69×10^5 simulation cycles, whereby each cycle contained 32.000 particle moves. During the first 1×10^4 MC cycles the values for the displacement are adjusted to obtain an acceptance rate of 50% for the proposed moves.

Experiments - Colloidal gels

Fluorescent core-shell particles are synthesized using the method reported in Ref. [33]. Cross-linked cores of 600 nm in diameter are obtained by a precipitation polymerization. The cross-linked core particles contain a fluorescent dye (DiI, Sigma-Aldrich) which is covalently attached to the polymer chains. Subsequently, a non-fluorescent shell is formed around the core particles using seed-dispersion polymerization. The total diameter of the particles equals $1.6\,\mu m$. Confocal images of these particles yield distinct fluorescent centers, even when particles are in direct contact.

The core-shell tFEMA-tBMA particles are washed in a solvent of 70:30 2,2 thiodiethanol:Milli-Q. Density matching of the particles is achieved by adding a small amount of 2,2 thiodiethanol to the solvent till particles do not sediment anymore (1h, 2000g). To induce depletion attraction 6.5 mg/mL polyethylene oxide (PEO, M_w 2.31×10^5, M_n 2.03×10^5, R_g = 23.1 nm)

is added to the samples. The overlap concentration c^* of this polymer equals approximately [34]:

$$c^* \approx \frac{M_w}{(4\pi/3)R_g^3 N_A} \approx 7.5 \text{ mg/mL} \tag{4.4}$$

with R_g the radius of gyration, M_w the molecular weight of the polymer and N_A Avogadro's constant. To screen electrostatic interactions, samples contain 10 mM of salt (NaCl). Samples are made with volume fractions between $\phi = 0.08$ and $\phi = 0.20$.

Sample chambers are constructed from glass slides and spacers, which are adhered and sealed using Norland Optical Adhesive 61 UV curable glue. First, two small pieces of Precision Brand plastic color coded shim (10 mm $\times$ 26 mm, thickness 0.318 mm) are attached to a microscopy slide (26 mm $\times$ 76 mm); leaving a space between them of approximately 1.0 cm. Next, a round cover slip (radius of 5 cm) is glued on top of the small pieces of plastic. Hereby, a hollow chamber is created with dimensions of approximately 10 $\times$ 26 $\times$ 0.318 mm. The sample chamber is loaded using capillary forces and both ends are sealed with Norland Optical Adhesive 61, without exposing the particles to UV light. Samples are measured after 12 hours of equilibration.

3D Z-stacks (50 $\times$ 50 $\times$ 50 μm) of the gel structure are obtained using an inverted Nikon $C2$ confocal with a Nikon APO 60$\times$ oil objective (NA = 1.4). For each sample 15 Z-stacks are made to get statistics throughout the sample. Locating the particle positions in each of these Z-stacks is done using the python based particle-tracking package Trackpy [35].

Results and discussion

Reduction Algorithm

To determine the network topology of a colloidal gel, a reduction algorithm is applied to all particles located in the gel (Fig. 4.1). Gels consist of many interconnected branches which are often multiple particles wide. First, the coordination number of each particle in the gel is determined. The outside of the strands contain particles with the lowest coordination number whereas particles inside the strands have more bonds. To make sure that the strands of the gel are reduced from the outside to the inside, particles with the lowest coordination number are checked first. When a particle of a specific coordination is randomly selected, all its neighbours -up to 5 generations- are identified. Subsequently, a check is performed to see whether deleting the

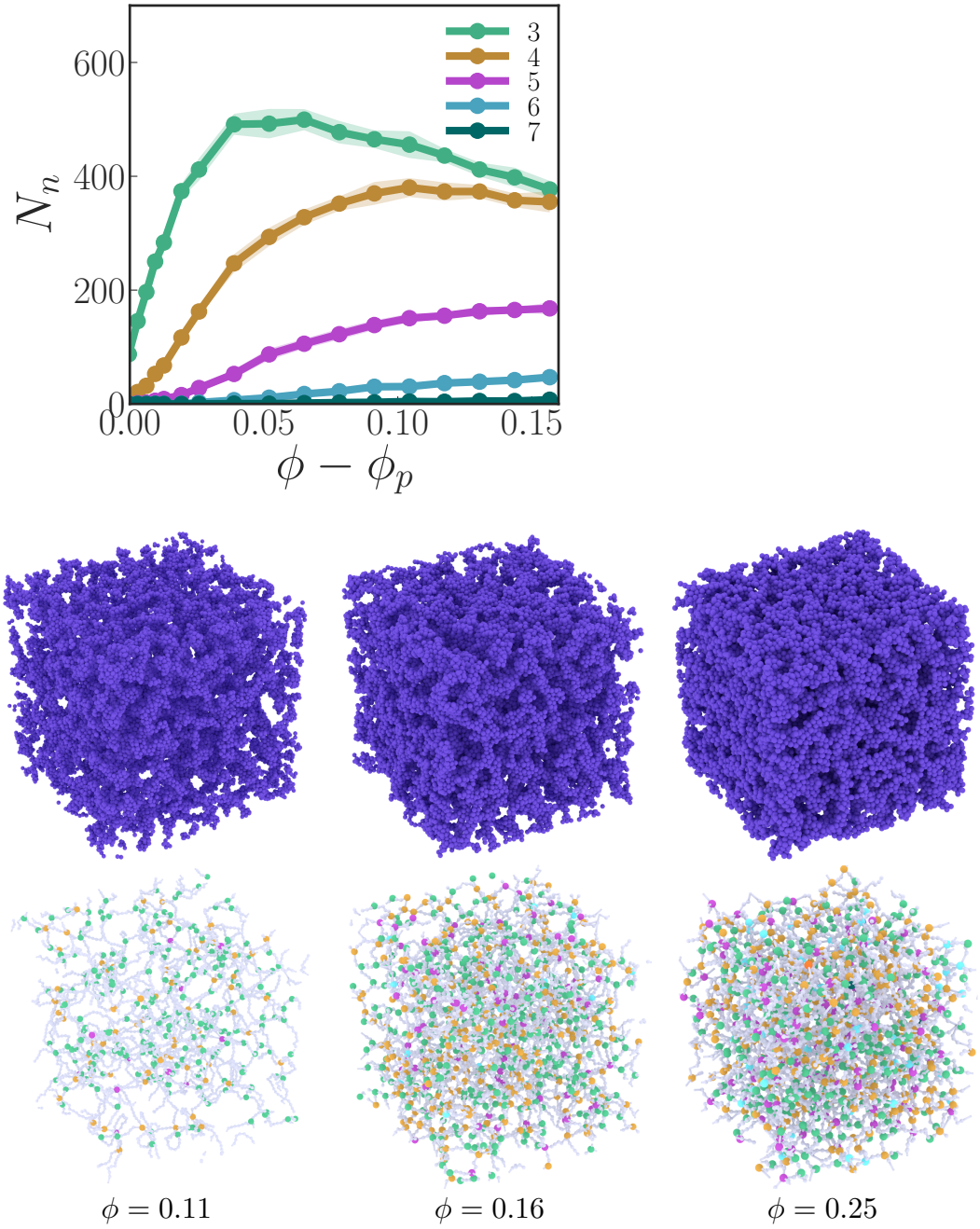

Figure 4.1 – (Top) The number of nodes N_n for each coordination number n upon increasing volume fraction ϕ. Averaging the number of nodes for all coordination numbers results in the average coordination number $\langle n \rangle$ of the gel. (Bottom) Visual representation of simulated colloidal gels at different volume fractions before and after reduction ($\beta\epsilon = 10$, $\phi_p = 0.092$, $C = 1.16$, $\Delta R = 2.0$).

selected particle breaks the identified neighbours into two clusters. When this is not the case, a particle is not essential for the basic network structure and will be deleted.

At points where a gel strand branches off, the network structure contains a node. In principle this node has a coordination number which is higher than 2. Yet, nodes can connect up to 12 different branches. The reduced network can be simplified further at the node positions, i.e. some particles around the nodes balance each other forming quadruplets or triplets [2]. The final reduced network contains 2-coordinated particles for the branches and higher coordinated particles at the nodes.

The reduction algorithm is tested on artificially produced test data. Here, a gel network is formed on a specified raster lattice. In this way, it is exactly known what the reduced network should look like. Using this test data (see Fig. A4.1 & Fig. A4.2) the effects of a number of parameters in the reduction algorithm are illustrated.

Based on cut-off C, it is determined whether particles are nearest neighbours or not. In simulations, this cut-off is simply the set interaction range between particles. For experiments, however, the interaction potential is often not known. Taking the location of the first minimum in the radial distribution function is a good estimate for this cut-off [36]. The parameter ΔR sets the distance over which two nodes are considered to be too close together. A value of ΔR = 2.0, would mean that two nodes that are closer than 2 particle diameters from each other will be considered as one node.

Reduction of the network takes place from low to high coordination number. Yet, between particles of the same coordination number, reduction takes place at random. Therefore, the length of the branches (Fig. A4.4a) is a good estimate but not necessarily the shortest distance between nodes. Reducing the same raster data, multiple times, shows a maximum overestimation of the segment length of 15%.

Dangling ends in a gel structure do not contribute to the mechanical stability of the network. Therefore, all dangling ends are removed. When a part of the gel is missing (see Fig. A4.3) this will effect the final reduced structure. Even though a branch is interrupted at a range of only a few particles, this entire segment will be removed.

To determine whether a particle is essential for the network structure a cluster analysis of the selected neighbours is performed. The neighbours of each particle are identified up to G_n = 5 generations. A gel composed of interconnected chains will contain loops [1]. The parameter G_n determines the size of the loops that stay part of the final structure. Upon considering fewer neighbours, smaller loops will remain.

After applying the reduction algorithm to a heterogeneous network a reduced network structure results. Besides gaining information about the

[2] See Appendix for further details about the simplification step at the nodes

number and coordination of the nodes, number of segments and segment lengths, the reduced network structure can now also be placed on top of the original network to determine the thickness of the different branches. At distance ΔR away from the node, a cylinder is positioned. The orientation of this cylinder is determined by the direction vector between the 2-coordinated particles. In this way, the branches of the network are covered with a tube-like structure of cylinders. The original particles inside these branches are assigned to this tube. The thickness distribution of all the branches (Fig. A4.4b) indicates the heterogeneity and the approximate thickness of the branches in the network structure. Note that the thickness T of the branches is determined in terms of the average number of particles in the branch per unit length of the strand.

At higher volume fractions, the mesh size of the network becomes smaller. Hence, the cylinder that covers the original configuration could overlap two different branches. To prevent this, the neighbours of particles belonging to the considered branch are determined. Particles in the cylinder that do not belong to this specific cluster are removed. Moreover, particles are not assigned to any branch in a range of ΔR around the nodes.

The size of the cylinder is set by r_c. Above a certain threshold the branch becomes independent of the set radius, as we correct for the radius overlapping multiple branches and 'mask' out particles around the nodes (Fig. A4.5).

Structure of colloidal gels - simulations

To see how the structure of colloidal gels change, both the interaction strength $\beta\epsilon$ between the particles as well as the volume fraction ϕ are varied. For this range of parameters the percolation of the gel structures is determined. In the gels each cluster of 50 particles or more is analyzed. If one of these clusters -upon replicating the box- touches with at least one neighbouring box the gel is considered to have a percolating structure. Upon touching with 9 or more replicating boxes, the network is reckoned to be percolating in 3D [37]. Upon increasing the volume fraction, the first point at which a percolating structure is found is marked as the percolation point ϕ_p. At low attraction between particles the percolation point shifts to higher volume fractions. In this case a higher number density is required to obtain a percolating structure.

Colloidal gels at low volume fraction contain long segments with few connection points. Upon increasing the volume fraction, segments become shorter and the network's connectivity increases (see the visual representation in Figure 4.1). The graph in Fig. 4.1 indicates how many nodes N_n a network contains of each specific coordination number n. Initially, the number of nodes of each coordination increases with increasing ϕ. Yet, after increasing the volume fraction, low coordinated nodes will start decreasing

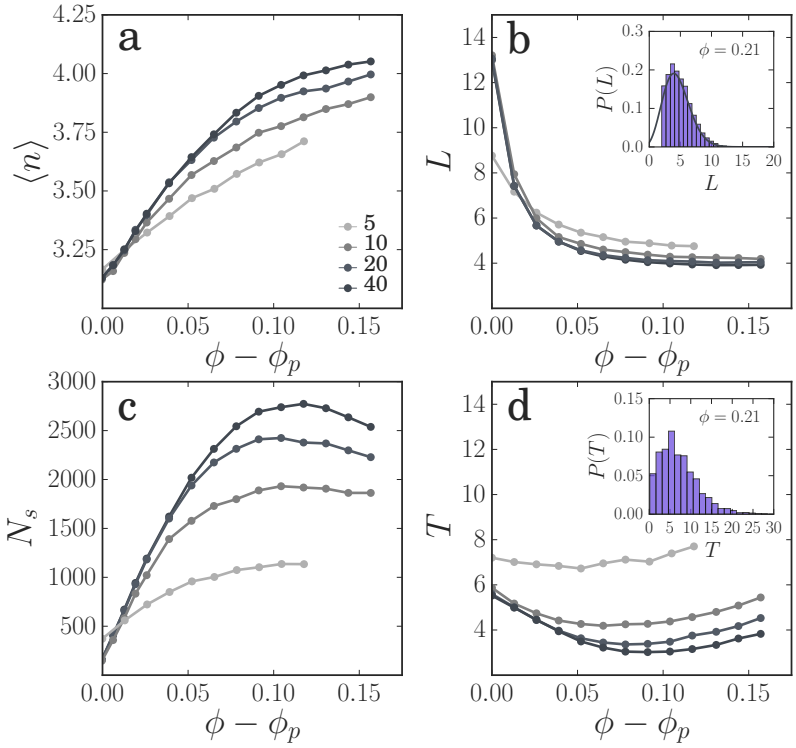

Figure 4.2 – (a) Average coordination number $\langle n \rangle$ at different interaction strengths $\beta\epsilon$. (b) Average segment length. The inset shows an example of a length distribution from which the average segment length is calculated ($\beta\epsilon = 5$, $\phi = 0.21$). The solid line indicates the fitted Poisson distribution. With the Poisson probability defined as $P(x;\mu) = (e^{-\mu})(\mu^x)/x!$. Here, x is the observed segment length and μ is the mean segment length (with a value of 4.75). The missing part at the left side of the distribution is due to the parameter ΔR (c) The number of segments in the network (d) The average thickness of the segments. The inset shows an example of a thickness distribution from which the average thickness is calculated ($\beta\epsilon = 5$, $\phi = 0.21$). Parameters algorithm: ($C = 1.16$, $\Delta R = 2.0$, $r_c = 7.0$).

again at the expense of higher coordinated nodes. Averaging the coordination number of all the different nodes gives the average coordination number $\langle n \rangle$ for networks at different volume fractions.

To see whether the obtained results are independent of the system size, simulation results of two different system sizes are compared (see Fig. A4.6). The same results are found for a system with N = 32.000 and N = 128.000 particles. This indicates that the smallest system size is sufficient to study the network topology of colloidal gels.

The different properties of colloidal gels are analysed as a function of volume fraction ϕ and interaction strength $\beta\epsilon$ (see Figure 4.2). Upon increasing the attraction between the particles the average coordination number

$\langle n \rangle$ is shown to increase as well. A comparison between histograms of the node's coordination numbers (Fig. A4.8) clearly indicates the increase in the number of nodes when particles become more attractive. Moreover, increasing the volume fraction favours the formation of higher coordinated nodes in the network structure.

Just above percolation, segment lengths are long. Yet, increasing the volume fraction results in the formation of more and more segments. Consequently, the segment length drops drastically until a plateau value is reached (Fig. 4.2b). The length of the segments in the network follow a Poisson distribution (see inset 4.2b). Both the segment length and the number of segments influence the thickness T of the branches. We observe that the branches decrease slightly in thickness, due to the large increase of the number of segments in the network. Yet, once the segment length reaches a plateau value (Fig. 4.2d) the thickness of the gel strands starts to increase again.

For gels at small attraction we find networks with fewer segments N_s (Fig. 4.2c). In all cases, increasing the volume fraction results in a higher network connectivity. Nonetheless, the network connectivity at small interaction strengths stays much lower due to the formation of thicker strands. The quantified thickness for gels at different interactions show a drastic increase when particles are less sticky. The visualization of gel morphologies at different bond strengths by Johnson et.al. confirms this [38]. Like observed in dilute network models [39], the formation of networks with higher connectivity results in a drop in the length of connecting segments. Yet, quantification of the length and thickness of strands in a colloidal gel indicates that dilute network models can only explain the network structure in the limit of very large interaction energies. In these dilute network models, plastic deformation which precedes strand failure cannot be taken into account [13, 14].

Structure of colloidal gels - experiments

Now that we successfully quantified the network topology of simulated gels, we apply the topological mapping to experimental gels. From confocal microscopy data the structure of experimental colloidal gels with a volume fraction between $\phi = 0.08$ and $\phi = 0.2$ is obtained (see Fig. 4.3). To study the network topology of these gels the same reduction algorithm is applied as used for the simulation data [3]. The cut-off C for the reduction algorithm is based on the minimum of the first peak in the radial distribution function

[3]For the experimental data a minor change is made in the reduction algorithm by removing periodic boundary conditions. To obtain the right network connectivity particles at the boundaries of the Z-stack are not allowed to be removed. To make sure that the obtained segment length distribution is correct, segments from a node towards a position touching a boundary in the Z-stack are not included.

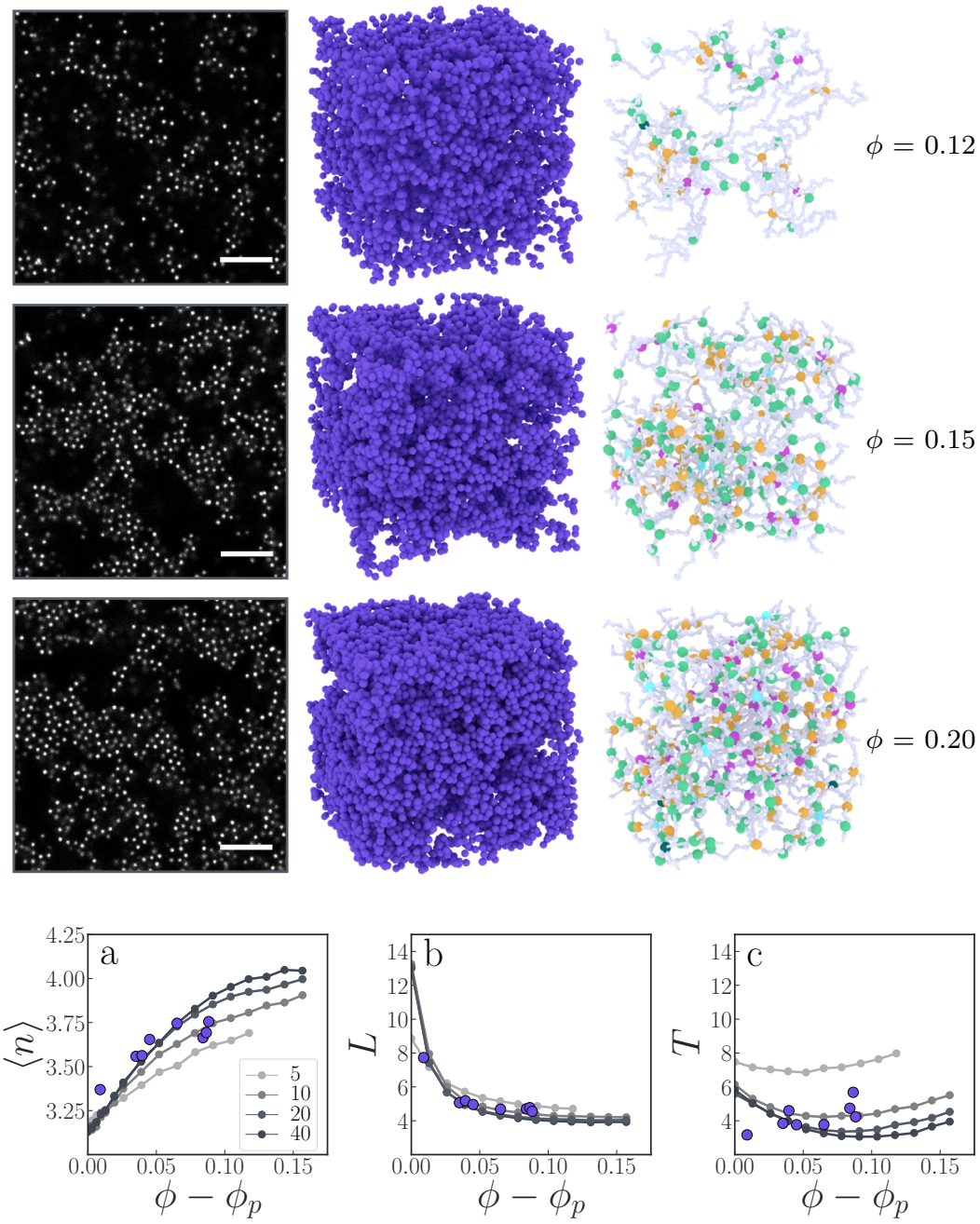

Figure 4.3 – (Top) Experimental images of colloidal gels at different volume fractions ϕ. The scale bar equals 10 μm. The renderings show the 3D experimental data before and after reduction. (Bottom) Data points of (a) the average coordination number (b) length and (c) thickness of experimental colloidal gels. The percolation threshold equals $\phi_p = 0.11$ for the experimental data.

(Fig. A4.7), other parameters are matched with the values used for the simulation data.

Experimental images show a visual increase in the amount of branches and the number of connection points upon increasing the number density of the samples (Fig. 4.3). The networks in the experiment start to percolate around a volume fraction of $\phi_p = 0.11$. This is slightly higher than in simulations where percolation for networks at attraction strengths of $\beta\epsilon = 10,\ 20,\ 40$ start at a volume fraction of $\phi_p = 0.093$.

The topological match between experimental and simulated networks is remarkable. Quantification of the coordination number and length of the segments in the colloidal gel (see graph Fig. 4.3), shows values very close to results obtained from simulations. The thickness distribution of the experimental samples shows an increasing trend which does not precisely overlay the thickness distributions obtained from simulations, yet is in very close proximity. Simulations already showed that segment length and coordination number of particle gels mainly depend on the volume fraction of the gel and are less affected by the interaction energy between particles. Experimentally, the attraction between particles depends heavily on the added depletant, but the precise interaction energy is difficult to estimate. However, the volume fraction of experimental gels can easily be controlled. Surprisingly, controlling the volume fraction is enough to match the topological mapping of experimental gels with those of simulated gels.

Thermal fluctuations

By overlaying the network structure on top of the simulated colloidal gels we obtain spatial information about particles in the network. Thermal fluctuations of particles can now be attributed to particles positioned in strands or nodes [4] (see Fig. 4.4). The mean square displacement of each particle is determined by calculating the moved distance between time t and $t + \Delta$, normalized by the particle diameter a:

$$d_0 = \frac{1}{Na^2} \sum_i |\boldsymbol{r}_i(t) - \boldsymbol{r}_i(t + \Delta)|^2 \tag{4.5}$$

with N the total number of particles and $\boldsymbol{r}_i(t)$ the time-dependent position vector of particle i. The highest thermal fluctuations are observed in colloidal gels with the lowest interaction energy. Here, single particle bonds –scaling with U/k_BT– are relatively weak, which allows particles to fluctuate more.

Particles around the nodes are observed to have smaller fluctuations, i.e. nodes are more rigid than strands (Fig. 4.4a). The difference in thermal fluctuations between nodes and strands is most pronounced at low volume fractions. Close to the percolation point the thermal fluctuations in the

[4] Here, all particles within a cutoff of 1.4 around the nodes are considered

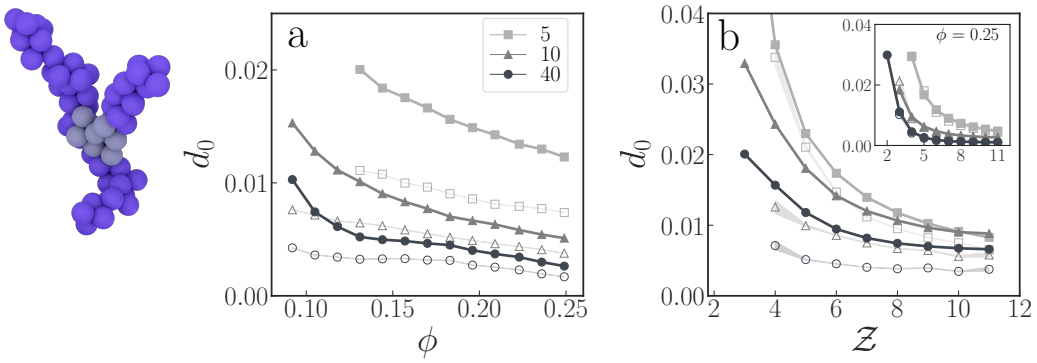

Figure 4.4 – (a) The average mean square displacement of particles in a colloidal gel as a function of volume fraction and interaction energy (5,10 and 40 k_BT) at t = 0.06 τ_B. A distinction between particles in the strands (closed markers) and particles around the nodes (open markers) is made, as shown in the rendering on the left. The rendering shows a single junction from a simulated gel ($\beta\epsilon = 10$, $\phi = 0.092$), with the node particles indicated in gray and particles in the strands indicated in purple. (b) Thermal fluctuations of the particles in the gel as a function of the number of neighbours $\mathcal{Z}$ per particle. Again, a distinction is made between particles in the strands and particles around the nodes. For each interaction energy the lowest volume fraction is plotted, which is respectively $\phi = 0.131$ for 5 k_BT and $\phi = 0.092$ for 10 and 40 k_BT. The inset shows the thermal fluctuations for a volume fraction of $\phi = 0.25$.

strands increase rapidly, which indicates that the network starts to loose its rigidity.

Previous experimental work shows that the mean square displacement of particles in colloidal gels strongly depends on the average coordination number $\mathcal{Z}$ per particle [24]. So, one might wonder whether the difference in thermal fluctuations between the nodes and strands cannot just be attributed to the difference in neighbours between particles in the strands and particles in the nodes, as one might assume that the average number of neighbours for particles in the nodes is higher. To check this, thermal fluctuations are plotted as a function of the number of neighbours per particle $\mathcal{Z}$ (see Fig. 4.4b). For colloidal gels at low volume fraction, clearly, particles around the nodes move less compared to their equally coordinated counterparts in the strands. However, at the highest volume fraction (see inset Fig. 4.4b) the difference between particles in the strands and particles in the nodes vanishes upon splitting thermal fluctuations based on the number of neighbours.

The weakest colloidal gels show a large difference in dynamics between nodes and strands (Fig. 4.4a). We can construct the following picture for thermal fluctuations in colloidal gels. At low volume fractions nodes are observed to be rigid, even when the number of neighbours per particle is taken into account. The movement of nodes is constrained by attached strands. This results in a low degree of freedom. Strands, on the other hand, have a higher degree of freedom and consequently fluctuate more.

Conclusions

In this Chapter, we demonstrate topological mapping of colloidal gels with different morphologies. The network topology of colloidal gels is obtained by a reduction method based on particle coordinates and their connectivity. The topology of the gel changes most significantly by increasing the volume fraction; segments in the network become shorter and the coordination and number of nodes increase. A strong link is observed between the number of segments, length of these segments and their corresponding thickness. The thickness of the gel strands decreases when the connectivity of the network increases. However, once the segment length stabilizes to a constant value, the thickness of the strands starts to increase again.

The network topology of experimental colloidal gels show surprisingly similar values for the coordination number of the nodes and the segment length distribution compared to simulation data. This indicates that these parameters follow a general trend in colloidal gels. To see whether results can be generalized further, future research could focus on colloidal gels with other kinds of inter-particle interactions. In soft matter physics, we find many more network structures. It would be highly interesting to apply a similar algorithm to glasses, to determine stress networks. Here, the nearest neighbour criterion should be replaced by a dynamic nearest neighbour criterion.

Information about the network topology is combined with single particle positions to study particle dynamics in nodes and strands. Close to percolation, thermal fluctuations of particles around the nodes are smaller compared to particles located in strands. This can be explained by nodes acting as rigid bodies, whereas strands are able to fluctuate more. Towards higher volume fractions the difference in particle dynamics between nodes and strands vanishes. We attribute this to the network becoming more highly connected and consequently strands becoming shorter.

Upon mechanically deforming a soft material the structure of the gel will start to yield. How the network topology of a colloidal gel changes in this solid-to-liquid transition is a very interesting, yet unanswered question. Besides, the demonstrated method can be used to study the network topology of colloidal gels while subjected to other types of external fields, such as gravity.

Acknowledgements

I would like to thank Thomas Kodger for the synthesis of the tFEMA-tBMA particles used in this Chapter. I would also like to thank Justin Tauber for useful discussions.

Bibliography

[1] AD Dinsmore, V Prasad, IY Wong, and DA Weitz. Microscopic structure and elasticity of weakly aggregated colloidal gels. *Physical Review Letters*, 96(18):185502, 2006.

[2] Myung Han Lee and Eric M. Furst. Response of a colloidal gel to a microscopic oscillatory strain. *Physical Review E*, 77:041408, Apr 2008.

[3] Gavin A. Buxton and Nigel Clarke. "bending to stretching" transition in disordered networks. *Physical Review Letters*, 98:238103, Jun 2007.

[4] Qun Wang, Limin Wang, Michael S Detamore, and Cory Berkland. Biodegradable colloidal gels as moldable tissue engineering scaffolds. *Advanced Materials*, 20(2):236–239, 2008.

[5] Denis Renard, Fred van de Velde, and Ronald W Visschers. The gap between food gel structure, texture and perception. *Food Hydrocolloids*, 20(4):423–431, 2006.

[6] Peter J Lu, Emanuela Zaccarelli, Fabio Ciulla, Andrew B Schofield, Francesco Sciortino, and David A Weitz. Gelation of particles with short-range attraction. *Nature*, 453(7194):499, 2008.

[7] V. Trappe, V. Prasad, Luca Cipelletti, P. N. Segre, and D. A. Weitz. Jamming phase diagram for attractive particles. *Nature*, 411(6839):772–775, 2001.

[8] S. Manley, L. Cipelletti, V. Trappe, A. E. Bailey, R. J. Christianson, U. Gasser, V. Prasad, P. N. Segre, M. P. Doherty, S. Sankaran, A. L. Jankovsky, B. Shiley, J. Bowen, J. Eggers, C. Kurta, T. Lorik, and D. A. Weitz. Limits to gelation in colloidal aggregation. *Physical Review Letters*, 93:108302, Sep 2004.

[9] Anthony D Dinsmore, Eric R Weeks, Vikram Prasad, Andrew C Levitt, and David A Weitz. Three-dimensional confocal microscopy of colloids. *Applied Optics*, 40(24):4152–4159, 2001.

[10] Vikram Prasad, Denis Semwogerere, and Eric R Weeks. Confocal microscopy of colloids. *Journal of Physics: Condensed Matter*, 19(11):113102, 2007.

[11] Emanuela Zaccarelli. Colloidal gels: equilibrium and non-equilibrium routes. *Journal of Physics: Condensed Matter*, 19(32):323101, 2007.

[12] A D Dinsmore and D A Weitz. Direct imaging of three-dimensional structure and topology of colloidal gels. *Journal of Physics: Condensed Matter*, 14(33):7581, 2002.

[13] Jan Maarten van Doorn, Joanne E Verweij, Joris Sprakel, and Jasper van der Gucht. Strand plasticity governs fatigue in colloidal gels. *Physical Review Letters*, 120(20):208005, 2018.

[14] Joanne E Verweij, Frans AM Leermakers, Joris Sprakel, and Jasper Van Der Gucht. Plasticity in colloidal gel strands. *Soft Matter*, 15(32):6447–6454, 2019.

[15] Emanuela Bianchi, Julio Largo, Piero Tartaglia, Emanuela Zaccarelli, and Francesco Sciortino. Phase diagram of patchy colloids: towards empty liquids. *Physical Review Letters*, 97(16):168301, 2006.

[16] Emanuela Del Gado and Walter Kob. Structure and relaxation dynamics of a colloidal gel. *EPL (Europhysics Letters)*, 72(6):1032, 2005.

[17] Emanuela Del Gado and Walter Kob. Length-scale-dependent relaxation in colloidal gels. *Physical Review Letters*, 98(2):028303, 2007.

[18] Clare J Dibble, Michael Kogan, and Michael J Solomon. Structure and dynamics of col-

loidal depletion gels: Coincidence of transitions and heterogeneity. *Physical Review E*, 74(4):041403, 2006.

[19] Nick Koumakis, Esmaeel Moghimi, Rut Besseling, Wilson C. K. Poon, John F. Brady, and George Petekidis. Tuning colloidal gels by shear. *Soft Matter*, 11:4640–4648, 2015.

[20] Peter J Lu, Jacinta C Conrad, Hans M Wyss, Andrew B Schofield, and David A Weitz. Fluids of clusters in attractive colloids. *Physical Review Letters*, 96(2):028306, 2006.

[21] Emanuela Zaccarelli, Peter J Lu, Fabio Ciulla, David A Weitz, and Francesco Sciortino. Gelation as arrested phase separation in short-ranged attractive colloid–polymer mixtures. *Journal of Physics: Condensed Matter*, 20(49):494242, 2008.

[22] Stefan B. Lindström, Thomas E. Kodger, Joris Sprakel, and David A. Weitz. Structures, stresses, and fluctuations in the delayed failure of colloidal gels. *Soft Matter*, 8:3657–3664, 2012.

[23] Roseanna N. Zia, Benjamin J. Landrum, and William B. Russel. A micro-mechanical study of coarsening and rheology of colloidal gels: Cage building, cage hopping, and smoluchowski's ratchet. *Journal of Rheology*, 58(5):1121–1157, 2014.

[24] Jan Maarten Van Doorn, Jochem Bronkhorst, Ruben Higler, Ties Van De Laar, and Joris Sprakel. Linking particle dynamics to local connectivity in colloidal gels. *Physical Review Letters*, 118(18):188001, 2017.

[25] Stefan B Lindström, David A Vader, Artem Kulachenko, and David A Weitz. Biopolymer network geometries: characterization, regeneration, and elastic properties. *Physical Review E*, 82(5):051905, 2010.

[26] M Wyart, H Liang, A Kabla, and L Mahadevan. Elasticity of floppy and stiff random networks. *Physical Review Letters*, 101(21):215501, 2008.

[27] Ting Xu, Dimitrios Vavylonis, Feng-Ching Tsai, Gijsje H Koenderink, Wei Nie, Eddy Yusuf, I-Ju Lee, Jian-Qiu Wu, and Xiaolei Huang. Soax: A software for quantification of 3d biopolymer networks. *Scientific Reports*, 5:9081, 2015.

[28] Andrew M Stein, David A Vader, Louise M Jawerth, David A Weitz, and Leonard M Sander. An algorithm for extracting the network geometry of three-dimensional collagen gels. *Journal of Microscopy*, 232(3):463–475, 2008.

[29] Louise M Jawerth, Stefan Münster, David A Vader, Ben Fabry, and David A Weitz. A blind spot in confocal reflection microscopy: the dependence of fiber brightness on fiber orientation in imaging biopolymer networks. *Biophysical Journal*, 98(3):L1–L3, 2010.

[30] Jasper N Immink, JJ Erik Maris, Peter Schurtenberger, and Joakim Stenhammar. Using patchy particles to prevent local rearrangements in models of non-equilibrium colloidal gels. *Langmuir*, 2019.

[31] Mani Diba, Huanan Wang, Thomas E Kodger, Shima Parsa, and Sander CG Leeuwenburgh. Highly elastic and self-healing composite colloidal gels. *Advanced Materials*, 29(11):1604672, 2017.

[32] C. Patrick Royall, Jens Eggers, Akira Furukawa, and Hajime Tanaka. Probing colloidal gels at multiple length scales: The role of hydrodynamics. *Physical Review Letters*, 114:258302, Jun 2015.

[33] Thomas E Kodger, Rodrigo E Guerra, and Joris Sprakel. Precise colloids with tunable interactions for confocal microscopy. *Scientific Reports*, 5:14635, 2015.

[34] Qicong Ying and Benjamin Chu. Overlap concentration of macromolecules in solution. *Macromolecules*, 20(2):362–366, 1987.

[35] Daniel B Allan, Thomas Caswell, Nathan C Keim, and Casper M van der Wel. Trackpy v0.4.1. *https://doi.org/10.5281/zenodo.1226458*, 2018.

[36] Emanuela Del Gado and Walter Kob. A microscopic model for colloidal gels with directional effective interactions: network induced glassy dynamics. *Soft Matter*, 6(7):1547–1558, 2010.

[37] Francesco Varrato, Lorenzo Di Michele, Maxim Belushkin, Nicolas Dorsaz, Simon H. Nathan, Erika Eiser, and Giuseppe Foffi. Arrested demixing opens route to bigels. *Proceedings of the National Academy of Sciences*, 109(47):19155–19160, 2012.

[38] Lilian C Johnson, Roseanna N Zia, Esmaeel Moghimi, and George Petekidis. Influence of structure on the linear response rheology of colloidal gels. *Journal of Rheology*, 63(4):583–

608, 2019.
[39] Jader Colombo and Emanuela Del Gado. Self-assembly and cooperative dynamics of a model colloidal gel network. *Soft Matter*, 10(22):4003–4015, 2014.

Appendix

To obtain the network topology of colloidal gels a reduction algorithm is described in the main text. The described algorithm is illustrated here on clearly structured test data. This test data is presented in Fig. A4.1 and a larger field of view is presented in Fig. A4.2. Especially, more information is provided about the last step (from Fig. A4.1c to Fig. A4.1d), where the connection points of the branches (the so-called nodes) are reduced further.

Simplification of nodes

Step 1: In first instance, simplification at the nodes takes place based on the coordination number of each particle (determined by cut-off C). Particles in the reduced structure (see Fig. A4.2c) with a coordination number higher than 2 are considered, when they are not yet exclusively surrounded by 2-coordinated particles. Contrary to the previous reduction step, in which reduction takes place from low to high connectivity, now first particles with the highest coordination number are considered. For the specific particle its direct neighbours are checked and these and the particle itself, are replaced with a single particle. In this way, particles that balance each other are removed. This step is illustrated in Fig. A4.2c to A4.2c1.
Step 2: Due to the random reduction of the network structure it is possible that a node is split in two. In this case, two nodes are present very close to each other. To make sure that the right coordination number Z is obtained for the network node, further simplification takes place over range ΔR defined in terms of particle diameter a. In this way, nodes next to each other (Fig. A4.2c1), or even a bit further away (Fig. A4.2c2) can be combined. In this second step of the simplification at the nodes 3-coordinated nodes are checked and if close enough together combined with other 3-, 4-, 5- and 6- coordinated nodes. Next, 4-coordinated nodes are combined with 4-, 5-, 6- and 7-coordinated nodes and so forth, until all options have been checked.

Dangling ends

To illustrate what happens to dangling ends in the structure, a slab of particles is removed from the test data (respectively between $x = -1.4$

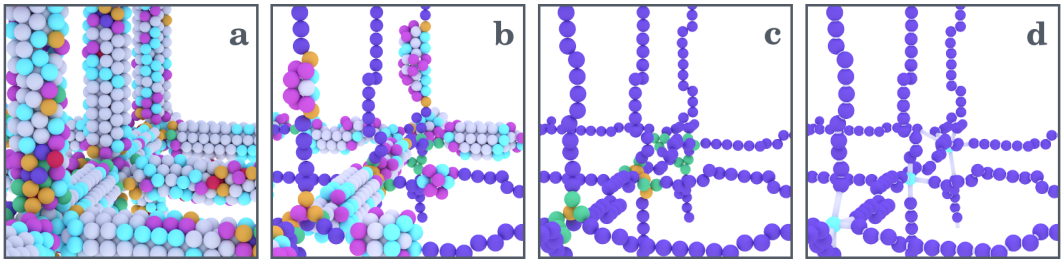

Figure A4.1 – Test data on a specified raster lattice. a) Complete network. Color coding indicates the coordination number of the different particles. 1 (red), 2 (purple), 3 (green), 4 (yellow), 5 (pink), 6 (light blue), >=7 (gray). b) Network during reduction c) Network after reduction d) Network after simplification step at the nodes. ($C = 1.1, \Delta R = 6.0$)

and $x = +1.4$). Fig. A4.3 shows this raster, with the gap in the structure indicated by the black dotted line. The lose ends that remain, due to the removal of particles, are completely reduced.

To increase the computational speed of the algorithm, each particle that cannot be deleted, because it destroys the network structure, is marked. During reduction, these marked particles are not considered again. This causes small parts of dangling ends still to be present after reduction (Fig. A4.3c). A very fast second reduction step, whereby all particles are again free to be deleted, removes these remaining dangling ends. Thus, in the end only the load-bearing structure of the network remains (Fig. A4.3d).

Lengths of segments

Even though reduction of the network takes place from low to high coordination number, segments in between the nodes will still not be straight. Therefore, the lengths of these segments is generally higher than the real length. The segment length is determined based on all the individual bonds between nodes and the 2-coordinated particles (Fig. A4.2d). The raster lattice can be used to test how much the obtained segment lengths deviate from the original raster spacing. The raster data is reduced 10 times at random, i.e. particles at the same coordination number are selected randomly. Fig. A4.4a shows the obtained histogram of the segment lengths. The original raster spacing is 17.1. Thus, due to random reduction the algorithm increases the average segment length with 2.5 particle diameter. As the test data contains quite thick strands compared to branches in simulations and experiments, we do not expect the overestimation of the segment length to exceed 15 %.

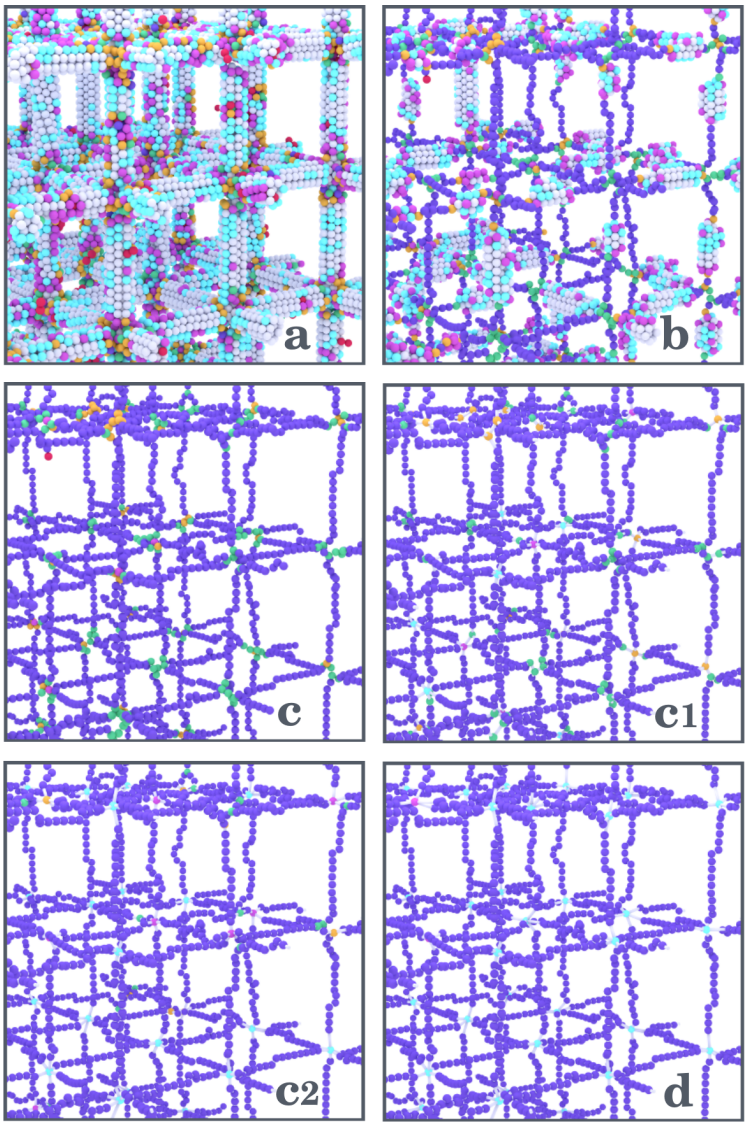

Figure A4.2 – Large field of view of test data on a specified raster lattice. a) Complete network. Color coding indicates the coordination number of the different particles. 1 (red), 2 (purple), 3 (green), 4 (yellow), 5 (pink), 6 (light blue), >=7 (gray). b) Network during reduction c) Network after reduction. After reduction simplification at the nodes takes place. First, particles that balance each other are replaced with a single particle (c1). Afterwards nodes are simplified over range ΔR; starting with nodes next to each other (c2) and followed by reduction of nodes further away from each other (d). d) Network after simplification step at the nodes ($C = 1.1, \Delta R = 6.0$).

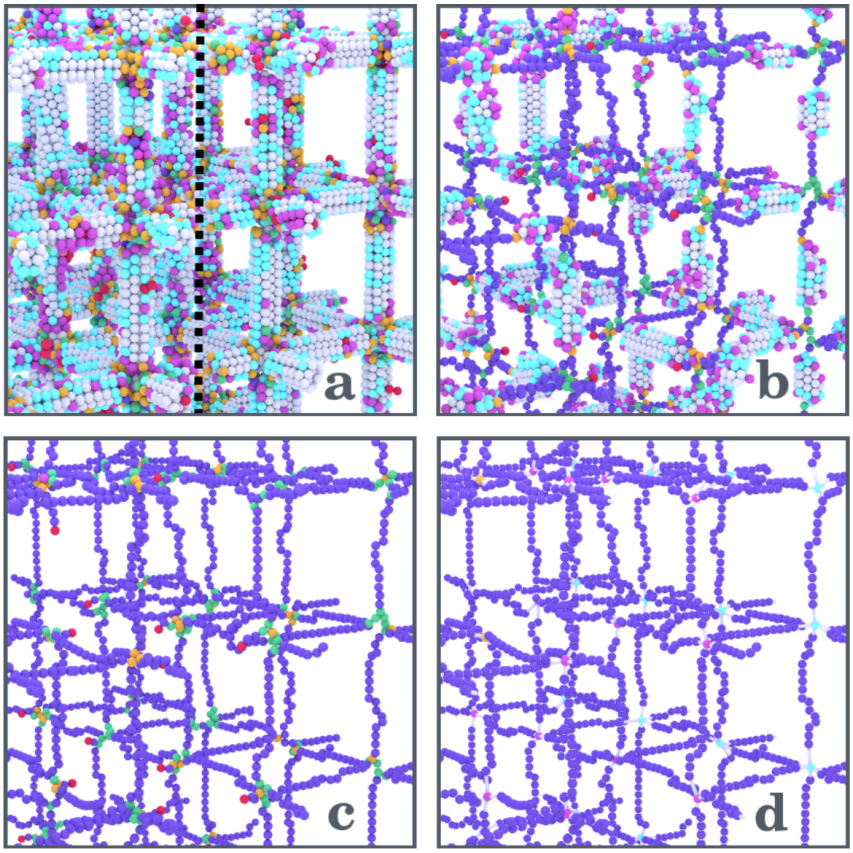

Figure A4.3 – Same data as shown in Figure A4.2. However, now a gap is made between $x = -1.4$ and $x = +1.4$ (indicated by the black dotted line). This figure shows how parts of the structure that are not mechanically stable, such as dangling ends, are removed.

Thickness of segments

As described in the main text, information is gained by placing the reduced network on top of the original gel. Starting at a distance of ΔR from the nodes, cylinders with radius r_c are placed between sets of 2-coordinated particles in the reduced structure. Particles from the original structure which are located inside this cylinder are marked. To make the thickness of the branches independent of the size of the cylinder, a cluster analysis is performed. If multiple clusters are found -due to a cylinder with large radius covering multiple branches- only particles belonging to the specific branch are kept. At a range of ΔR around the nodes particles cannot be assigned to a specific branch.

A final measure for the thickness of the branches is obtained by aver-

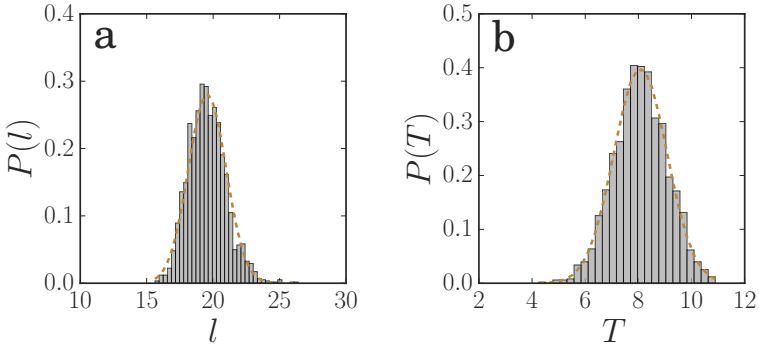

Figure A4.4 – (a) Probability distribution of the obtained segment lengths for the raster lattice. In this case the raster is reduced 10 times, in a random fashion. In yellow the Gaussian distribution with mean 19.55 ± 1.42 (SD) (b) Thickness distribution of the branches in the network. In yellow the Gaussian distribution with mean 8.08 ± 1.00 (SD). ($C = 1.1, \Delta R = 6.0, r_c = 7.0$)

aging the amount of particles in a branch by the total length l of this branch. Resulting in an average thickness T per unit length of the strand.

System size

To check the effect of the system size, a comparison between two different system sizes of N = 32.000 and N=128.000 is made. The number of nodes for each node coordination (Fig. A4.6a) are very similar upon dividing the number of nodes for system size N=128.000 by 4. Also the segment length distribution and the thickness distribution look similar. Thus, a system size of 32.000 particles is large enough to exclude size effects.

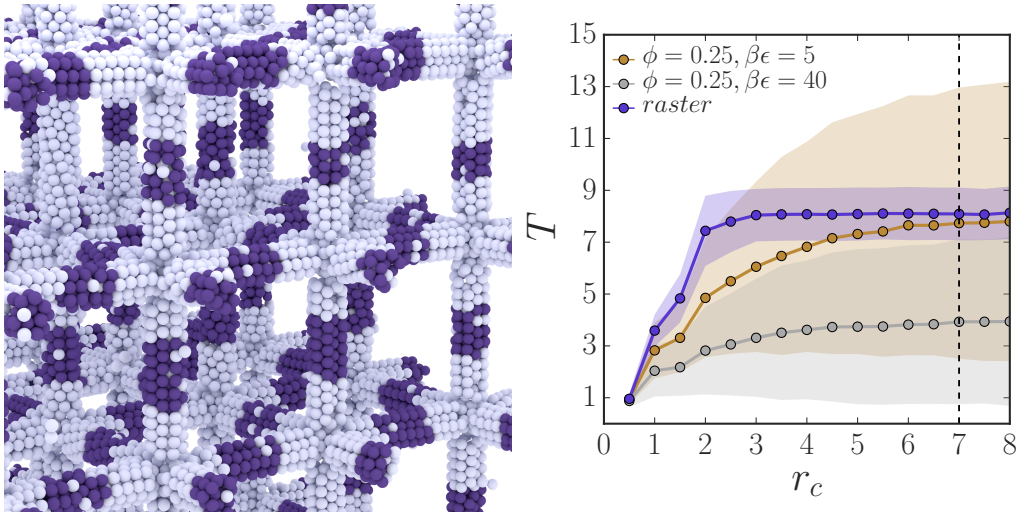

Figure A4.5 – **(left)** Visual representation of the raster data. The purple parts on the raster indicate in which areas the thickness is measured ($C = 1.1, \Delta R = 6.0, r_c = 7.0$). Note that the cut-off, which determines whether particles are neighbours or not, is quite small. Therefore, some particles that seem to be part of the structure by eye are still excluded. **(right)** Thickness of segments as a function of the radius r_c of the cylinder. Both raster data ($C = 1.1, \Delta R = 6.0$) and two simulation points of colloidal gels ($C = 1.16, \Delta R = 2.0$) are shown. The dotted line indicates the chosen value for parameter r_c.

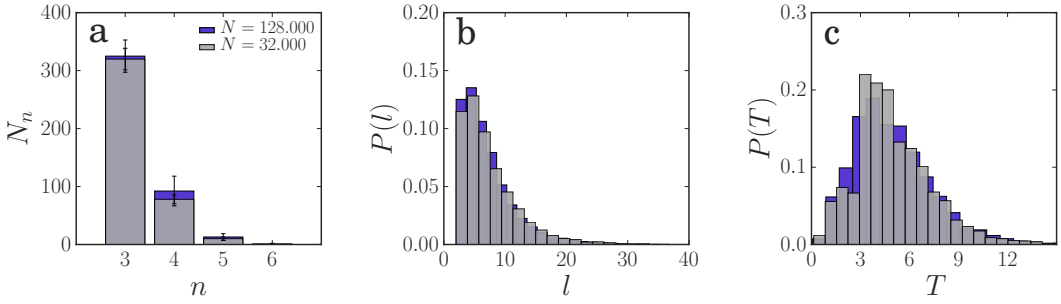

Figure A4.6 – Comparison between system size N=128.000 and N=32.000 (a) Number of nodes (N_n) for nodes n with different coordination numbers (b) Length and (c) Thickness distribution of the branches. ($\beta\epsilon = 20$, $\phi = 0.105$, $C = 1.16, \Delta R = 2.0, r_c = 7.0$). The length distribution gives a mean of 7.43 ± 4.73 (SD) for a system size of 32.000 and 7.11 ± 4.54 (SD) for a system size of 128.000. The thickness distribution has a mean of 5.01 ± 2.49 (SD) and 5.01 ± 2.61 (SD) for a system size of N=32.000 and N=128.000 respectively.

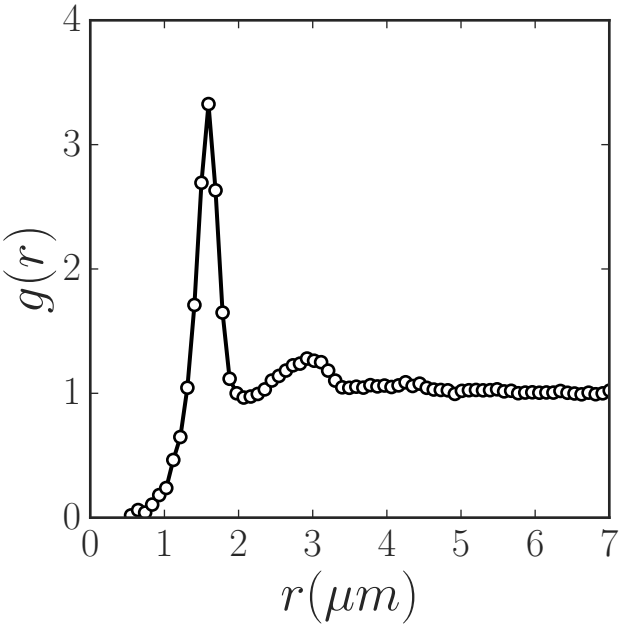

Figure A4.7 – The radial distribution function $g(r)$ of experimental data at a volume fraction of $\phi = 0.2$. The minimum of the first peak is located at 2.1 μm . This value is a good measure for the interaction range between the particles. The cut-off C in the reduction algorithm is set to $C = 2.1/a$. The particle diameter a of the colloids equals 1.6 μm, resulting in a cut-off value C of 1.31.

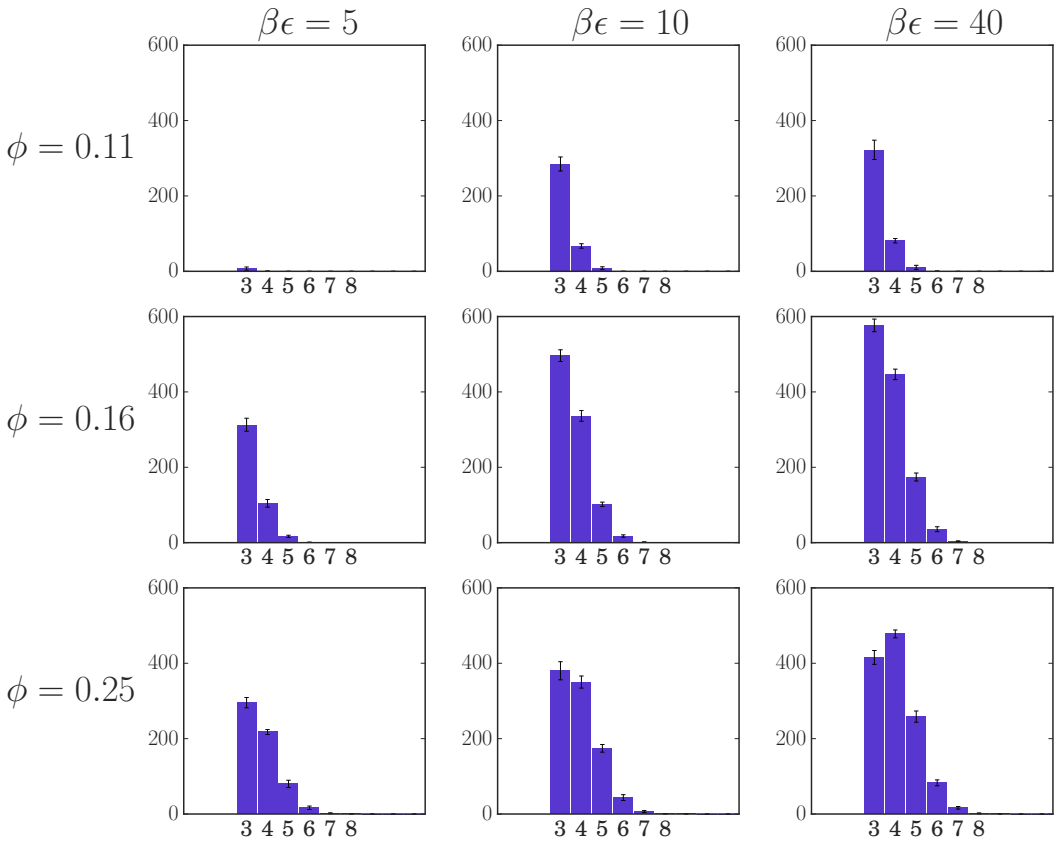

Figure A4.8 – Number of nodes N_n for different coordination numbers n. Histograms are shown for three different volume fractions ($\phi = 0.11, \phi = 0.16, \phi = 0.25$) and three different interaction strengths ($\beta\epsilon = 5, \beta\epsilon = 10, \beta\epsilon = 40$). Parameters algorithm: $C = 1.16$, $\Delta R = 2.0$, $r_c = 7.0$.

Colloidal gel networks under shear

5

The yielding transition of gels is highly relevant to understand the initiation of flow and deformation in food products, paints and coatings. Yet, how the network topology of gels affects or is affected by yielding is still unexplored. Here, we investigate the yielding transition of colloidal gels both in simulations and experiments. For the first time we quantify the full network topology of colloidal gels during deformation. We examine different gel topologies, formed at varying interaction energies and volume fractions. Upon increasing strain, the number of segments in the gel rapidly decreases, whereas strands in the network become thicker. Simulations reveal that close to percolation applying shear increases the connectivity of the network. This is due to dangling ends in the network which can form new connections. Networks at higher volume fraction, on the other hand, decrease in connectivity due to the applied deformation. These results indicate that the initial network topology has a considerable effect on the resulting yielding response of colloidal gels.

Joanne E. Verweij, Thomas E. Kodger, Frans A. M. Leermakers, Joris Sprakel & Jasper van der Gucht[1]

"Colloidal Gel Networks under Shear"
To be submitted (2020)

[1]*Physical Chemistry and Soft Matter, Wageningen University, Wageningen, 6708 WE, The Netherlands.*

Introduction

Food products [1, 2], paints [3], coatings [4], our blood [5] and cells [6] can be initiated to flow, migrate or deform. In food products, such as gelatin, yoghurt, cheese and butter, attractive particles form fractal space-spanning networks [7]. Upon applying a shear deformation these gels will yield, exhibiting a solid-to-liquid transition. Yielding has been extensively studied in model colloidal systems using rheology [8–11], microscopy [12–18], static light scattering or a combination of these techniques.

So far, a universal picture of yielding has not yet been presented. Some papers describe yielding as a gel network breaking into clusters [9, 14, 19], whereas other papers report how the gel network becomes more compact and heterogeneous [12, 20–22]. However, in both cases the gel undergoes complex rearrangement processes. It is not yet clear whether these rearrangement processes are dominated by bond breakage at the particle level, or whether process at the network level, such as strand failure or fusion, dominate. To answer these questions it is important to be able to quantify structural changes in the network. To this end we employ the method developed in Chapter 4, which can reveal the network topology of a colloidal gel. Ultimately, yielding is a shear-induced solid-to-liquid transition that must involve the loss of connectivity in the network, at least locally. Yet, a network-scale picture of yielding in these inhomogeneous solids has not been presented.

To determine what microstructural changes underlie this mechanical transition from a solid to a freely-flowing state, one can look at the number of neighbours $\mathcal{Z}$ of each individual particle in the structure. However, quantifying the number of bonds per particle does not provide information about the network topology itself. Topological mapping of the network provides a way to determine the number, length and thickness of strands in the network. Moreover, we can also quantify segments that do not contribute to the rigid backbone, so-called dangling ends. Topological mapping of the network and quantification of dangling ends, allows us to study the effect of yielding on the network topology, upon varying the interaction strength $\beta\epsilon$ and volume fraction ϕ.

So far, shear has been applied experimentally using a shear cell [13, 14, 19], electrical field [23], microchannel flow [24] or a rheo-confocal [25]. Still, making sure that a sample is merely sheared is quite challenging, as one has to make sure that wall slip [26] and squeeze flow [16] are absent. We experimentally study the early stress response of the network and see how

the gel morphology changes upon applying small deformation steps. Here, a home-built setup is used, which can fully resolve the three-dimensional structure of colloidal gels under shear.

Previously, two-dimensional shear experiments on low volume fraction colloidal gels showed how, after initial affine deformation, at a strain of $\gamma = 0.3$ break-up events start to happen. These initial events are followed by an avalanche of break-up events at higher strains, resulting in local compaction and the structure becoming more heterogeneous [12]. Yet, here the backbone of which the network consists was very thin, restricting these results to dilute networks at high interaction energy. In this Chapter, we will focus on colloidal networks with both thin and bulky strand structures.

In this work, we combine simulations and experiments to study how yielding affects the network topology of colloidal gels. A reduction algorithm is used to go from all three-dimensional particle positions in the gel to the topology of the gel structure. This allows for the quantification of the network structure upon applying shear deformation. Results show how the network becomes more heterogeneous, due to strand fusion. Simulations reveal how close to percolation the connectivity of the network increases, due to dangling ends which can form new connections. At higher volume fractions, however, shear induces a decrease in the network connectivity. This indicates that the initial network topology has a large effect on the nature of the yielding transition in colloidal gels.

Methods

Simulations - yielding

Brownian Dynamics simulations are performed to study yielding in large colloidal gels (N = 32.000) at different interaction strengths ($\epsilon = 5, 10$ and $40\ k_BT$) with a volume fraction range from $\phi = 0.11$ up to $\phi = 0.25$.

The motion of a particle i with position $\boldsymbol{r}_i$ is obtained by solving the overdamped Langevin equation:

$$\dot{\boldsymbol{r}}_i(t) = \beta D_0[-\nabla_i U(t)] + \sqrt{2D_0}\boldsymbol{\xi}_i(t) \tag{5.1}$$

where $\boldsymbol{\xi}_i(t)$ is random white noise, sampled with zero mean and unit variance, to model the thermal fluctuations of the particles. $D_0 = k_BT/\zeta_f$ is the short-time diffusion coefficient with ζ_f the friction coefficient, set to unity. The time step δt for the numerical integration is set to $\delta t = 1 \times 10^{-6}\ \tau_B$. The unit of time is expressed in terms of the short-time self-diffusion $\tau_B = a^2/D_0$ with particle diameter a.

A Morse potential is used to calculate the force between particles [27]:

$$\beta u(r) = \beta\epsilon \, \exp(\rho_0[a-r]) \, (\exp[\rho_0(a-r)] - 2) \tag{5.2}$$

with $\beta = 1/k_B T$ and energy scale $\beta\epsilon$. Parameter ρ_0 determines the width of the potential, which equals approximately $\Delta = 0.16\, a$ for $\rho_0 = 33$ [1].

The equilibration time of the gel structures is set to $10\ \tau_B$. Whether these gel structures are percolating is defined by using the method described in Chapter 4. Afterwards, shear is applied with a shear rate of $\dot{\gamma} = 1.0\ \tau_B^{-1}$. The gel is deformed from $\gamma = 0 - 10$ and Lees-Edwards boundary conditions [28] are applied. For every set of chosen quantities 10 independent measurements are performed.

Particle Synthesis

Based on previously reported work, we synthesize micrometer-sized core-shell particles that are easy to locate in confocal microscopy experiments and can be index- and density matched in non-hazardous polar solvents [29]. These tFEMA-tBMA particles are electrostatically stabilized by a corona of polymeric hairs grown by surface-initiated ATRP. When electrostatic interactions are screened by adding salt, this results in a hard-sphere-like interaction.

First, fluorescent cores are synthesized by adding 6.4 mL of a 28:72 tFEMA: tBMA mixture (by volume, 2,2,2-trifluoroethyl methacrylate: tert-butyl methacrylate, TCI), 80.7 g methanol, 20.1 g distilled water, 64 mg SPMA (3-sulfopropyl methacrylate potassium salt, Sigma-Aldrich), 64 mg AIBN (azobisisobutyronitril, Sigma-Aldrich), 128.4 μL EGDMA (ethylene glycol dimethacrylate, TCI) and 300 μL cyanine dye (synthesis protocol of this fluorophore is described in Ref. [30]) in a 250 mL round bottom flask. This mixture reacts for 4 hours at 80 °C in an oil bath under reflux cooling, while stirring continuously. Afterwards the mixture is filtered and diluted with a 90:10 methanol:Milli-Q mixture to a total volume of 200 mL.

In the second step the non-fluorescent shell is synthesized around the cores. Here, 100 mL of the core suspension (synthesized in the previous step), 300 mL 90:10 methanol:Milli-Q, 20 g PVP (polyvinylpyrrolidone, Sigma-Aldrich), 30 mL of a 28:72 tFEMA:tBMA mixture, 300 μL inimer (synthesis protocol is described in [29]) and 400 mg AIBN are added to a 1 L round bottom flask. In a cyclic manner vacuum and N_2 purging is applied for over half an hour. The mixture reacts overnight at 65 °C in an oil bath under continues tumbling of the flask using an IKA overhead stirrer.

In the last step, polymeric hairs are grown on the outside of the particles

[1] Here, Δ is determined by taking the end of the well at 1% of the original well-depth.

via ATRP. In a 1 L round bottom flask 133 mL of Milli-Q, 133 mL formamide (Sigma-Aldrich), 10 gr SPMA, 5 gr DMA (dimethylacrylamide, Sigma-Aldrich), 200 μL MBSI (methyl bromopropionate, Sigma-Aldrich), 490 μL HMTETA (hexamethyltriethylenetetramine, Sigma-Aldrich) and 100 mg copper(II)chloride (Sigma-Aldrich) are added. Lastly, the core-shell particles obtained in the previous steps are added to this mixture. The round bottom flask is purged with nitrogen gas for 2.5 hours and vacuum is applied for 1 hour. Finally, copper(I)chloride (Sigma-Aldrich) is added, while purging the head space of the flask, to start the reaction. After properly mixing in the copper(I)chloride the mixture is allowed to react overnight on a stir plate at room temperature.

After filtering the reaction mixture, particles are centrifuged down and washed with 90:10 methanol:distilled water. Next, particles are washed with 50:50 methanol:Milli-Q. In this washing step a small amount of EDTA (ethylenediaminetetraacetic acid tetrasodium salt >99.5%, Sigma-Aldrich) is added to remove copper. The particles are washed 2$\times$ towards a density and index matched solvent with 30:70 Milli-Q: 2,2 thiodiethanol (TCI). Finally, drops of distilled water are added to optimize the index matching by eye.

To determine the size of the particles, a Dynamic Light Scattering (DLS) measurement is performed on an ALV instrument equipped with an ALV5000/60X0 external correlator and a 300 mW Cobolt Samba-300 DPSS laser (λ = 532 nm), at a detection angle of 90°. The particle diameter equals 1.84 μm, based on the second order cumulant of the normalized first-order correlation function. The polydispersity index (PDI) of the synthesized particles is lower than 10% as the particles do crystallize at high volume fraction [31, 32].

Experiments - sample preparation

Colloidal gels are formed by adding depletant to a particle suspension of synthesized tFEMA-tBMA particles. In this case, depletion attraction between the colloids is induced by adding polyethylene oxide (PEO, M_w 2.31×10^5, M_n 2.03×10^5, R_g = 23.1 nm). The sample has a volume fraction between 0.23-0.25 and a polymer concentration of 7.6 mg/mL ($c/c^* = 1.01$). 10 mM salt is added to screen electrostatic interactions. Particles in the Z-stack are located using the Matlab locating algorithm of Gao and Kilfoil [33]. The deformation field is determine by calculating the difference between confocal XZ images in time using the ImageJ BUnwarpJ-plugin [34].

Experiments - setup

We develop a low cost shear setup which can be installed on top of a conventional inverted microscope (see picture in Fig. 5.1 and schematic in Fig. 5.5).

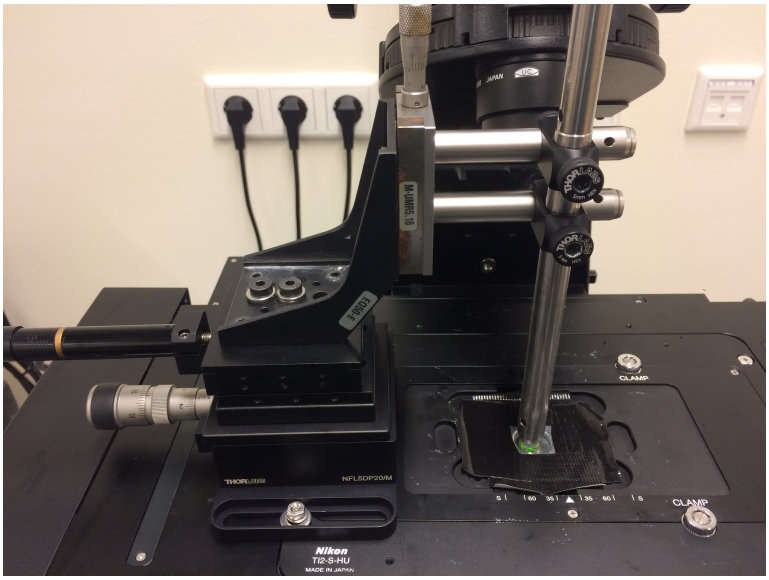

Figure 5.1 – Shear setup on the stage of an inverted confocal microscope. The top plate of the shear cell is attached to the metal post. By moving the motorized actuator, the sample will be sheared towards the right.

The aim of the experiments is to resolve large parts of the three-dimensional structure of colloidal gels upon applying shear deformation.

On top of a base plate (NF53, Thorlabs) a single-axis translation stage (MT1B/M, Thorlabs) with a motorized actuator (Z825B, Thorlabs) is mounted. The actuator is controlled by a K-Cube Brushed DC Servo Motor Controller (KDC101, Thorlabs), which can be controlled using Thorlabs' Kinesis software. On top of the translation stage an outer bracket (EQ50-E, Newport) is attached, with a linear stage (M-UMR5.16, Newport) and micrometer head (BM11.166, Newport) to determine the Z-position of the metal post at the side. Posts are fixed together using right-angle clamps. At the bottom of the post the top plate (10 mm $\times$ 10 mm) is glued to a M4 screw using 5 minute epoxy gel (Devcon). The sample holder consists of a round cover slip (50 mm, Thermo Scientific), connected to a metal ring (M16, Sencys, inner diameter 16 mm, thickness 4 mm) using Norland Optical Adhesive 61 UV curable glue. The metal ring is not visible in Fig. 5.1, as it is held in place by tape.

To ensure a stick boundary condition, we coat the cover slip with a layer of oppositely charged polymer onto which the colloids strongly adsorb by electrostatic complexation. The round cover slip is first washed with soap and successively coated with one layer of positive, one layer of negative and one layer of positive polymer. The cationic polymer layer is made from a 1% w/w solution of polydiallyldimethylammonium chloride (M_w = 4 $\times$ 10^5 $-$ 5 $\times$ 10^5, Sigma-Aldrich) with 1M of NaCl, whereas for the anionic layer a 1% w/w solution of sodium polystyrene sulfonate

($M_w \approx 2 \times 10^5$, Sigma-Aldrich) with 1M of NaCl is used. After applying each polymer solution the cover slip is thoroughly rinsed with Milli-Q. The cover slip is blown dry after applying all polymer layers. On top of the last positively charged layer a bit of our particle stock is deposited. Rinsing these particles with Milli-Q leaves a single heterogeneous layer of particles attached to the glass. Finally, the cover slip is blown dry and glued to the metal ring.

The top plate of this shear setup consists of a glass plate with 250 μm spacers (Precision Brand, 0.254 mm). Between these spacers a TEM grid is glued (Agar Scientific, G27 60C Hex 700 thin bar copper, 3.05 mm). Figure 5.5 shows a schematic of the top plate. The colloidal gel can penetrate through the TEM grid which creates a non-slip boundary.

To perform the shear experiments the following protocol is followed. First, the metal ring with the attached cover slip is taped to the microscope. The top plate is placed on the cover slip. After installing the shear setup on the microscope stage the post at the right side of the shear setup is lowered and glued to the top glass plate. After half an hour, the micrometer is moved 500 μm up and 15 μL of sample is pipetted between the two plates. Afterwards, the gap between the cover slip and the TEM grid is adjusted to 200 μm and 150 μL of fluorinated oil (DuPont Krytox, GPL101) is pipetted in the metal ring to prevent evaporation. After an hour, shear is applied by moving the piezo in steps of 25 μm (with a velocity of 5 μm per second). After each step a pause is taken to record a Z-stack of $102 \times 102 \times 80$ μm. Data is obtained using an inverted Nikon C2 confocal with a Nikon SR HP Plan Apo 100$\times$ silicone immersion oil objective (NA=1.35).

Quantifying the Network Topology

We determine the complete network topology of the gel network from the three-dimensional coordinates of all particles in our field-of-view. This is done in silico by deleting particles in the gel structure which are not essential to maintain the overall network connectivity. For each particle, its neighbours up to 5 generations are determined. If deleting a particle will split the cluster of neighbouring particles, this particle cannot be removed. After additional simplification steps, the final structure contains segments and nodes (see Fig. 5.2). This allows for the quantification of the connectivity of the network and the number, length and thickness of the segments. The used method can be applied to both simulations and experiments and is described in Chapter 4.

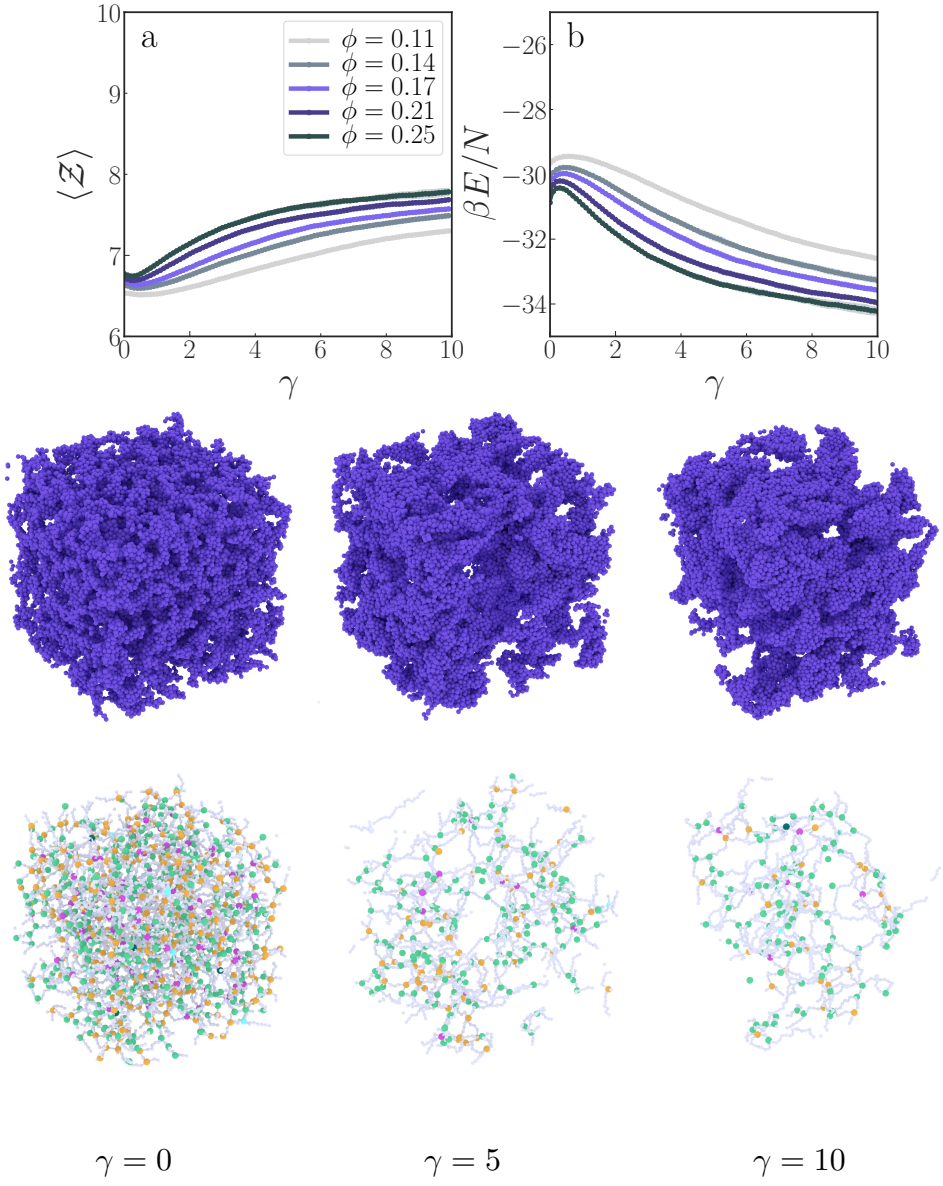

Figure 5.2 – Simulation data at $10\ k_BT$ for volume fractions $\phi = 0.11$, 0.14, 0.17, 0.21 and 0.25. A close-up of the graphs is present in Fig. A5.1 (a) Average number of nearest neighbours $\langle \mathcal{Z} \rangle$ per particle as a function of strain. (b) Average energy per particle in the system as a function of strain. (Image) Visualization of a simulated colloidal gel at a deformation of $\gamma = 0, 5$ and 10 ($\phi = 0.17$, $10\ k_BT$). The upper row shows the full colloidal gels whereas the bottom row shows their network structures. The nodes in the network structure are colour-coded according to their respective coordination number, being successively green (3), yellow (4), pink (5), light blue (6) and dark green (7).

Results and discussion

To answer the question how the topology of gels alters upon shear deformation numerous shear simulations are performed at different interaction energies and volume fractions. Visual inspection of the resulting gels reveals a drastic structural change after deforming the gel 500 % (see image Fig. 5.2). A common method to quantify the deformation of a colloidal gel is to analyse the evolution of the nearest neighbour distribution $\mathcal{Z}$ [15, 21, 35, 36]. Upon plotting the average number of nearest neighbours per particle $\langle \mathcal{Z} \rangle$ for deformations up to γ = 10 (Fig. 5.2a, zoom Fig. A5.1), we observe a clear dip in the average number of neighbours at low strain. This decrease in particle connectivity signals a yielding transition. At higher strains, however, the number of nearest neighbours increases again, indicating coarsening of the gel structure due to shear deformation.

Studying yielding at different interaction energies (Fig. A5.3) shows how the minimum of $\langle \mathcal{Z} \rangle$ shifts to lower strains with increasing interaction strength $\beta\epsilon$. This suggest that increasing stickiness between particles brings the yield strain down, an effect which is also observed with increasing volume fraction. Interestingly, the dip in $\langle \mathcal{Z} \rangle$ completely disappears at an interaction energy of $40\ k_B T$. Here, the rate of bond breakage, apparently, does not become higher than the rate of bond formation as the structure is observed to keep increasing its number of nearest neighbours. At this interaction energy, we also do not observe a clear yield peak in the stress-strain curves (Fig. A5.2).

The minimum in the number of bonds appears at higher strains than one might expect for yielding. Therefore, we compare this data with the evolution of the stress tensor $\boldsymbol{\sigma}$ in the shear direction (Fig. A5.2). Here, the shear stress is calculated as:

$$\sigma_{xy} = -\frac{1}{V} \sum_{i=1}^{N} r_{i,x} F_{i,y} \tag{5.3}$$

with V the volume of the simulation box, $r_{i,x}$ the x-component of the particle position vector, $F_{i,y}$ the y-component of the total force of particle i and N the total number of particles. From the stress-strain curves it is observed that the yield point is positioned at much lower strains, in line with previously reported results [10]. Thus, the yield point represents the onset of bond breakage, whereas the minimum in the nearest neighbour distribution is found at higher strains.

The average number of neighbours $\langle \mathcal{Z} \rangle$ per particle shows clear yielding behaviour through bond breakage and bond formation. From the simulation data the total energy of the system E can also be obtained (Fig. 5.2b). As

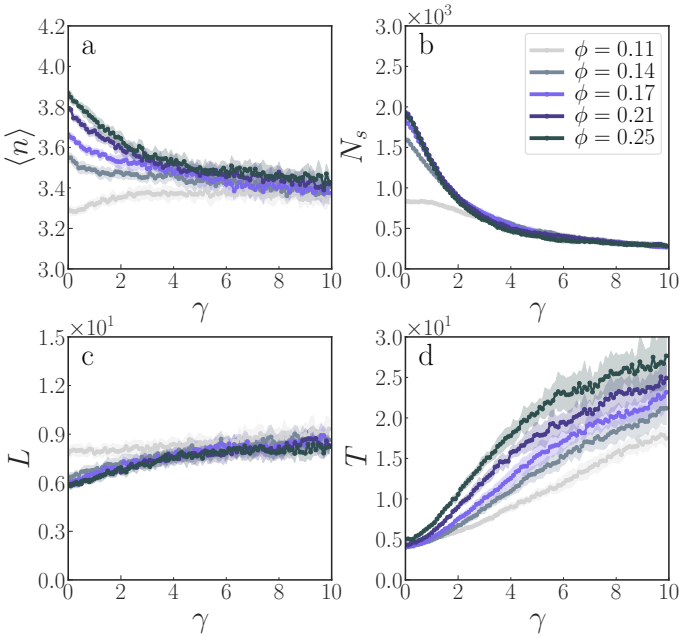

Figure 5.3 – The network structure as a function of deformation γ in simulations. (a) The average coordination number $\langle n \rangle$ for the nodes in the network (b) Number of segments in the network (c) Length of the segments (d) Thickness of the segments. Parameters network structure ($\beta\epsilon = 10$, $C = 1.16$, $\Delta R = 2.0$, $r_c = 12.0$).

expected, the energy per particle in the system indeed drops when particles start to form bonds with neighbouring particles. Here, the shape of the curves is identical to the evolution of the average number of neighbours per particle (Fig. 5.2a). A second yielding transition, as reported in some studies [8, 20], is not observed in this simulation data. Indeed, previously reported second yielding transitions were observed at much higher deformations ($\gamma \approx 100$) and higher volume fractions [25].

Looking at both the average number of nearest neighbours $\langle \mathcal{Z} \rangle$ and the energy E of the system provides information about bond breakage and bond formation in the gel. The question arises how this actually affects the network topology. To answer this question a recently developed algorithm is used to quantify colloidal gels based on the number and coordination of nodes, and the amount, length and thickness of the segments (see Chapter 4). For each network a coordination number $\langle n \rangle$ can be determined (see image Fig. 5.2). The coordination number is the average connectivity of all branching points and in this way points out the degree of connectivity of the network. In general the coordination number of the network decreases when the network is sheared (see Fig. 5.3a). This indicates that the coordination number of the branching points goes down. Consequently, a decrease in the number of segments N_s, of which the network consists, is visible. At the same time, we observe a slight increase in the average length of the segments L. Yet, the strongest effect is observed in the average thickness T of

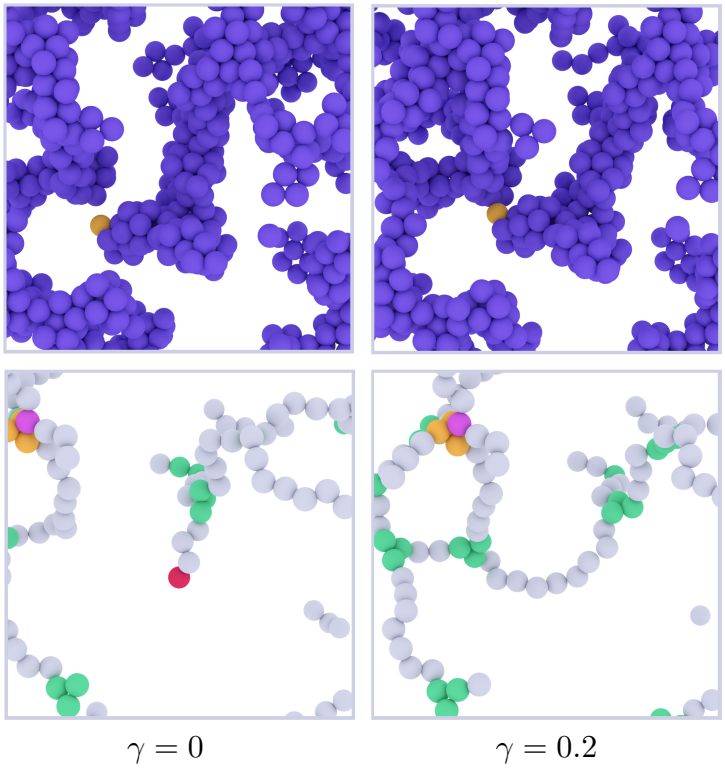

Figure 5.4 – Close-up of a colloidal gel at $\phi = 0.11$, with an interaction strength of 10 k_BT. The upper row shows the original gel structure. Here, the newly formed connection is colored orange to guide the eye. The lower row shows the gel structure during network reduction. As the reduction is not completely finished the nodes in the network are not yet simplified and dangling ends are still present. The particles are colour-coded according to their coordination number being respectively, red (1), gray (2), green (3), yellow (4) and pink (5). At this low volume fraction a dangling end forms a new connection when shear is applied.

the strands. A drastic increase in strand thickness results in coarsening of the gel. At high shear deformations particles collect into such large blobs that one could argue not to call this strands anymore, an effect which becomes even more substantial at higher interaction strengths.

Surprisingly, at low volume fraction the coordination number of the network increases. Instead of a network structure losing its coordination, the structure actually creates more highly coordinated branching points. All analyzed simulations are percolating structures, yet gels at the lowest volume fraction contain most dangling ends (See Fig. A5.4) [2]. During shear these dangling ends have the possibility to form new branching points, allowing the gel to increase coordination number (see Fig. 5.4). Due to dangling ends forming new connections the number of segments does not start decreasing

[2]To increase the computational speed of the reduction algorithm, each particle that cannot be deleted, because this destroys the network structure, is marked and not considered again. This allows for the detection of dangling ends (see Chapter 4). However, only dangling ends with a segment length of at least 5 particles or more are detected, due to the fact that connectivity of the network structure is based on 5 generations of nearest neighbours. When a dangling end is exactly reduced from the outer end towards a junction, it can also be completely reduced. As a result, the number of dangling ends are an underestimation of the real number of dangling ends

straight away after applying shear (see Fig. 5.3b, ϕ = 0.11). For the lowest volume fraction at 40 k_BT, we even observe a clear increase in the number of segments (Fig. A5.5), until the strands start to fuse at much higher strains.

Now that dangling ends are shown to effect the connectivity of the network during shear, lets take a closer look at the amount of dangling ends at different interaction energies and volume fractions. In general, both a higher volume fraction and stronger attraction between particles gives fewer dangling ends. Gels with most dangling ends (5 k_BT, see Fig. A5.4) are observed to reach a lower average coordination number. Remarkably, the number of dangling ends in these weak gels increases under shear, indicating strand rupture in the gel network. For gels at stronger attraction (40 k_BT) the coordination number of all volume fractions converges to the same value. These gels have hardly any dangling ends. Conclusively, the presence of dangling ends influences how and how fast the connectivity of a network evolves. Moreover, the evolution of dangling ends under shear indicates strand failure and strand fusion.

How the gel network topology alters during shear deformation can be summarized as follows. Upon applying shear, strands of the network start to fall on top of each other and fuse together. As a result the coordination number and the number of segments in the gel decreases, except at very low ϕ. The thickness of the segments increases significantly, due to strand fusion. This densification has been observed experimentally as well [12, 21, 22]. At volume fractions just above the percolation point we observe an increase in network connectivity due to the fusion of dangling ends in the gel structure.

Shear experiments are performed to see whether the network topology of a colloidal gel evolves similarly as observed in simulations. To this end a shear setup is developed that can be used on top of a conventional inverted confocal microscope (see Fig. 5.1 and Fig. 5.5a). Repeatedly shearing a sample between two glass plates results in plug flow, i.e. the displacement of the sample is constant as a function of the sample height. Therefore, the upper glass plate is replaced with a TEM grid with small 30 μm holes (see Fig. 5.5b). Now the gel can penetrate through the grid, which creates a non-slip boundary. The glass plate at the bottom of the shear cell is also coated with particles to prevent slip. Next, the deformation field is quantified (Fig. 5.5c). Clearly, shear deformation is observed, which becomes more pronounced higher up in the sample. The obtained XZ confocal microscopy images (Fig. 5.5d) show how the gel structure becomes more heterogeneous upon applying more strain, as also observed in the simulations.

Experiments were carried out to see how the network topology of an experimental gel is altered by shear. For two experimental samples that clearly showed shear deformation we analysed the network topology. In this case, three-dimensional particle locations were extracted from the confocal microscopy data. The observed changes in the network structure are a small decrease in coordination number, a decrease in the number of segments, a

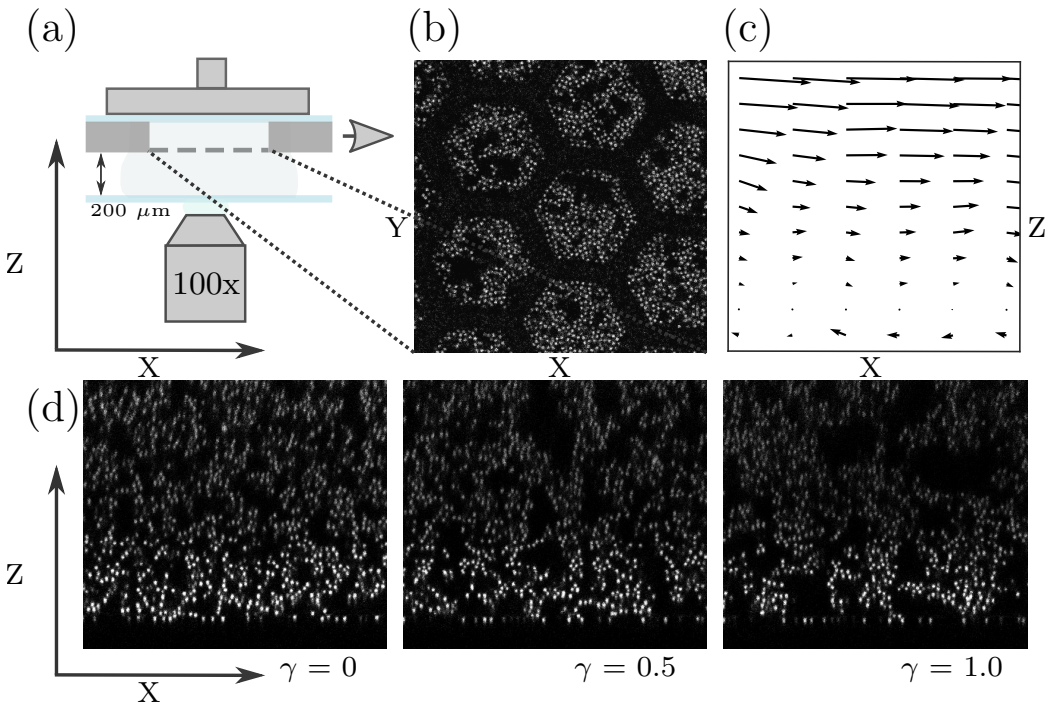

Figure 5.5 – (a) Schematic of the experimental setup. (b) TEM grid used at the top of the shear cell (c) Vector plot of the deformation between $\gamma = 0.625$ and $\gamma = 0.75$. The vectors at the top of this image represent an average shear flow of 19 μm to the right. (d) XZ projection of the experimental data at $\gamma = 0$, 0.5 and 1.0. The dimensions of the X- and Z-direction are 102 and 80 μm respectively.

slight increase in segment length and a major increase in thickness of the strands (Fig. 5.6). To show that these trends follow the results found in simulations, we also plot the simulation data for one particular volume fraction ϕ and interaction strength $\beta\epsilon$.

The evolution of both experimental samples is the same. However, the network structure (at $\gamma = 0$) is not the same, even though the initial composition of these samples is identical. The difference in network structure can be attributed to the difference in strain history between these two samples. By setting the gap of the shear cell to 200 μm applying pre-strain cannot be avoided. Nonetheless, the strain applied by the motorized actuator is the same for both samples. The changes in the network topology indeed confirm that both samples respond similarly to this applied deformation.

There are some subtle differences between the simulations and experiments. That is, the number of segments in the simulations is higher

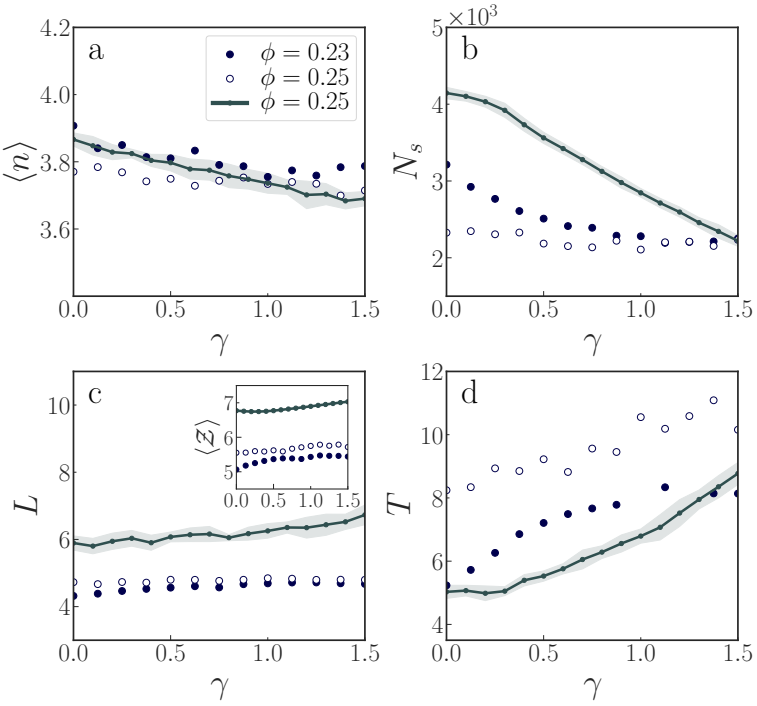

Figure 5.6 – Network structure as function of deformation γ. The solid line shows simulation data at 10 k_BT and volume fraction $\phi = 0.25$. The open markers represent the experimental data. a) Average coordination number b) Number of segments in the network c) Length of the segments. The inset shows the average number of neighbours per particle $\langle \mathcal{Z} \rangle$ as a function of strain d) Thickness of the segments. Parameters of the network structure for experimental data ($C = 1.3$, $\Delta R = 2.0$, $r_c = 12.0$).

compared to the number of segments in the experiments [3]. As a result, the experimental segments are thicker. Another difference in the network topology can be found in the average length of the segments, which are found to be slightly shorter in the experimental networks. Variance in network topology between simulations and experiments is not surprising, as equilibration time and flow history are important factors in the network formation. Therefore, we should look at trends instead of making a one-on-one comparison. The number of neighbours per particle $\langle \mathcal{Z} \rangle$ (see inset Fig. 5.6c) is smaller for the experimental gels. This can be explained by the difference in determining particle neighbours in simulations and experiments [4]. Consistently, in both cases the number of neighbours increases upon applying shear.

Experimentally, a shear driven densification of the gel structure is observed. Analysing the network structure of these gels for the first time shows how the number of segments in the gel decreases and strands get thicker. Densification of aggregates in colloidal suspensions [37] and colloidal gels [12, 20–22] has been reported previously. However, there are

[3] Here, the number of segments are scaled to the same volume.

[4] In simulations, the cut-off between nearest neighbours equals 1% of the original well depth (1.16 a center-to-center distance). In experiments, the cut-off is based on the first minimum of the radial distribution function (1.30 a center-to-center distance).

several papers that report opposite results. In these studies the number of neighbours per particle goes down, and the network completely falls apart [9, 14, 19]. Based on the results in this paper, we argue that in these studies the applied deformation field probably corresponds to plug flow instead of shear. One of these papers indeed reports that during shear the network is detached from the cone surface and yielding of the gel is primarily induced by fluid drag and hydrodynamic interactions [19].

Conclusions

In this Chapter we looked at the network topology of colloidal gels during shear. At low strains, a dip in the number of nearest neighbours per particle $\mathcal{Z}$ indicated the yield point of these colloidal gels. Through mapping of the network topology, we quantified what actually happens with the network topology of colloidal gels during the subsequent yielding transition. In general, the number of segments in the network rapidly decreases whereas the thickness of the remaining strands quickly increases. This indicates that strands meet each other and fuse, forming thicker strands. At high shear deformation strand fusion causes the formation of particle blobs, an effect which is enhanced by increasing the stickiness between particles.

Upon applying shear, the total connectivity of the network will go down. However, there is an exception for gel structures close to percolation. At these very low volume fractions dangling ends in the network structure can form new connections. The role of dangling ends in shear deformation has been overlooked so far. It would be interesting to see whether shear deformation of colloidal gels with different particle-particle interactions shows the same increase in network connectivity close to percolation.

Experimental shear was realized by using a shear setup with a TEM grid as top boundary. After resolving the three-dimensional structure of these gels the effect of shear deformation on the experimental network topology was shown. The network topology showed a significant loss of segments and a major increase in strand thickness. This confirms the microscopic picture that we obtained from the simulations; upon applying shear strands meet each other and start to fuse.

The observed thickening of strands during yielding of colloidal gels, raises many new interesting research questions. As shown in our previous work [38, 39], gel strands can ´unravel´ during deformation which causes the formation of a necking region at which a strand can fail. Whether strand failure, due to strand plasticity, also plays a role in local compaction during the yielding transition remains to be understood. It would be very valuable

to quantify the breakage and formation of strands during yielding more precisely. Moreover, being able to track strand movements, between mapped topologies in time, would be highly informative as well.

In this work we show what happens to the network topology of gels upon applying shear deformation. The experimental realization of shear is challenging and requires characterization of the deformation field. An initial shear deformation can change into plug flow as the network detaches from its boundaries. Future research should focus on quantifying the deformation fields throughout a shear experiment to disentangle the different stages of colloidal gel yielding. This will help to get a clear picture of how both the deformation field and gel structure change during the experiment.

Acknowledgements

I would like to thank Qimeng Wu for useful discussions about the shear experiments. I would like to thank Thomas Kodger for his help with developing the shear setup and shear protocol.

Bibliography

[1] Raffaele Mezzenga, Peter Schurtenberger, Adam Burbidge, and Martin Michel. Understanding foods as soft materials. *Nature Materials*, 4(10):729, 2005.

[2] Georges Debregeas, Herve Tabuteau, and J-M Di Meglio. Deformation and flow of a two-dimensional foam under continuous shear. *Physical Review Letters*, 87(17):178305, 2001.

[3] Hanne M Van Der Kooij, Remco Fokkink, Jasper Van Der Gucht, and Joris Sprakel. Quantitative imaging of heterogeneous dynamics in drying and aging paints. *Scientific Reports*, 6:34383, 2016.

[4] AL Volynskii, S Bazhenov, OV Lebedeva, and NF Bakeev. Mechanical buckling instability of thin coatings deposited on soft polymer substrates. *Journal of Materials Science*, 35(3):547–554, 2000.

[5] Timothy W Secomb. Blood flow in the microcirculation. *Annual Review of Fluid Mechanics*, 49:443–461, 2017.

[6] Benoit Ladoux and René-Marc Mège. Mechanobiology of collective cell behaviours. *Nature Reviews Molecular Cell Biology*, 18(12):743, 2017.

[7] Peter J Lu and David A Weitz. Colloidal particles: crystals, glasses, and gels. *Annual Review of Condensed Matter Physics*, 4(1):217–233, 2013.

[8] N Koumakis and G Petekidis. Two step yielding in attractive colloids: transition from gels to attractive glasses. *Soft Matter*, 7(6):2456–2470, 2011.

[9] Thomas Gibaud, Damien Frelat, and Sébastien Manneville. Heterogeneous yielding dynamics in a colloidal gel. *Soft Matter*, 6(15):3482–3488, 2010.

[10] Joris Sprakel, Stefan B Lindström, Thomas E Kodger, and David A Weitz. Stress enhancement in the delayed yielding of colloidal gels. *Physical Review Letters*, 106(24):248303, 2011.

[11] Gabriele Colombo, Sunhyung Kim, Thomas Schweizer, Bram Schroyen, Christian

Clasen, Jan Mewis, and Jan Vermant. Superposition rheology and anisotropy in rheological properties of sheared colloidal gels. *Journal of Rheology*, 61(5):1035–1048, 2017.

[12] Kasper Masschaele, Jan Fransaer, and Jan Vermant. Direct visualization of yielding in model two-dimensional colloidal gels subjected to shear flow. *Journal of Rheology*, 53(6):1437–1460, 2009.

[13] PA Smith, G Petekidis, SU Egelhaaf, and WCK Poon. Yielding and crystallization of colloidal gels under oscillatory shear. *Physical Review E*, 76(4):041402, 2007.

[14] Lilian C Hsiao, Richmond S Newman, Sharon C Glotzer, and Michael J Solomon. Role of isostaticity and load-bearing microstructure in the elasticity of yielded colloidal gels. *Proceedings of the National Academy of Sciences*, 2012.

[15] D Rocklin, Lilian C Hsiao, Megan Szakasits, Michael J Solomon, and Xiaoming Mao. Elasticity of colloidal gels: structural heterogeneity, foppy modes, and rigidity. *arXiv preprint arXiv:1808.01533*, 2018.

[16] Priya Varadan and Michael J Solomon. Direct visualization of flow-induced microstructure in dense colloidal gels by confocal laser scanning microscopy. *Journal of Rheology*, 47(4):943–968, 2003.

[17] Eric M Furst and John P Pantina. Yielding in colloidal gels due to nonlinear microstructure bending mechanics. *Physical Review E*, 75(5):050402, 2007.

[18] Myung Han Lee and Eric M. Furst. Response of a colloidal gel to a microscopic oscillatory strain. *Physical Review E*, 77:041408, Apr 2008.

[19] Bharath Rajaram and Ali Mohraz. Dynamics of shear-induced yielding and flow in dilute colloidal gels. *Physical Review E*, 84(1):011405, 2011.

[20] Hubert K Chan and Ali Mohraz. Two-step yielding and directional strain-induced strengthening in dilute colloidal gels. *Physical Review E*, 85(4):041403, 2012.

[21] Bharath Rajaram and Ali Mohraz. Microstructural response of dilute colloidal gels to nonlinear shear deformation. *Soft Matter*, 6(10):2246–2259, 2010.

[22] Benjamin J Landrum, William B Russel, and Roseanna N Zia. Delayed yield in colloidal gels: Creep, flow, and re-entrant solid regimes. *Journal of Rheology*, 60(4):783–807, 2016.

[23] Michael Kogan and Michael J Solomon. Electric-field-induced yielding of colloidal gels in microfluidic capillaries. *Langmuir*, 26(2):1207–1213, 2010.

[24] Jacinta C Conrad and Jennifer A Lewis. Structure of colloidal gels during microchannel flow. *Langmuir*, 24(15):7628–7634, 2008.

[25] Nick Koumakis, Esmaeel Moghimi, Rut Besseling, Wilson C. K. Poon, John F. Brady, and George Petekidis. Tuning colloidal gels by shear. *Soft Matter*, 11:4640–4648, 2015.

[26] HJ Walls, S Brett Caines, Angelica M Sanchez, and Saad A Khan. Yield stress and wall slip phenomena in colloidal silica gels. *Journal of Rheology*, 47(4):847–868, 2003.

[27] C. Patrick Royall, Jens Eggers, Akira Furukawa, and Hajime Tanaka. Probing colloidal gels at multiple length scales: The role of hydrodynamics. *Physical Review Letters*, 114:258302, Jun 2015.

[28] Michael P. Allen and Dominic J. Tildesley. Computer simulation of liquids. *Clarendon Press, Oxford*, 1987.

[29] Thomas E Kodger, Rodrigo E Guerra, and Joris Sprakel. Precise colloids with tunable interactions for confocal microscopy. *Scientific Reports*, 5:14635, 2015.

[30] Thomas E Kodger, Peter J Lu, G Reid Wiseman, and David A Weitz. Stable, fluorescent polymethylmethacrylate particles for the long-term observation of slow colloidal dynamics. *Langmuir*, 33(25):6382–6389, 2017.

[31] PN Pusey. The effect of polydispersity on the crystallization of hard spherical colloids. *Journal de Physique*, 48(5):709–712, 1987.

[32] PN Pusey, E Zaccarelli, C Valeriani, E Sanz, Wilson CK Poon, and Michael E Cates. Hard spheres: crystallization and glass formation. *Philosophical Transactions of the Royal Society A: Mathematical, Physical and Engineering Sciences*, 367(1909):4993–5011, 2009.

[33] Yongxiang Gao and Maria Kilfoil. Accurate detection and complete tracking of large populations of features in three dimensions. *Optics Express*, 17:4685–704, 04 2009.

[34] Ignacio Arganda-Carreras, Carlos OS Sorzano, Roberto Marabini, José María Carazo, Carlos Ortiz-de Solorzano, and Jan Kybic. Consistent and elastic registration of histolo-

gical sections using vector-spline regularization. In *International Workshop on Computer Vision Approaches to Medical Image Analysis*, pages 85–95. Springer, 2006.
[35] Esmaeel Moghimi, Alan R Jacob, Nick Koumakis, and George Petekidis. Colloidal gels tuned by oscillatory shear. *Soft Matter*, 13(12):2371–2383, 2017.
[36] Jun Dong Park, Kyung Hyun Ahn, and Seung Jong Lee. Structural change and dynamics of colloidal gels under oscillatory shear flow. *Soft Matter*, 11(48):9262–9272, 2015.
[37] Alessio Zaccone, Daniele Gentili, Hua Wu, Massimo Morbidelli, and Emanuela Del Gado. Shear-driven solidification of dilute colloidal suspensions. *Physical Review Letters*, 106(13):138301, 2011.
[38] Jan Maarten van Doorn, Joanne E Verweij, Joris Sprakel, and Jasper van der Gucht. Strand plasticity governs fatigue in colloidal gels. *Physical Review Letters*, 120(20):208005, 2018.
[39] Joanne E Verweij, Frans AM Leermakers, Joris Sprakel, and Jasper Van Der Gucht. Plasticity in colloidal gel strands. *Soft Matter*, 15(32):6447–6454, 2019.

Appendix

On the next few pages the additional figures from the appendix can be found.

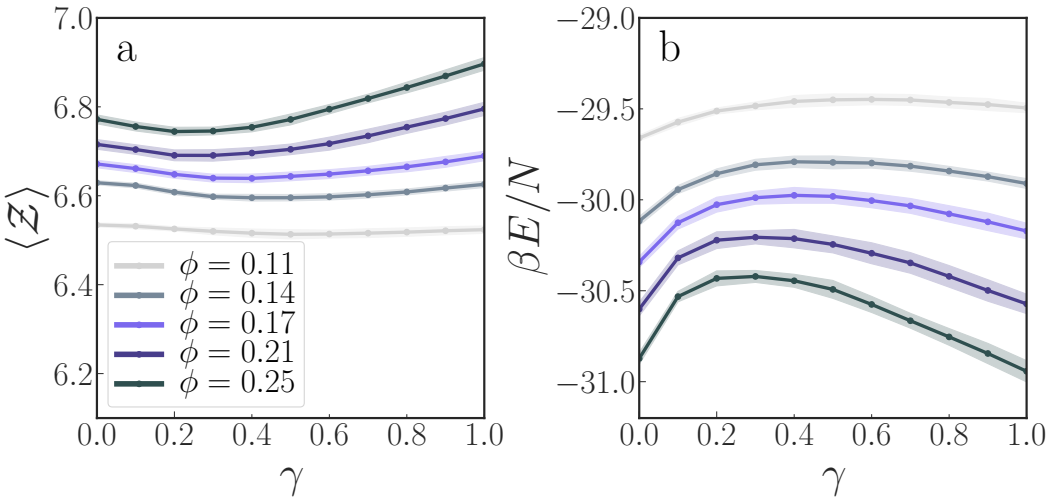

Figure A5.1 – Simulation data for 10 k_BT at a strain from 0 - 1.0 γ. (a) Average number of nearest neighbours $\langle z \rangle$ of the full colloidal gel structure versus strain. (b) Energy E per particle N in the system as a function of strain.

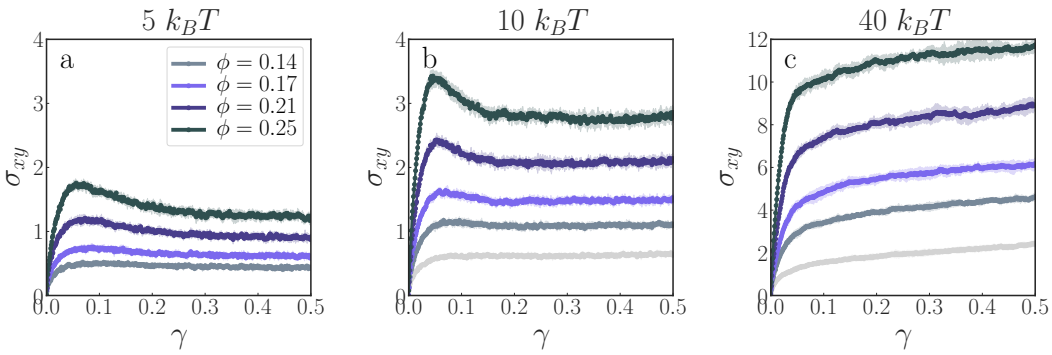

Figure A5.2 – Stress versus strain curves at different interaction energies and volume fractions. Note that the y-axis of plot c is larger than for plot a and b.

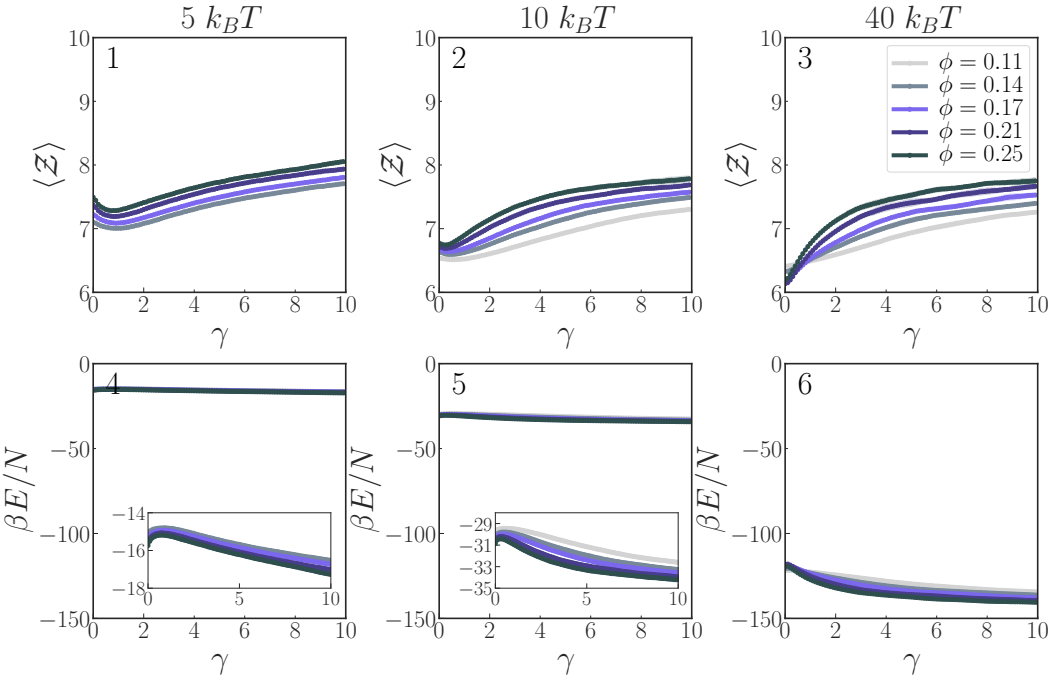

Figure A5.3 – Simulation data for different interaction strengths $\beta\epsilon$ (Upper row, 1-3) Average number of nearest neighbours $\langle Z \rangle$ of the full colloidal gel structure versus strain. (Lower row, 4-6) Energy E per particle N in the system as a function of strain.

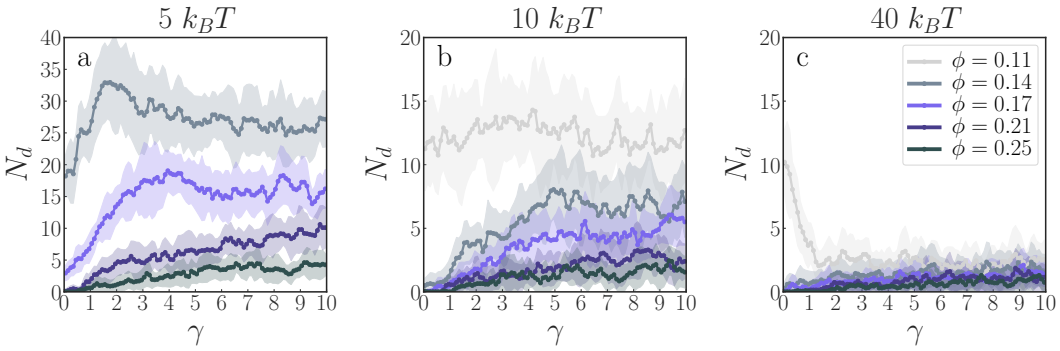

Figure A5.4 – The number of dangling ends N_b obtained during reduction of the network structure. Note that after complete reduction of the gels (see Fig. 2 main text) dangling ends are absent in the obtained network topologies. A volume fraction of $\phi = 0.11$ at 5 k_BT does not give a fully percolated structure and is therefore not analysed. In plot a) the y-axis is larger than for the other plots.

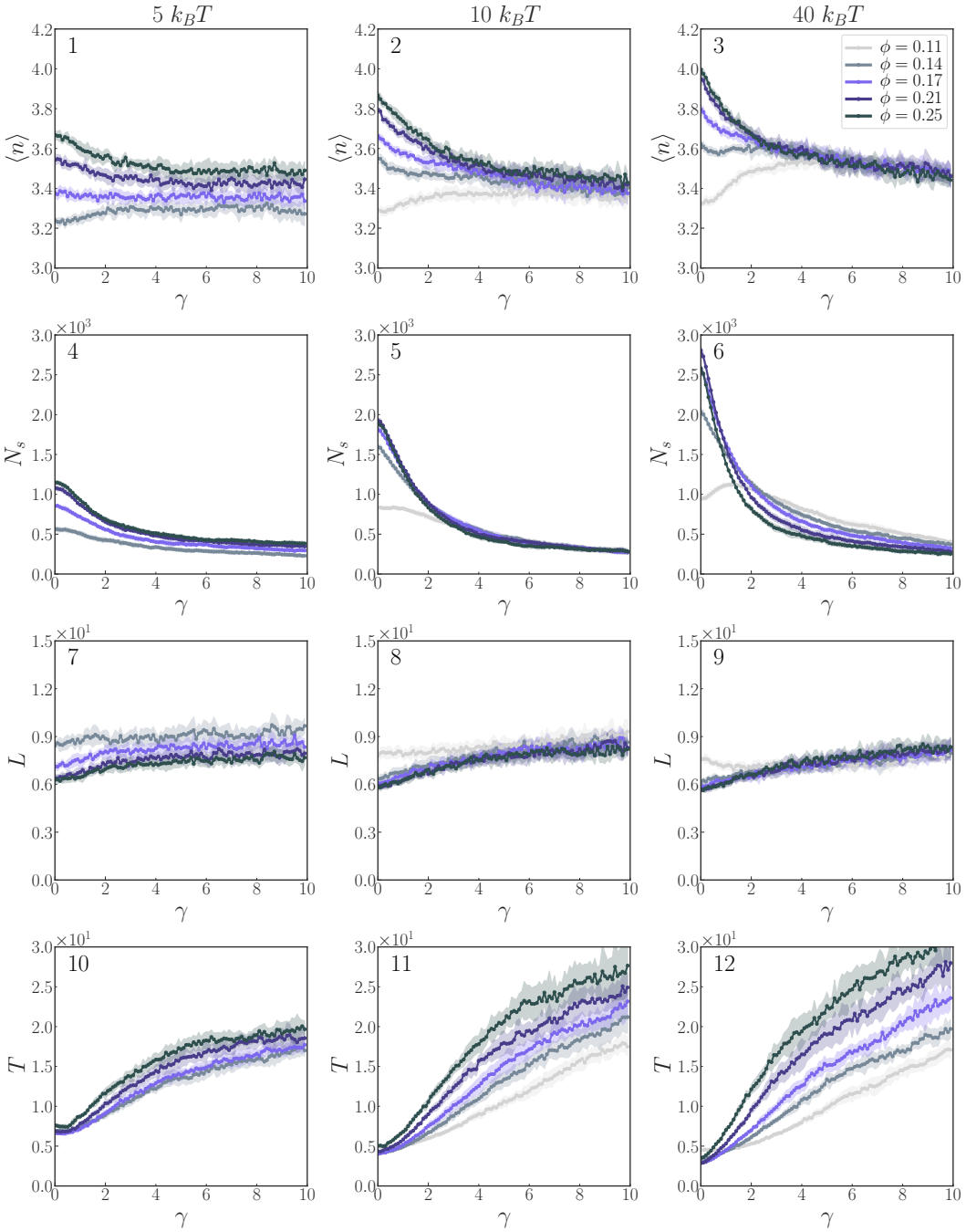

Figure A5.5 – Simulation data for different interaction strengths $\beta\epsilon$. First row (1-3): The average coordination number $\langle n \rangle$ for the nodes in the network as a function of deformation γ. Second row (4-6): Number of segments in the network. Third row (7-9): Length of the segments. Fourth row (10-12): Thickness of the segments.

Anomalous large-scale motion during the gravitational collapse of colloidal gels

6

Using confocal microscopy, we study the gravitational collapse of colloidal gels in three dimensions at the single-particle level. After a short delay time, the colloidal gels are observed to detach from the top of the sample, and a macroscopic interface emerges. The sedimentation dynamics of this interface are governed by poroelastic compression of the gel that lies beneath. Large-scale collective motions in the direction perpendicular to the gravitational field, induced by internal stresses in the gel, lead to shear deformation in the network that accelerates gel failure. These motions are present both during the induction period and the subsequent rapid-settling stage of the gel, and subside as the gel reaches its final height. These results highlight that not only external gravitational stresses, but also internal stresses in the network play a crucial role in the failure of these heterogeneous networks.

Joanne E. Verweij[*1,2], Berend van der Meer[*2], Taiki Yanagishima[2], Jasper van der Gucht[1], Joris Sprakel[1] & Roel P.A. Dullens[2]

"Anomalous large-scale motion during the gravitational collapse of colloidal gels"
In preparation (2020)

[*] *These authors contributed equally.*
[1] *Physical Chemistry and Soft Matter, Wageningen University, Wageningen, 6708 WE, The Netherlands.*
[2] *Department of Chemistry, Physical and Theoretical Chemistry Laboratory, University of Oxford, South Parks Road, Oxford OX1 3QZ, United Kingdom*

Introduction

Suspensions of attractive colloidal particles form space-spanning, fractal networks at relatively low volume fractions [1]. These arrested gels, whose elastic properties are determined by the structure and connectivity of the network [2], find applications in many food and personal care products. As such, understanding the (in)stability of these networks to both internal and external stresses, such as shear or gravity, is crucial to control the stability of these complex materials.

One striking example of an instability in particle gels is the collapse of the gel network due to gravity; a general phenomenon observed in a wide range of materials and at different interaction strengths [3–6]. Depending on the strength and range of the attraction between the particles, two different types of gravitational collapse can be distinguished. Namely, the gel collapse can either be immediate and steady [5, 7, 8] or "delayed", where no macroscopic sedimentation is observed up to a characteristic delay period [3, 4, 8–13]. This delayed collapse consists of three stages [3, 5, 14], starting with a slow induction process that suddenly gives way to a rapid-sedimentation regime, followed by a stage where the structure slowly densifies.

To date, most experimental studies have examined the gel collapse at a macroscopic level [3–5, 7–13, 15–17], for example by following the top of the collapsing gel in time through direct observation or via light scattering techniques. These studies have been instrumental in acquiring a basic understanding of the role of various system properties on the gel collapse – such as strength and range of the attraction, particle volume fraction, the degree of density-(mis)matching, and the initial height of the gel. Several structural changes have been identified during the collapse of these gels, including the breakup of the network into clusters [3, 11, 15], and the formation of channels, so-called "streamers" and "volcanoes" [5, 18]. The formation of all these features are understood to play a role in expelling fluid from the gel [3, 5, 18, 19]. Furthermore, the sedimentation of the gel can be accurately captured by a poroelastic model [9, 20]. Yet, a major limitation of this description is that it does not provide insight into the microscopic dynamics of the gel structure.

The microscopic details of gel collapse have primarily been investigated in simulations [14, 19, 21], and to a limited extent in experiments using confocal microscopy [3, 4, 22]. Importantly, confocal microscopy studies have identified that the gel coarsens through rupture and reassocation events of gel strands in the network prior to collapse [3]. Yet, a direct connection between single-particle dynamics and changes in the network structure at

different length scales during gel collapse remains largely unexplored. Besides, the interplay between internal and external stresses in the failure of colloidal gels has not been given much attention so far.

In this work, we follow the gravitational collapse of colloidal gels in three dimensions at the single-particle level using confocal microscopy. After a short delay time, the colloidal gel detaches from the top of the sample, and a macroscopic interface emerges. The evolution of the height of the gel is well-described by the poroelastic model. Analysis of the network topology reveals that strands become significantly longer in the top region of the sample while strands at the bottom become shorter due to the densification of the gel network. Interestingly, large-scale displacements, perpendicular to the direction of gravity, are observed to affect the gel structure and enhance failure, both during the induction period and the rapid-sedimentation regime. This suggests that the gravitational force on the gel leads to an imbalance of internal stresses in the network, which causes a perpendicular shear-like motion. We hypothesize this imbalance to originate from the gel collapsing at slightly different rates at different locations within the sample.

Methods

Fluorescent tFEMA-tBMA core-shell particles are synthesized according to the method described in Ref. [23]. The exact synthesis protocol for these particles can be found in Chapter 5. The diameter of the synthesized particles is measured using Dynamic Light Scattering and equals σ = 1.84 μm. The advantage of this particle system is that density and index matching can be reached simultaneously using non-hazardous polar solvents. The excellent index matching makes it possible to image colloidal gels over the entire height of a 100 μm sample chamber, using confocal microscopy.

Colloidal gels are prepared for a range of volume fractions ϕ_s = 0.12-0.18. To induce depletion attraction 2.4 mg/mL polyethylene oxide is added (PEO, M_w 2.31 $\times$ 10^5, M_n 2.03 $\times$ 10^5, R_g = 23.1 nm, c^* = 7.5 mg/mL). The core-shell particles are suspended in 2,2 thiodiethanol:Milli-Q, 70:30, containing 10mM of NaCl to screen electrostatic interactions.

To induce gravitational collapse within a reasonable time span, the solvent in the samples has a slight density mismatch. The gravitational length is extracted from the equilibrium density profile of a dilute sample without depletant. Specifically, after a sedimentation-equilibrium is established the tail of the density profile was fitted using:

$$\rho(z) = \rho(0)\exp(-z/l_g) \tag{6.1}$$

from which the gravitational length l_g=10 μm was extracted. This corresponds to a Péclet number of $Pe = \sigma/2l_g \approx 0.1$ [21].

A rectangular capillary (0.10 × 2.00 mm, Vitrocom) is filled with sample and sealed using Norland Optical Adhesive 63 UV curable glue. Subsequently, the sample is rotated for half an hour on a mini-rotator (PTR-25, Grant Bio). This allows for the formation of a gel where the effect of gravity is essentially averaged out. After rotation, the sample is placed on an inverted confocal microscope to image the gel collapse. To follow the gravitational collapse in time, a Z-stack is made every 10 minutes for a period of 15 hours up to 60 hours. For each sample at least two independent measurements are taken. The confocal consists of a Thorlabs confocal 12kHz resonant point scanner mounted on an Olympus IX73 microscope with an 60× oil immersion Olympus Plan Apochromat objective (NA = 1.42).

Particles are located using the Matlab implementation of the locating algorithm of Gao and Kilfoil [24]. We determine the complete network topology of the gel from the three-dimensional coordinates of all particles in our field-of-view as described in Chapter 4. In short, this is done by deleting particles in the gel structure that are not essential to maintain the overall network connectivity. For each particle, its neighbours up to 5 generations are determined. If deleting a particle will split the cluster of neighbouring particles, this particle cannot be removed. After additional simplification steps, the final structure contains segments and nodes (see Fig. 6.3). This allows for the quantification of the connectivity of the network and the number and length of the segments.

Results and discussion

We study the microscopic structure of colloidal gels during gravitational collapse using three-dimensional confocal microscopy. A three-dimensional reconstruction and various projections of the raw confocal image data are shown in Fig. 6.1, at three different moments in time (sample ϕ_s = 0.153). From these data, we observe the formation of a macroscopic interface as the top of the capillary is depleted by colloids. In the remainder of this chapter we will refer to this interface between the gel and the colloid-poor supernatant as the gel interface.

To investigate the collapse of the gel and the emergence of the gel interface, we plot the local volume fraction ϕ as function of height Z at various times in Fig. 6.2a. Clearly, the local volume fraction at the top of the capillary rapidly decreases, whereas the local volume fraction at the bottom of the capillary increases. This displays the formation of three distinct zones; a

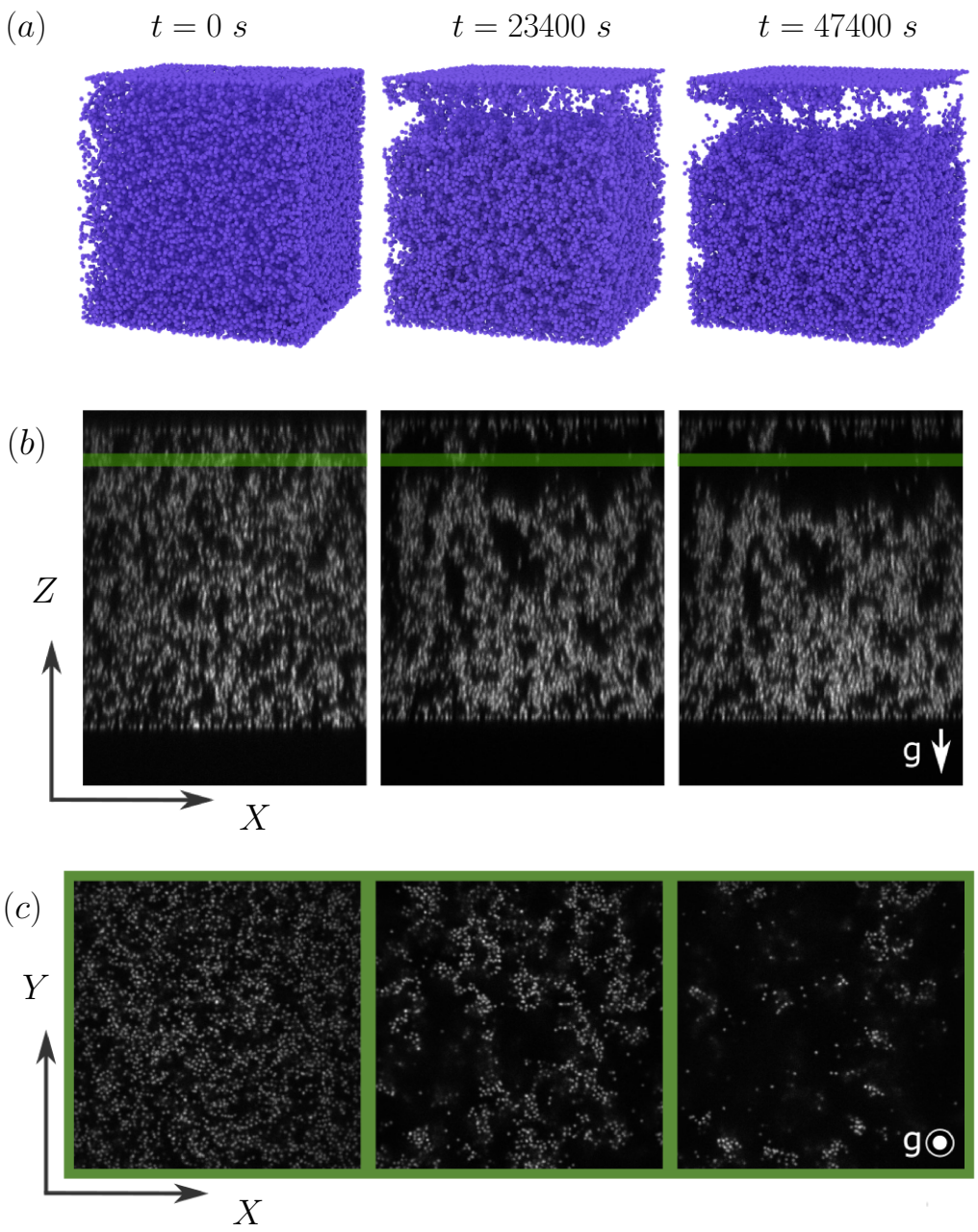

Figure 6.1 – Gravitational collapse of a colloidal gel (ϕ_s = 0.153, c = 2.4 mg/mL). A total sample volume of 102 μm x 102 μm x 100 μm is imaged (XYZ). a) Three-dimensional visualization of experimental data at three different times b) Corresponding XZ representation of confocal microscopy data (projection of Y = 49-53 μm). The highlighted area shows the position of the XY data in subplot c. c) Corresponding XY representation of the experimental data (projection of Z = 88-92 μm).

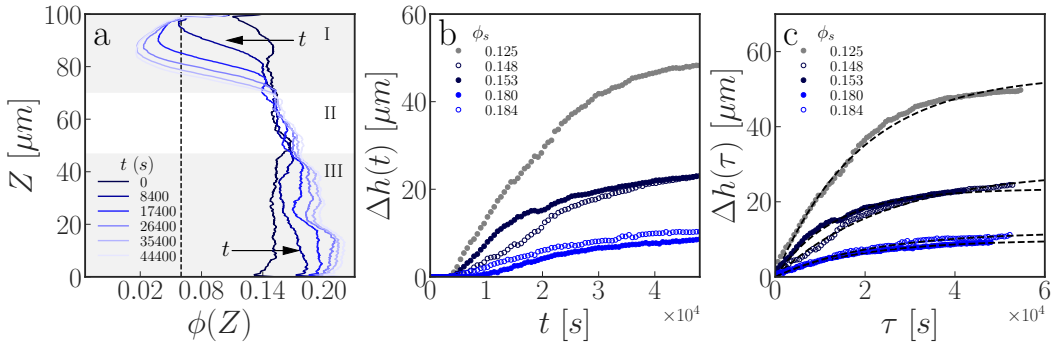

Figure 6.2 – a) The local volume fraction ϕ as a function of Z in time ($\phi_s = 0.153$, $c = 2.4$ mg/mL). The dotted line indicates the cutoff used to determine the height of the interface. The shaded areas indicate (I) the colloid-poor zone, (II) the falling or non-compressing zone, (III) the densifying zone. b) Change in height of the gel interface in time for different samples. Here, $\Delta h(t) = h(0) - h(t)$. Markers with the same color correspond to samples taken from the same mixture of particles, polymer and solvent. c) Change in height of the interface shifted by the delay time τ_D ($\tau = t - \tau_D$ on the x-axis). The data is fitted by the exponential poroelastic model (black dotted lines).

colloid-poor region at the top, a falling, non-compressing zone in the middle, and a densifying zone at the bottom of the sample cell (see Fig. 6.2a), which is in good agreement with previous studies [13–15, 25]. The evolution of the local volume fraction ϕ indicates how failure takes place at the top of the sample cell, whereas the bottom of the sample densifies.

To quantify the position of the gel interface, we make use of the height detection algorithm described in Ref. [14]. Specifically, the colloidal gel is divided into columns which span 30 μm x 30 μm in the X- and Y-direction and the entire height of the sample ($\approx 100\ \mu m$) in the Z-direction. The local height of the interface for each column is then taken to be the height where the local volume fraction becomes lower than ϕ = 0.06. At this volume fraction the gel is not assumed to percolate anymore. The global interface height is taken as the average over all local interface heights of the different columns. In this way, the interface height of the gel can be assessed during the gravitational collapse. In Fig. 6.2b, we plot the change in height of the interface $\Delta h(t) = h(0) - h(t)$ as a function of time, for a range of samples. Evidently, the collapse of the gel is "delayed" as it takes a while before the interface of the gel starts to decrease in height. In general, the delay time τ_D before the sudden collapse becomes longer with increasing volume fraction (see Fig. A6.1b). Additionally, the amount by which the height of the gel is reduced becomes lower at higher volume fractions. This is in good agreement with prior macroscopic investigations where the height of the gel interface was studied in vials [3, 9, 13].

Interestingly, we observe that while the rate of collapse is initially fast, a distinct slowing down of the sedimentation occurs over time, which leads to

a clear plateau in height of the gel. Previous studies of the height of macroscopic gel interfaces have revealed that at short times the rate of gel collapse is limited by the rate at which fluid is expelled from the network, while at longer times the gel height is determined by a balance between the network elasticity and the gravitational stress. Within this context, the height of the gel over time can be well-described by the theory of poroelasticity [9]. To test the validity of this approach, we plot the height of the gel after rescaling the time with respect to the delay time, i.e. $\tau = t - \tau_D$. For all data, the rescaled time evolution of the height is described by the exponential poroelastic model, as shown in Fig. 6.2c:

$$\Delta h(\tau) = \Delta h_f(1 - \exp(-\tau/\tau_p)) \tag{6.2}$$

with Δh_f the total change in height, and τ_p the poroelastic timescale, which among others depends on the solvent viscosity, permeability and modulus of the gel [9]. This suggests that the gravitational stress in first instance is balanced by the stress due to fluid flow. Subsequently, the gravitational stress is balanced by the elasticity of the network when the height of the gel approaches a plateau.

Even though for individual samples the height of the gel can be described by the poroelastic model, the height evolution between experiments show quite some variation – even when the collapse of a gel is measured twice from the same mixture of solvent, particle and polymer composition (see Fig. A6.1a). There are two reasons which could account for this observation. Firstly, as the added polymer stock is viscous, it is to be expected that the polymer concentration between samples of different volume fractions deviates slightly. It is well known that lower attraction strengths correspond to a faster collapse and permit denser compaction [11, 12, 14]. Indeed, the change in height of the interface for samples with a higher amount of polymer (c_p = 2.8 mg/mL, see Fig. A6.1c) show a slower compaction in time. This implicates that a small error in the amount of polymer between samples with different volume fractions can give rise to changes in the time-dependent interface height. Another explanation for the observed statistical differences could be that the interface is heterogeneous. In other words, at different locations within the sample the gel may collapse at slightly different rates. To check this, the interface after collapse could be measured at different positions in the same capillary.

To study the gravitational collapse at the microscopic level, we determine the network topology of the gel using the method described in Chapter 4. A plot of the gel network at different times, color-coded by the segment length, is shown in Fig. 6.3. Clearly, the gel starts to fail at the top of the sample where the segment density of the network decreases and segments elongate. Meanwhile, the segment density at the bottom part of the network increases and segments become shorter. We quantify this observation by plotting the average segment length as function of the height Z in Fig. 6.4a.

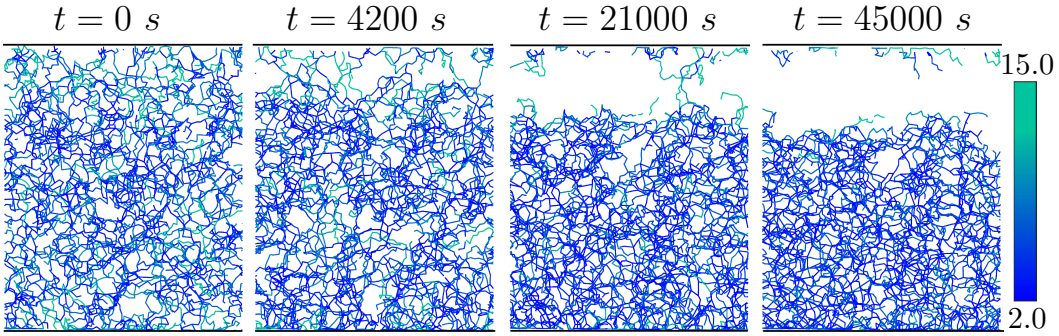

Figure 6.3 – The network topology of a colloidal gel during gravitational collapse ($\phi_s = 0.153$, $c = 2.4$ mg/mL, settings network topology: $G_n = 5$, $C = 1.3\ \sigma$, $\Delta r = 1.3\ \sigma$ [see Chapter 4]). The visualization shows a XZ projection of the gel (Y = 40-80 μm). The segments in the network are color-coded from blue to green according to their respective length in micron, as indicated by the color bar.

During the collapse, gel strands become significantly longer in the top region of the sample while gel strands at the bottom become shorter due to densification of the network. Likewise, a plot of the average number of strands N_s^* intersecting a plane at a height Z reveals a gradual breakdown of the network at the top region of the sample and an increase in segments at the bottom. As expected, we thus observe a similar evolution for the segment density and the volume fraction (Fig. 6.4b and Fig. 6.2a).

The clear distinction between the colloid-poor, falling, and densification regions of the gel becomes very apparent when the key parameters of the network topology are plotted for four different slabs (as shown in see Fig. 6.4c). During the collapse, gel strands become longer at the top part of the sample, and a significant reduction in the connectivity of the gel occurs (Fig. 6.4d-f). Simultaneously, this leads to an increased network connectivity at the bottom of the gel, where strands get shorter.

Strikingly, during gravitational collapse the gel structure moves significantly in the direction perpendicular to gravity, as shown in Fig. 6.5. This motion is observed for all samples (see Fig. A6.2). To investigate these anomalous motions, which are perpendicular to the direction of gravity, we quantify these displacements in three dimension using non-rigid image alignment between sequential Z-stacks [26, 27]. The observed motion is split up in the vector components in the X-, Y- and Z-direction and plotted in time (see Fig. 6.5). The movement is mainly observed in the X-direction, which corresponds to the long axis of the capillary. This suggests that the network does not only undergo a external stress due to gravity, but that there are also internal stresses at play. From the displacements in the XY plane we are unable to extract a correlation length, as clearly the displacements are correlated over a distance larger than our field of view (see Fig. 6.5c).

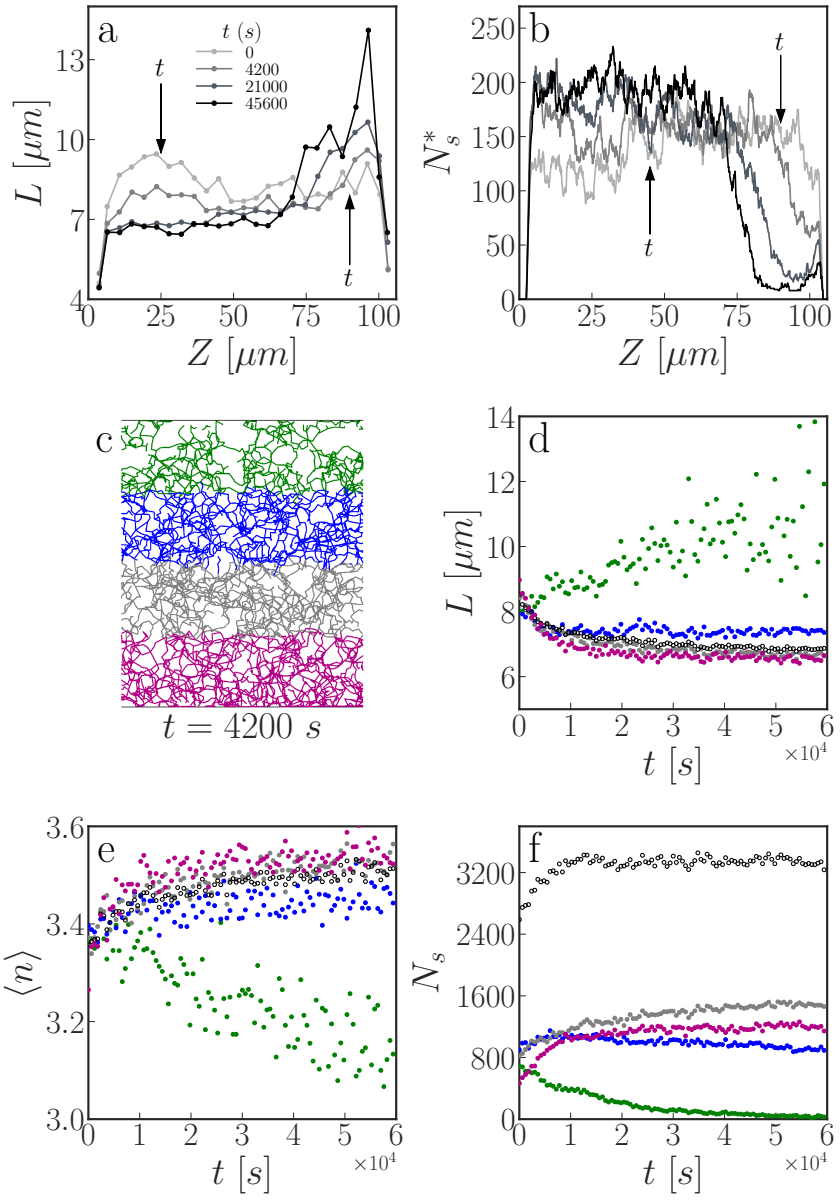

Figure 6.4 – Quantification of the network topology of a colloidal gel during gravitational collapse ($\phi_s = 0.148$, $c = 2.4$ mg/mL). a) Segment length as a function of the height of the gel. The segment length profile is shown in time (from light to dark), indicated by the arrows. b) The number of segments as a function of the height of the gel. Here, N_s^* is the number of segments crossing this specific Z-height. The number of segments are plotted in time (from light to dark). c) Visualization of the segments in the network structure. The colors indicate 4 different slabs in the gel. Parameters in subplot d, e and f are plotted based on these slabs. Subplot d), e) and f) show the length of the segments, connectivity of the network and number of segments in time. The different colors correspond to the slabs indicated in subplot c). The black open markers indicate the average of these parameters over the whole gel.

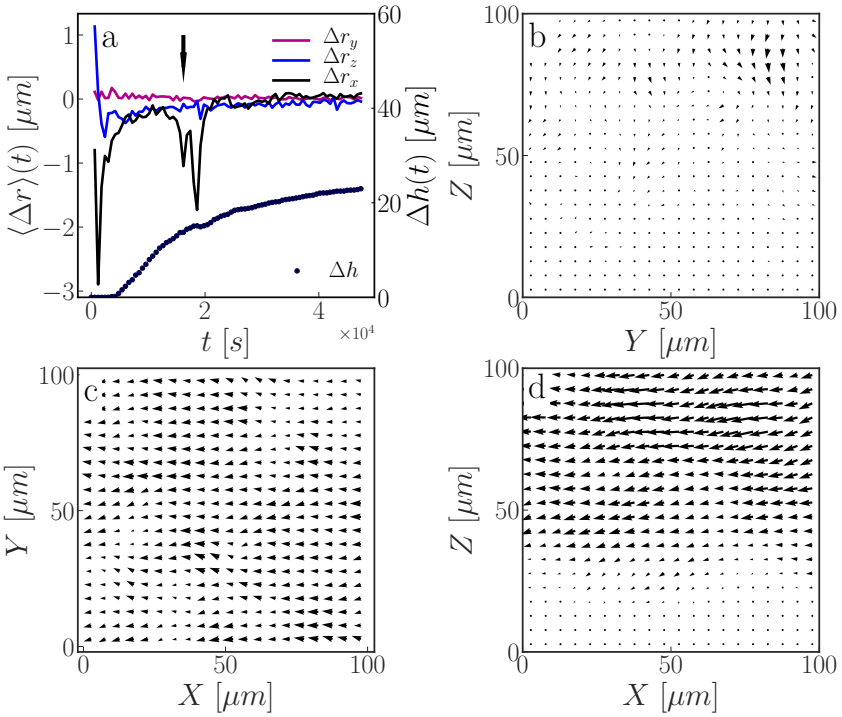

Figure 6.5 – a) The average displacement Δr of a colloidal gel ($\phi_s = 0.153$), split up in the vector components in the X,Y and Z direction. The arrow indicates the time point of subplots b,c and d ($t = 16200$ seconds). The second y-axis indicates the time-dependent height of this sample in time (closed markers). b) Vector plot of YZ displacements (X = 63 μm) c) Vector plot of XY displacements (Z = 43 μm) d) Vector plot of XZ displacements (Y = 63 μm). All vectors are scaled with factor 2.0.

Importantly, these motions are observed during both the induction period and the subsequent rapid-settling of the gel, but subside as the gel reaches its final height (see Fig. 6.5a). Note that we have checked that this motion does not arise due to mechanical drift of the sample as a whole. This is verified by the fact that both particles at the top and bottom of the capillary stay stationary in time.

This of course raises the question as to what may be the origin of these large perpendicular motions. We hypothesize that these shear-like motions arise due to the gel collapsing at slightly different rates at different locations within the sample. Namely, if the gel collapses locally it will create regions of high deformation within the sample. Due to the elasticity of the gel network these localized "micro-collapses" are expected to create a large-scale elastic deformation field. When the gel collapses slightly faster in one region of the sample compared to a neighboring region, we expect the downward motion

of this region to exert a sideways pull on the other region, essentially dragging it down. Note that the emergence of large-scale motion, arising from elastic relaxation of heterogeneous internal stresses, has been explored in various studies [3, 28–32], yet so far, such anomalous motion has not been observed directly on the single-particle level.

Conclusions

In this Chapter, we have studied the gravitational collapse of colloidal gels in three dimensions on the single-particle level using confocal microscopy. After a short delay time, the colloidal gel detaches from the top of the sample, and a macroscopic interface emerges. The evolution of the height of the gel is captured by the poroelastic model.

Our analysis of the gel network reveals that gel strands at the top of the sample get significantly longer during the collapse of gel. This raises the interesting question whether segments become longer due to fracture [33] of side branches or because strands start to unwind and thus elongate [34, 35]. Furthermore, large-scale simulations pointed out that particles moving from strands to junctions may trigger the onset of rapid collapse [14]. It would therefore be informative to study what type of particle dynamics are responsible for the observed changes at the top of the sample. We plan to study the dynamics of these particles by taking very fast Z-stacks in the top region of the sample.

Furthermore, variations in the time-dependent local height of the gel are observed between similar samples – even when taking great care to ensure similar solvent, particle and polymer composition. We hypothesize that these variations originate from the gel interface being heterogeneous, i.e. the interface might be much higher in certain regions of the sample than others. An observation indicative of these inhomogeneities are the large-scale horizontal motions observed during the collapse. We speculate that this motion arises from the gel collapsing at slightly different rates at different locations within the sample. Due to the elasticity of the gel network these localized "micro-collapses" are expected to create a large-scale elastic deformation field. A simple experiment that can test our hypothesis would be to quantify the interface height at different positions within the same sample.

The emergence of large-scale elastic motion, due to the elastic relaxation of heterogeneous internal stresses, has been explored in various studies [3, 28–31]. Recent research shows how the increased microscopic dynamics of a gel under mechanical load weakens a gel network thousands of seconds before its macroscopic failure [36]. Furthermore, concurrence of spatially localized

microquakes with system-spanning macroquakes was reported for colloidal gels during aging [31]. This suggests that the observed motion during the collapse of colloidal gels is a general phenomenon in the course of colloidal gel failure.

Acknowledgements

This work was carried out in collaboration with Berend van der Meer. Taiki Yanagishima provided technical support with the confocal microscope. This research has been performed in the group of Roel Dullens (Physical and Theoretical Chemistry Laboratory at the University of Oxford).

Bibliography

[1] Peter J Lu and David A Weitz. Colloidal particles: crystals, glasses, and gels. *Annual Review of Condensed Matter Physics*, 4(1):217–233, 2013.

[2] AD Dinsmore, V Prasad, IY Wong, and DA Weitz. Microscopic structure and elasticity of weakly aggregated colloidal gels. *Physical Review Letters*, 96(18):185502, 2006.

[3] Paul Bartlett, Lisa J Teece, and Malcolm A Faers. Sudden collapse of a colloidal gel. *Physical Review E*, 85(2):021404, 2012.

[4] Maria L Kilfoil, Eugene E Pashkovski, James A Masters, and DA Weitz. Dynamics of weakly aggregated colloidal particles. *Philosophical Transactions of the Royal Society of London. Series A: Mathematical, Physical and Engineering Sciences*, 361(1805):753–766, 2003.

[5] Laura Starrs, WCK Poon, DJ Hibberd, and MM Robins. Collapse of transient gels in colloid-polymer mixtures. *Journal of Physics: Condensed Matter*, 14(10):2485, 2002.

[6] Nynke AM Verhaegh, Daniela Asnaghi, and Henk NW Lekkerkerker. Transient gels in colloid–polymer mixtures studied with fluorescence confocal scanning laser microscopy. *Physica A: Statistical Mechanics and its Applications*, 264(1-2):64–74, 1999.

[7] C Allain, M Cloitre, and M Wafra. Aggregation and sedimentation in colloidal suspensions. *Physical Review Letters*, 74(8):1478, 1995.

[8] Chanjoong Kim, Yaqian Liu, Angelika Kühnle, Stephan Hess, Sonja Viereck, Thomas Danner, L Mahadevan, and David A Weitz. Gravitational stability of suspensions of attractive colloidal particles. *Physical Review Letters*, 99(2):028303, 2007.

[9] Suliana Manley, JM Skotheim, L Mahadevan, and David A Weitz. Gravitational collapse of colloidal gels. *Physical Review Letters*, 94(21):218302, 2005.

[10] V Gopalakrishnan, Kenneth S Schweizer, and CF Zukoski. Linking single particle rearrangements to delayed collapse times in transient depletion gels. *Journal of Physics: Condensed Matter*, 18(50):11531, 2006.

[11] Stephen W Kamp and Maria L Kilfoil. Universal behaviour in the mechanical properties of weakly aggregated colloidal particles. *Soft Matter*, 5(12):2438–2447, 2009.

[12] JJ Liétor-Santos, C Kim, PJ Lu, A Fernandez-Nieves, and DA Weitz. Gravitational compression of colloidal gels. *The European Physical Journal E*, 28(2):159–164, 2009.

[13] Rim Harich, TW Blythe, Michiel Hermes, Emanuela Zaccarelli, AJ Sederman, Lynn F Gladden, and Wilson CK Poon. Gravitational collapse of depletion-induced colloidal gels. *Soft Matter*, 12(19):4300–4308, 2016.

[14] Poornima Padmanabhan and Roseanna Zia. Gravitational collapse of colloidal gels: non-

equilibrium phase separation driven by osmotic pressure. *Soft Matter*, 14(17):3265–3287, 2018.

[15] Eleonora Secchi, Stefano Buzzaccaro, and Roberto Piazza. Time-evolution scenarios for short-range depletion gels subjected to the gravitational stress. *Soft Matter*, 10(29):5296–5310, 2014.

[16] Theo BJ Blijdenstein, Erik van der Linden, Ton van Vliet, and George A van Aken. Scaling behavior of delayed demixing, rheology, and microstructure of emulsions flocculated by depletion and bridging. *Langmuir*, 20(26):11321–11328, 2004.

[17] Ji Yeon Huh, Matthew L Lynch, and Eric M Furst. Microscopic structure and collapse of depletion-induced gels in vesicle-polymer mixtures. *Physical Review E*, 76(5):051409, 2007.

[18] C Derec, D Senis, L Talini, and C Allain. Rapid settling of a colloidal gel. *Physical Review E*, 67(6):062401, 2003.

[19] Zsigmond Varga, Jennifer L Hofmann, and James W Swan. Modelling a hydrodynamic instability in freely settling colloidal gels. *Journal of Fluid Mechanics*, 856:1014–1044, 2018.

[20] Giovanni Brambilla, Stefano Buzzaccaro, Roberto Piazza, Ludovic Berthier, and Luca Cipelletti. Highly nonlinear dynamics in a slowly sedimenting colloidal gel. *Physical Review Letters*, 106(11):118302, 2011.

[21] Azaima Razali, Christopher J Fullerton, Francesco Turci, James E Hallett, Robert L Jack, and C Patrick Royall. Effects of vertical confinement on gelation and sedimentation of colloids. *Soft Matter*, 13(17):3230–3239, 2017.

[22] Lisa J Teece, Malcolm A Faers, and Paul Bartlett. Ageing and collapse in gels with long-range attractions. *Soft Matter*, 7(4):1341–1351, 2011.

[23] Thomas E Kodger, Rodrigo E Guerra, and Joris Sprakel. Precise colloids with tunable interactions for confocal microscopy. *Scientific Reports*, 5:14635, 2015.

[24] Yongxiang Gao and Maria Kilfoil. Accurate detection and complete tracking of large populations of features in three dimensions. *Optics Express*, 17:4685–704, 04 2009.

[25] Richard Buscall and Lee R White. The consolidation of concentrated suspensions. part 1.—the theory of sedimentation. *Journal of the Chemical Society, Faraday Transactions 1: Physical Chemistry in Condensed Phases*, 83(3):873–891, 1987.

[26] Jean-Philippe Thirion. Image matching as a diffusion process: an analogy with maxwell's demons. 1998.

[27] Tom Vercauteren, Xavier Pennec, Aymeric Perchant, and Nicholas Ayache. Diffeomorphic demons: Efficient non-parametric image registration. *NeuroImage*, 45(1):S61–S72, 2009.

[28] Luca Cipelletti, Suliana Manley, RC Ball, and DA Weitz. Universal aging features in the restructuring of fractal colloidal gels. *Physical Review Letters*, 84(10):2275, 2000.

[29] J-P Bouchaud and E Pitard. Anomalous dynamical light scattering in soft glassy gels. *The European Physical Journal E*, 6(3):231–236, 2001.

[30] Luca Cipelletti, Laurence Ramos, Suliana Manley, Estelle Pitard, David A Weitz, Eugene E Pashkovski, and Marie Johansson. Universal non-diffusive slow dynamics in aging soft matter. *Faraday Discussions*, 123:237–251, 2003.

[31] Zeno Filiberti, Roberto Piazza, and Stefano Buzzaccaro. Multiscale relaxation in aging colloidal gels: From localized plastic events to system-spanning quakes. *Physical Review E*, 100(4):042607, 2019.

[32] Luca Cipelletti, Kirsten Martens, and Laurence Ramos. Microscopic precursors of failure in soft matter. *Soft Matter*, 16(1):82–93, 2020.

[33] Mathieu Leocmach, Christophe Perge, Thibaut Divoux, and Sébastien Manneville. Creep and fracture of a protein gel under stress. *Physical Review Letters*, 113(3):038303, 2014.

[34] Jan Maarten van Doorn, Joanne E Verweij, Joris Sprakel, and Jasper van der Gucht. Strand plasticity governs fatigue in colloidal gels. *Physical Review Letters*, 120(20):208005, 2018.

[35] Joanne E Verweij, Frans AM Leermakers, Joris Sprakel, and Jasper Van Der Gucht. Plasticity in colloidal gel strands. *Soft Matter*, 15(32):6447–6454, 2019.

[36] Stefano Aime, Laurence Ramos, and Luca Cipelletti. Microscopic dynamics and failure

precursors of a gel under mechanical load. *Proceedings of the National Academy of Sciences*, 115(14):3587–3592, 2018.

Appendix

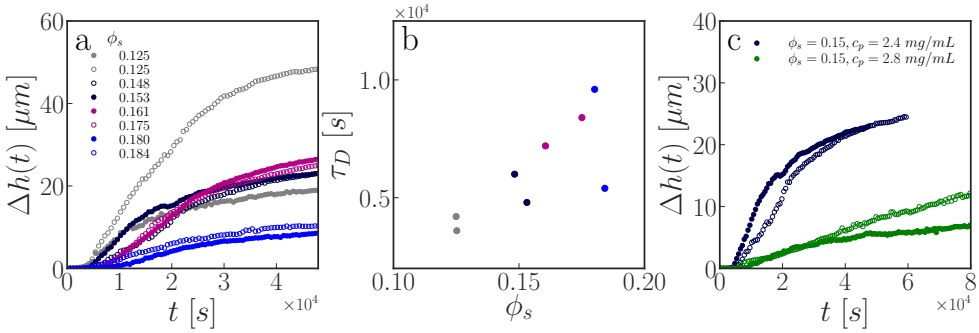

Figure A6.1 – a) All height profiles of samples at different volume fraction ϕ (c_p = 2.4 mg/mL). b) Delay time τ_D before gravitational collapse. c) Height profiles of samples at a polymer concentration c_p of 2.4 and 2.8 mg/mL, with a volume fraction of $\phi = 0.15$.

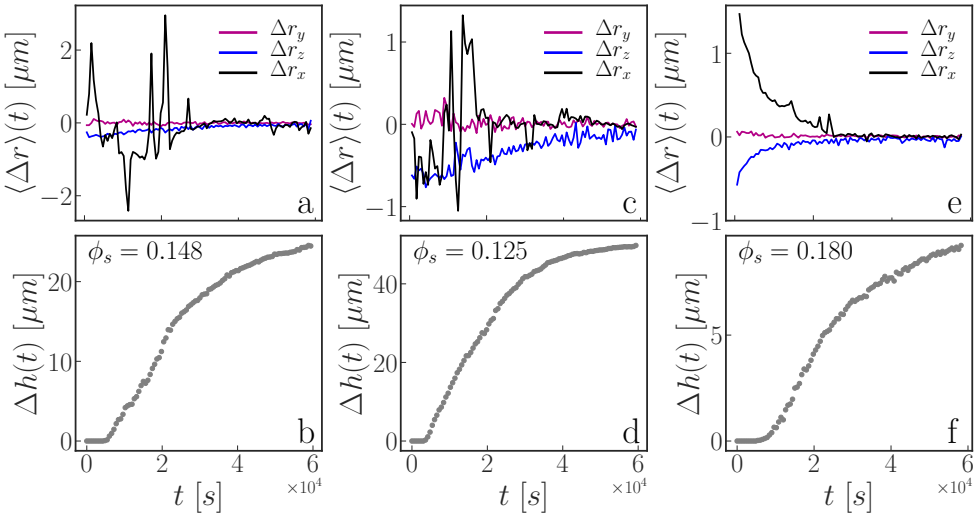

Figure A6.2 – The average displacement Δr of colloidal gels during gravitational collapse, split up in the vector components in the X,Y and Z direction. a) $\phi = 0.148$, with the height profile of this sample in subplot b. c) $\phi = 0.125$ with the height profile of this sample in subplot d. e) $\phi = 0.180$, with the height profile of this sample in subplot f.

General discussion

7

In this thesis we study the microstructural dynamics of colloidal gels, to learn more about the mechanical (in)stability of these highly heterogeneous structures. Acquiring a basic understanding of gel stability and failure on the microscopic level is crucial to design gels that are more resilient against internal or external stresses. In the previous Chapters, we quantified the microstructure of colloidal gels in absence or presence of external fields. Specifically, we took a closer look at phenomena such as fatigue, shear and gravitational collapse and studied how the microstructure and network topology of particle gels alters due to deformation or gravity. In this Chapter, we discuss the research in this thesis in a broader context. Subsequently, we highlight some interesting directions for further exploration.

The role of plasticity in colloidal gel failure

In Chapter 2 and 3 of this thesis we studied fatigue in colloidal gels. We showed that strand rupture is preceded by significant plastic deformations that cause irreversible lengthening and softening of gel strands. Plasticity in the gel strands gives rise to the formation of weak spots or so-called necking regions. This mechanism of failure is observed for strands of different lengths and thicknesses and for interaction potentials of different strength and range. This suggests that plasticity in colloidal gel strands as a precursor for failure is relevant for a wide range of colloidal systems.

So far, fatigue in colloidal gels was mainly studied on a macroscopic scale, for instance in colloidal gels made out of carbon black particles of which the stress-strain response was followed using a combined rheometer and ultrasound device [1, 2]. There has been one study where fatigue has been attributed to erosion of the strand structure [3]. Yet, in this study strand fracture is considered to be brittle, whereas our work shows that strands fail in a ductile manner. That is, before failure plastic deformations cause the

formation of weaker necking regions.

Chapter 2 and 3 of this thesis are some of the first studies to explain fatigue at the microscopic level. As plastic events are also present in gels during aging and when applying mechanical load [4, 5], this raises the question whether the formation of necking regions is a mechanism through which colloidal gels fail more often. A recent simulation study on the gravitational collapse of colloidal gels, shows how particles in a strand move towards the junctions of the network [6], which gives rise to the formation of a necking region. Consequently, the gel strand gets weaker and will fail. When this happens to many strands, a gravitational collapse results. We argue that the formation of necking regions in colloidal gels is not limited to fatigue, but probably also happens during gravitational collapse and even aging. Experimentally, the formation of necking regions during aging can be studied with the particle system utilized in Chapter 4, 5 and 6. Optimizing the density matching in this system will make it possible to follow the three-dimensional structure of a gel as it evolves in time. Furthermore, the shear setup described in Chapter 5 is also suitable to experimentally study the evolving network topology in colloidal gels during cyclic loading. Instead of applying shear in one direction, the motorized actuator can reverse direction in an alternating manner.

Extending the network topology analysis of colloidal gels

In Chapter 4, we presented a method to map the complete topology of a colloidal gel network. The topological structure is obtained by reducing the network based on the particle coordinates and the connectivity of the network. The final network topology is the mechanical backbone of the gel which does not contain any dangling ends. During reduction, however, long dangling ends can be quantified. In Chapter 5, we saw that depending on the initial network topology shear can increase or decrease the number of dangling ends. Therefore, it would be useful to determine all dangling ends in the system, including short loose ends.

We showed how weak colloidal gels have more dangling ends compared to stronger gels. Dangling ends are known to be more flexible structures than strands fixed between two nodes [7]. Yet, these flexible dangling ends are not known to play a role in colloidal gel mechanics. However, as dangling ends can form new connections in time, this raises the question how the formation of these new connections changes the network's stiffness [8]. It would be very interesting to use the topology method to see how gels actually form during the gelation process, and how the structure of a gel evolves as the gel ages in time.

To study the evolution of the network structure it would also be benefi-

cial to link strands and nodes in time. Now, it is possible to locate strands and nodes, but it is not yet possible to follow their movement. This is essential to study processes, such as local stress-relaxation, where single strands may move or elongate. Thus, linking nodes and strands in time will complete the picture of how the network structure of a gel alters during failure or when stress is applied. An extended version of the method to determine the network topology, as described in Chapter 4, would allow for such an investigation.

In Chapter 3 of this thesis, the mechanical response of colloidal gel strands is observed to depend on both the strand length and thickness. This raises the question whether colloidal gels can also be described by a bead-spring model, were complete strands in the network are represented by springs. Bead-spring models with less than 6 springs per bead in three-dimensions, so-called sub-isostatic networks, have proven to be a powerful tool to study elastic networks composed of stiff biopolymers, like actin and collagen [9–11]. It would be interesting to see whether these subisostatic networks can also predict the rheological behaviour of colloidal gels.

Towards a systematic definition of shear deformation in colloidal gels

In Chapter 5 we showed how the network structure of colloidal gels is affected when shear is applied. From computer simulations and experiments we see that the network structure densifies upon applying shear, as strands start to fuse. Some papers, report densification upon shear as well [12–14]. Other papers, however, report completely opposite results. Here, the network falls apart upon applying shear and the the number of neighbours per particle goes down [15–17]. In one of these papers it is reported that during shear the network is detached from the cone surface and yielding of the gel is primarily induced by fluid drag and hydrodynamic interactions [16]. In other words, wall slip makes it challenging to perform good rheology experiments on colloidal gels.

In Chapter 5 we report that shear in the network is only obtained by using non-slip boundaries. Otherwise, the gel will immediately slip and detach from the glass plate, which results in plug flow. In simulations, of course, applying shear is much more feasible. The definition of shear in experiments, however, is poorly defined as instead of shear one could also be looking at plug flow, creep flow or a combination of these effects. This makes it difficult to compare experimental and simulation data, but also to compare experimental data between scientific groups. Since colloidal gels are weak in itself and often have fewer particles connected to the walls [1, 2, 18], it is just a matter of time before a gel will eventually break from its boundaries [16, 19–21]. To reproduce and compare experimental data it is thus important to quantify and report the applied deformation field, for instance

by plotting the particle trajectories in time [16].

A general framework for mechanical instabilities

Processes such as fatigue, gravitational collapse, aging and syneresis in colloidal gels share common features. Here, we describe a few of these similarities. Colloidal gels are out-of-equilibrium structures and will evolve in time. In Chapter 2 and 3 we show how the number of bonds in colloidal gel strands rapidly increase when a repetitive oscillatory deformation is applied. In this way fatigue is reminiscent of activated aging, i.e. a gel coarsens quicker in time by applying an external force. It would be very interesting to experimentally compare the evolution of the microstructre of colloidal gels with and without external deformation.

Both aging and syneresis have been ascribed to rearrangements of particles in the network due to stress relaxation. A recent study by Wu et. al. shows that for small hydrostatic pressure differences - applied by taking a scope out of a model mayonnaise system- a delay period is observed before syneresis takes place [22]. This delay might coincide with the period before the gravitational collapse of the particle gel. This raises the question how these processes are intertwined and whether syneresis might be a consequence of the gravitational collapse of particle gels. Similar questions arise in the case when aging is followed by a gravitational collapse [23].

In Chapter 6, the gravitational collapse of colloidal gels is studied experimentally. During gravitational collapse, large-scale, cooperative motion is observed in the direction perpendicular to the gravitational field. This shear-like motion is induced by internal stresses in the gel and accelerates gel failure. A recent study shows the occurrence of spatially localized microquakes in aging colloidal gels [4]. It is too early to conclude that microquakes observed in aging are similar to the large-scale, cooperative motion observed during gravitational collapse. However, studying whether these processes are (inter)related would be highly relevant to design soft materials which are mechanically (more) stable. A combination of confocal microscopy and scattering techniques, such as diffusing wave spectroscopy (DWS), can increase our understanding of both the microstructure and long-ranged dynamics of gels during failure.

Multi-component gels

Although gels are out-of-equilibrium structures and hence manifest slow aging dynamics they are still able to withstand large mechanical stresses. It

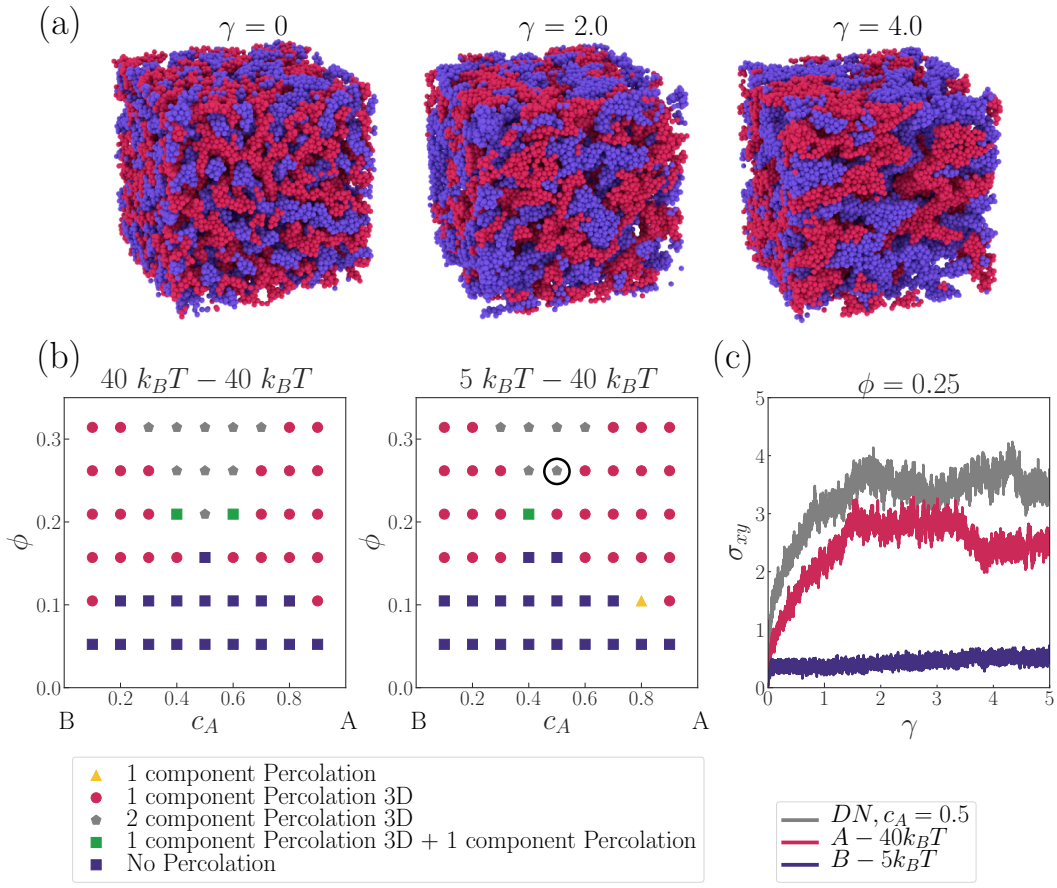

Figure 7.1 – a) Three-dimensional reconstructions of a hybrid particle network of which the two independent networks differ in strength. The total volume fraction of this gel equals $\phi = 0.25$, the weak network has an interaction strength of 5 k_BT (purple) and the strong network has an interaction strength of 40 k_BT (pink). b) Phase diagrams for two different hybrid networks. The circle indicates the sample in subplots a and c. c) Stress-strain curve of the deformation of a hybrid particle network. The double network is represented in gray, whereas single network A and B are represented in pink and purple. Network A (40 k_BT) is stronger compared to network B (5 k_BT). The yielding behaviour of the hybrid network is very similar to the strongest network. Surprisingly, adding the weak network makes the double network stronger than a single network at a volume fraction of $\phi = 0.25$ and interaction strength of 40 k_BT. In this way, combining weak and stronger networks can be used to tune material properties.

is well-known that the toughness of a polymer gel can increase dramatically upon combining a weak sacrificial network and a stronger network [24–27]. The question arises whether this is also the case for colloidal gels.

Formation of interpenetrating networks, or so-called bigels, hybrid networks or double networks, has been realised in experiments and simulations

using DNA-crafted colloids [28–32], proteins [33], patchy particles [34], micelles [35] and dipolar colloids [36]. In these cases, a specific interaction makes it possible for particles of one type to bind to each other. At certain positions in the phase diagram this allows for the formation of intertwined networks. Just as for single particle networks, the number of particles of each type must be high enough to get a space-spanning network. One can imagine that there are regions in the phase diagram where one type of particles forms a network, whereas the other type of particles just forms aggregates in between.

Simulations where hybrid networks are strained show the break up of the two intertwined networks into clusters [29]. This is very different from the coalescence of particle strands as observed for a single network (Chapter 5). Two component gels appear to be stiffer at low strains, have a higher yield stress and retain higher stresses at large deformations [29]. The proposed microscopic mechanism for the increase in toughness of a interpenetrating network would be that bigels prevent demixing. The repulsion between particles of different types prevent the gel from complete failure.

A recent simulation study shows the difference in mechanical response between single, double and three component gels [37]. Upon increasing the number of networks, strands of the individual networks get thinner. Three component gels are softer than their single and double component counterparts, however, they yield at larger strains. Ferreiro-Córdova and coworkers showed that the microscopic rearrangements in three component gels are much higher [37]. This is probably due to the steric repulsion between the different networks, which forces the individual gel networks to restructure.

The formation of double or even three component gels opens up a wide range of possibilities to design materials with different mechanical properties, such as stronger and tougher materials, which have applications in flexible electronics and soft-robotics [38]. For these multi-component gels a wide variety of parameters can still be investigated. What happens for instance when you would apply repetitive oscillatory deformations to these multi-component gels? Is the microscopic mechanism of fatigue different in these networks? And what happens with the stress response of a double network if we combine networks of different strength? Figure 7.1 shows preliminary data of a hybrid network where two networks of different strength are combined. Individually these networks will yield at different moments in time. Yet, combining two networks of different strength permits to tune both the strength, yielding behaviour and reversibility of the gel. Moreover, mapping the network topology of double networks –using the method described in Chapter 4 of this thesis– can elucidate the distinct network response in these multi-component gels.

Oppositely charged particle networks

Gelation of colloidal systems has been extensively studied for purely attractive systems. Yet, gelation can also occur in systems where attractive interactions compete with repulsive interactions. In these so-called binary gels attractive interactions are caused by oppositely charged particles whereas repulsive interactions are due to like-charged particles. Binary gel formation has been studied before both in experiments and simulations using mixtures of equally sized oppositely charged colloids [39–41]. Besides, it was shown that long-ranged oppositely charged interactions can also be used to design binary colloidal clusters [42].

A recent study by Diba and coworkers, shows how mixing oppositely charged silica and gelatin nanoparticles results in the formation of self-healing composite gels [43]. These colloidal gels are able to withstand substantial compressive or tensile loads and show remarkable self-healing after failure through cutting or shear. Oppositely charged particle gels are therefore highly relevant to develop self-healing gels [44].

So far, binary gels have not yet been studied using differently sized anionic and cationic particles. Even though gels are out of equilibrium structures a charge ratio between the small and large particles might induce local order in the network structure. Here, we show preliminary data of a gel of cationic and anionic particles (see Fig. 7.2). The negatively charged –anionic– particles consist of poly (methyl methacrylate) PMMA particles with a poly (12-hydroxystearic acid) (PHSA) based stabiliser, whereas the positively charged –cationic– particles consist of PMMA with a polydimethylsiloxane (PDMS) based stabiliser. Figure 7.2a shows that the cationic particles (in blue) are larger compared to the anionic particles (in orange), their sizes are respectively 2.4 and 1.4 μm. The structure of the gel results from a balance between repulsive forces of like-charged particles and attractive forces of oppositely charged particles. This gives rise to the formation of a highly sparse network, where particles have a low number of connections. We clearly see how cationic particles (in blue) act as branching points when they are surrounded by three anionic particles (in orange). The gel shows this local order, as the positive charge of the large particles is approximately $3\times$ higher compared to the negative charge of the small particles. The stoichiometry of anionic and cationic particles also plays a major role in whether a compact or fractal network will be obtained [30]. In this case the stoichiometry between large and small particles equals 1:3.

Using Monte Carlo simulations we study the formation of clusters in this system (see Fig 7.2). We determine the angle between two anionic particles on one cationic particle and find well defined peaks. Upon increasing the volume fraction we see how the peaks shift from a broad peak at 120 degrees

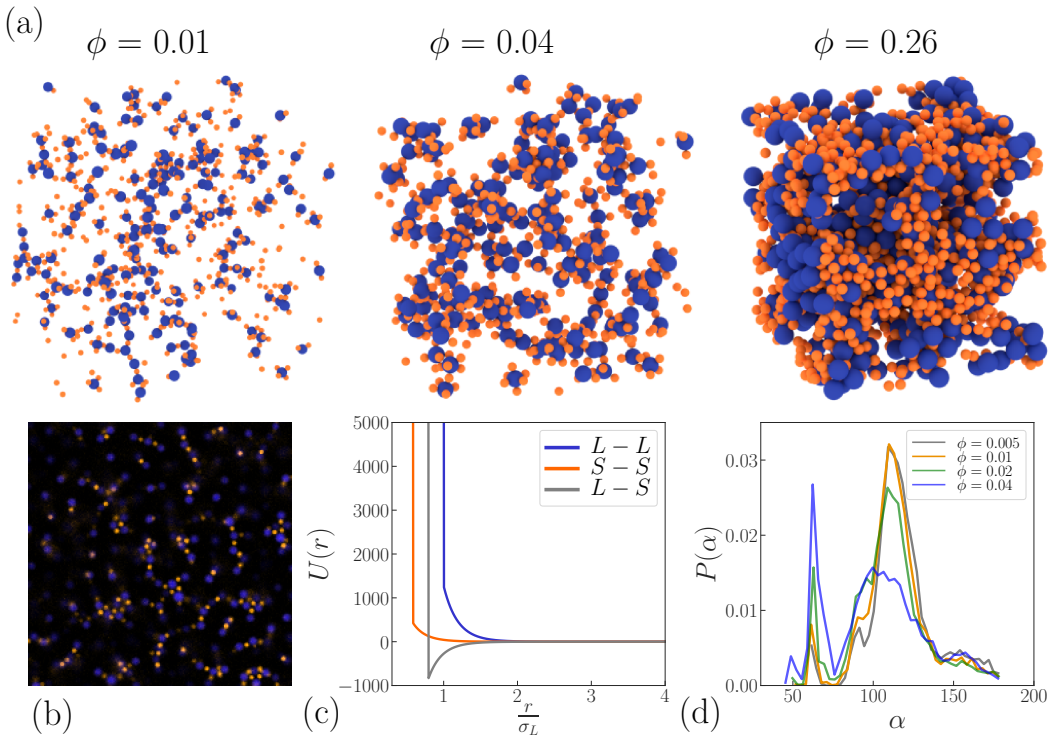

Figure 7.2 – a) Three-dimensional reconstructions of Monte Carlo simulations of oppositely charged particles. b) Confocal microscopy image of a gel formed from oppositely charged particles of different sizes (*Experimental data: Ruben Higler, Particle synthesis: Thomas E. Kodger*). c) The used Yukawa potential for repulsion and attraction between the cationic and anionic particles. d) Probability distribution of the angle between large cationic and small anionic particles at different volume fractions. In this case the ratio in which the cationic and anionic particles are present is 1:3.

towards a sharper peak at 60 degrees. At higher volume fractions these clusters will form a percolating gel structure, as shown in the experimental data and the three-dimensional reconstruction of the simulations.

The mechanical properties of these charge based networks, with different size ratio and stoichiometry, have not been studied as such. Microstructural dynamics of these oppositely charged particle gels might be very different from colloidal gels studied in these thesis, as particle rotations could be hindered due to charge effects. How these oppositely charged gels, consisting of differently sized anionic and cationic particles, respond to mechanical deformation remains an open question for future research.

Internal stress and friction in colloidal gels

The work in Chapter 2 and 3 of this thesis shows how gel strands are plastically deformed upon repetitive oscillatory deformation. Naturally, this makes one wonder whether particles rotate or slide during this deformation. The recent development of eccentric colloidal particles now allows for the investigation of particle rotations in experimental systems. Eccentric colloidal spheres, which for instance contain two differently labelled fluorescent cores, provide not only the center of mass but also the local orientation of a particle [45]. So far, rotational dynamics of particles has been investigated for fluids and crystals [45, 46], but not yet for gels. Quantifying the emergence of friction is essential to understand particle dynamics in colloidal gels. An interesting experiment would be to stretch colloidal gel strands of these eccentric spheres using optical manipulation tools, to determine whether particles in the gel are rolling or sliding with respect to each other. Experimentally stretching bulky colloidal gel strands, like the simulations in Chapter 2 and 3 of this thesis, would be interesting to detect additional modes of deformation with respect to stretching single particle chains [47].

More and more simulation studies are performed to understand the role of sliding and rolling friction in colloidal gels [48, 49] and suspensions [50, 51]. Recently, it was shown that shear thickening in suspensions is due to the formation of a frictional contact network between particles [52, 53]. Friction between particles is not only relevant for colloidal gels and suspensions, but also for granular matter and frictional glasses. A simulation study by Nguyen and coworkers, shows how hindered particle rotations affect the gel morphology of colloidal gels [48]. When particles can rotate freely they form densely packed gels. When rotation dynamics are hindered, however, this leads to more diffuse networks. These gels are generally also stiffer. The development of eccentric colloidal particles opens up a wide range of opportunities to study rotational motion of colloidal particles in arrested networks. This will give new insights into particle dynamics during gravitational collapse, fatigue and shear.

Optical tweezers have been used to study micromechanics in gel networks and single particle chains [47, 54, 55]. In this thesis, the microstructural response of colloidal networks has been studied by applying external fields. However, we know that processes such as aging and syneresis are due to internal stresses in the gel network. This raises the question how these internal stresses in colloidal networks are dissipated. Computer simulations of simplified networks, by Bouzid and coworkers, show a long ranged elastic response when a rupture event takes place. This response extends over several network meshes [56]. However, the effect of these internal stresses on the network topology of gels, has not yet been studied in experiments. Here,

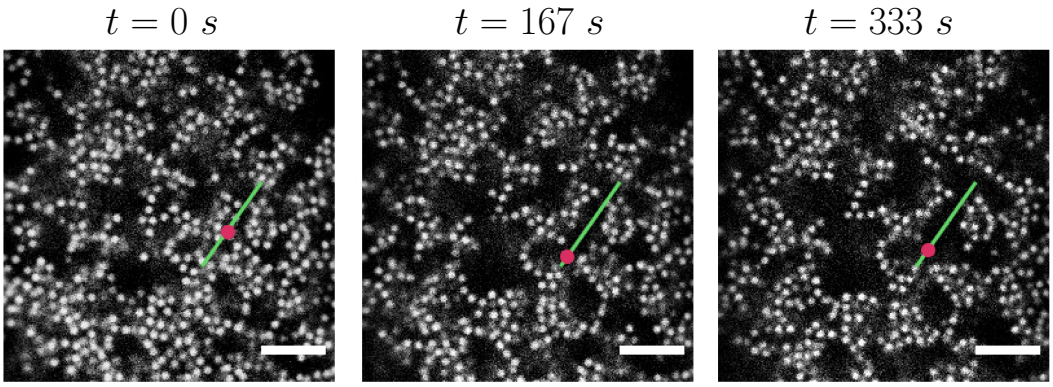

Figure 7.3 – Confocal images of a colloidal gel at a volume fraction of approximately $\phi = 0.15$ and a polymer concentration of 7.2 mg/mL. A trapped particle with an diameter of 2.8 μm is indicated in pink. The optical trap moves in an oscillatory fashion along the green line at a speed of 200 nm/second. The scale bar equals 10 μm (*Setup and Software development by Arran Curran, University of Oxford*).

we show a first proof-of-principle to execute such an experiment. Moving an optical trap through a colloidal gel in a linear oscillatory fashion ruptures the gel from the inside (see Fig 7.3). At the same time Z-stacks are recorded, to obtain three dimensional data around the point of rupture. The particle system is the same as used in Chapter 4,5 and 6 of this thesis. However, as this system is index and density matched a very small amount of larger polystyrene beads ($2.8 \pm 0.04\ \mu m$, microparticles GmbH), which can be trapped by the laser, are added. The network topology algorithm described in Chapter 4 of this thesis can be used to study the precise network response.

Following the stress response of these networks in time will give us more information about how the network copes with internal stresses. Questions, such as at which length scales the network is affected and how stress-relaxation becomes different in gels with higher volume fraction or larger interaction strength are highly relevant to understand the dissipation of internal stresses in colloidal gels. Moreover, it will increase our understanding of how the network topology evolves as a consequence of internal strand rupture.

Outlook

In this Chapter we described how future research can further boost our understanding of the structure-function relationship of colloidal gels. We discussed unresolved questions for multi-component gels and oppositely

charged networks. Besides, we considered quantifying internal stresses and friction to complete the picture of stress relaxation and rotational dynamics in colloidal gels. This knowledge will promote the development of new types of particle gels which are more stable, can self heal or are more resilient to fatigue.

Bibliography

[1] Christophe Perge, Nicolas Taberlet, Thomas Gibaud, and Sébastien Manneville. Time dependence in large amplitude oscillatory shear: A rheo-ultrasonic study of fatigue dynamics in a colloidal gel. *Journal of Rheology*, 58(5):1331–1357, 2014.

[2] Thomas Gibaud, Christophe Perge, Stefan B Lindström, Nicolas Taberlet, and Sébastien Manneville. Multiple yielding processes in a colloidal gel under large amplitude oscillatory stress. *Soft Matter*, 12(6):1701–1712, 2016.

[3] Stefan B Lindström, Thomas E Kodger, Joris Sprakel, and David A Weitz. Structures, stresses, and fluctuations in the delayed failure of colloidal gels. *Soft Matter*, 8(13):3657–3664, 2012.

[4] Zeno Filiberti, Roberto Piazza, and Stefano Buzzaccaro. Multiscale relaxation in aging colloidal gels: From localized plastic events to system-spanning quakes. *Physical Review E*, 100(4):042607, 2019.

[5] Stefano Aime, Laurence Ramos, and Luca Cipelletti. Microscopic dynamics and failure precursors of a gel under mechanical load. *Proceedings of the National Academy of Sciences*, 115(14):3587–3592, 2018.

[6] Poornima Padmanabhan and Roseanna Zia. Gravitational collapse of colloidal gels: non-equilibrium phase separation driven by osmotic pressure. *Soft Matter*, 14(17):3265–3287, 2018.

[7] Emanuela Del Gado and Walter Kob. Length-scale-dependent relaxation in colloidal gels. *Physical Review Letters*, 98(2):028303, 2007.

[8] Hang-Shing Ma, Rémi Jullien, and George W Scherer. Dangling bond deflection model: Growth of gel network with loop structure. *Physical Review E*, 65(4):041403, 2002.

[9] A Sharma, AJ Licup, KA Jansen, R Rens, M Sheinman, GH Koenderink, and FC MacKintosh. Strain-controlled criticality governs the nonlinear mechanics of fibre networks. *Nature Physics*, 12(6):584–587, 2016.

[10] Federica Burla, Justin Tauber, Simone Dussi, Jasper van Der Gucht, and Gijsje H Koenderink. Stress management in composite biopolymer networks. *Nature physics*, 15(6):549–553, 2019.

[11] Federica Burla, Simone Dussi, Cristina Martinez-Torres, Justin Tauber, Jasper van der Gucht, and Gijsje H Koenderink. Connectivity and plasticity determine collagen network fracture. *Proceedings of the National Academy of Sciences*, 117(15):8326–8334, 2020.

[12] Kasper Masschaele, Jan Fransaer, and Jan Vermant. Direct visualization of yielding in model two-dimensional colloidal gels subjected to shear flow. *Journal of Rheology*, 53(6):1437–1460, 2009.

[13] Bharath Rajaram and Ali Mohraz. Microstructural response of dilute colloidal gels to nonlinear shear deformation. *Soft Matter*, 6(10):2246–2259, 2010.

[14] Benjamin J Landrum, William B Russel, and Roseanna N Zia. Delayed yield in colloidal gels: Creep, flow, and re-entrant solid regimes. *Journal of Rheology*, 60(4):783–807, 2016.

[15] Lilian C Hsiao, Richmond S Newman, Sharon C Glotzer, and Michael J Solomon. Role of isostaticity and load-bearing microstructure in the elasticity of yielded colloidal gels. *Proceedings of the National Academy of Sciences*, 2012.

[16] Bharath Rajaram and Ali Mohraz. Dynamics of shear-induced yielding and flow in dilute colloidal gels. *Physical Review E*, 84(1):011405, 2011.
[17] Thomas Gibaud, Damien Frelat, and Sébastien Manneville. Heterogeneous yielding dynamics in a colloidal gel. *Soft Matter*, 6(15):3482–3488, 2010.
[18] Pierre Ballesta, Nick Koumakis, Rut Besseling, Wilson CK Poon, and George Petekidis. Slip of gels in colloid–polymer mixtures under shear. *Soft Matter*, 9(12):3237–3245, 2013.
[19] HJ Walls, S Brett Caines, Angelica M Sanchez, and Saad A Khan. Yield stress and wall slip phenomena in colloidal silica gels. *Journal of Rheology*, 47(4):847–868, 2003.
[20] N Koumakis, P Ballesta, R Besseling, WCK Poon, JF Brady, and G Petekidis. Colloidal gels under shear: Strain rate effects. In *AIP Conference Proceedings*, volume 1518, pages 365–371. American Institute of Physics, 2013.
[21] P Ballesta, G Petekidis, L Isa, WCK Poon, and R Besseling. Wall slip and flow of concentrated hard-sphere colloidal suspensions. *Journal of Rheology*, 56(5):1005–1037, 2012.
[22] Qimeng Wu, Melle TJJM Punter, Thomas E Kodger, Luben Arnaudov, Bela M Mulder, Simeon Stoyanov, and Jasper Van Der Gucht. Gravity-driven syneresis in model low-fat mayonnaise. *Soft Matter*, 15(46):9474–9481, 2019.
[23] Lisa J Teece, Malcolm A Faers, and Paul Bartlett. Ageing and collapse in gels with long-range attractions. *Soft Matter*, 7(4):1341–1351, 2011.
[24] Jian Ping Gong. Why are double network hydrogels so tough? *Soft Matter*, 6:2583–2590, 2010.
[25] Hugh R. Brown. A model of the fracture of double network gels. *Macromolecules*, 40(10):3815–3818, 2007.
[26] Hyun Joon Kong, Emma Wong, and David J. Mooney. Independent control of rigidity and toughness of polymeric hydrogels. *Macromolecules*, 36(12):4582–4588, 2003.
[27] Y. Tanaka. A local damage model for anomalous high toughness of double-network gels. *EPL (Europhysics Letters)*, 78(5):56005, 2007.
[28] Francesco Varrato, Lorenzo Di Michele, Maxim Belushkin, Nicolas Dorsaz, Simon H. Nathan, Erika Eiser, and Giuseppe Foffi. Arrested demixing opens route to bigels. *Proceedings of the National Academy of Sciences*, 109(47):19155–19160, 2012.
[29] L. Di Michele, D. Fiocco, F. Varrato, S. Sastry, E. Eiser, and G. Foffi. Aggregation dynamics, structure, and mechanical properties of bigels. *Soft Matter*, 10:3633–3648, 2014.
[30] Fabian M Hecht and Andreas R Bausch. Kinetically guided colloidal structure formation. *Proceedings of the National Academy of Sciences*, 113(31):8577–8582, 2016.
[31] Lorenzo Di Michele, Francesco Varrato, Jurij Kotar, Simon H. Nathan, Giuseppe Foffi, and Erika Eiser. Multistep kinetic self-assembly of dna-coated colloids. *Nature Communications*, 4(2007), 2013.
[32] Mykolas Zupkauskas, Yang Lan, Darshana Joshi, Z Ruff, and E Eiser. Optically transparent dense colloidal gels. *Chemical Science*, 8(8):5559–5566, 2017.
[33] Alice Blumlein and Jennifer J. McManus. Bigels formed via spinodal decomposition of unfolded protein. *Journal of Materials Chemistry B*, 3:3429–3435, 2015.
[34] Daniel de las Heras, Jose Maria Tavares, and Margarida M. Telo da Gama. Bicontinuous and mixed gels in binary mixtures of patchy colloidal particles. *Soft Matter*, 8:1785–1794, 2012.
[35] A. Klymenko, T. Nicolai, L. Benyahia, C. Chassenieux, O. Colombani, and E. Nicol. Multiresponsive hydrogels formed by interpenetrated self-assembled polymer networks. *Macromolecules*, 47(23):8386–8393, 2014.
[36] Amit Goyal, Carol K. Hall, and Orlin D. Velev. Bicontinuous gels formed by self-assembly of dipolar colloid particles. *Soft Matter*, 6:480–484, 2010.
[37] Claudia Ferreiro-Córdova, Emanuela Del Gado, Giuseppe Foffi, and Mehdi Bouzid. Multi-component colloidal gels: interplay between structure and mechanical properties. *Soft Matter*, 2020.
[38] Steven I Rich, Robert J Wood, and Carmel Majidi. Untethered soft robotics. *Nature Electronics*, 1(2):102–112, 2018.
[39] Eduardo Sanz, Mirjam E. Leunissen, Andrea Fortini, Alfons van Blaaderen, and Marjolein Dijkstra. Gel formation in suspensions of oppositely charged colloids: Mechan-

ism and relation to the equilibrium phase diagram. *The Journal of Physical Chemistry B*, 112(35):10861–10872, 2008.

[40] Evan Spruijt, Henriette E. Bakker, Thomas E. Kodger, Joris Sprakel, Martien A. Cohen Stuart, and Jasper van der Gucht. Reversible assembly of oppositely charged hairy colloids in water. *Soft Matter*, 7:8281–8290, 2011.

[41] Emily R. Russell, Joris Sprakel, Thomas E. Kodger, and David A. Weitz. Colloidal gelation of oppositely charged particles. *Soft Matter*, 8:8697–8703, 2012.

[42] Ahmet Faik Demirörs, Johan C. P. Stiefelhagen, Teun Vissers, Frank Smallenburg, Marjolein Dijkstra, Arnout Imhof, and Alfons van Blaaderen. Long-ranged oppositely charged interactions for designing new types of colloidal clusters. *Physical Review X*, 5:021012, Apr 2015.

[43] Mani Diba, Huanan Wang, Thomas E Kodger, Shima Parsa, and Sander CG Leeuwenburgh. Highly elastic and self-healing composite colloidal gels. *Advanced Materials*, 29(11):1604672, 2017.

[44] Danielle Lynne Taylor and Marc in het Panhuis. Self-healing hydrogels. *Advanced Materials*, 28(41):9060–9093, 2016.

[45] Stefan Schütter, Jörg Roller, Andrea Kick, Janne-Mieke Meijer, and Andreas Zumbusch. Real-space imaging of translational and rotational dynamics of hard spheres from the fluid to the crystal. *Soft Matter*, 13(44):8240–8249, 2017.

[46] Lilian C Hsiao, Indranil Saha-Dalal, Ronald G Larson, and Michael J Solomon. Translational and rotational dynamics in dense suspensions of smooth and rough colloids. *Soft Matter*, 13(48):9229–9236, 2017.

[47] Simon Stuij, Jan Maarten van Doorn, Thomas Kodger, Joris Sprakel, Corentin Coulais, and Peter Schall. Stochastic buckling of self-assembled colloidal structures. *Physical Review Research*, 1(2):023033, 2019.

[48] Hong T Nguyen, Alan L Graham, Peter H Koenig, and Lev D Gelb. Computer simulations of colloidal gels: how hindered particle rotation affects structure and rheology. *Soft Matter*, 16(1):256–269, 2020.

[49] Ruru Li and Daniel Lester. Hierarchical jamming in frictional particle assemblies. *arXiv preprint arXiv:2002.00313*, 2020.

[50] Vikram Rathee, Srishti Arora, Daniel L Blair, Jeffrey S Urbach, AK Sood, and Rajesh Ganapathy. Unraveling the role of frictional contacts and particle orientational order during shear-thickening in suspensions of colloidal rods. *arXiv preprint arXiv:1906.06356*, 2019.

[51] James A Richards, Ben M Guy, Elena Blanco, Michiel Hermes, Guilhem Poy, and Wilson CK Poon. The role of friction in the yielding of adhesive non-brownian suspensions. *Journal of Rheology*, 64(2):405–412, 2020.

[52] Jean Comtet, Guillaume Chatté, Antoine Niguès, Lydéric Bocquet, Alessandro Siria, and Annie Colin. Pairwise frictional profile between particles determines discontinuous shear thickening transition in non-colloidal suspensions. *Nature Communications*, 8(1):1–7, 2017.

[53] Cécile Clavaud, Antoine Bérut, Bloen Metzger, and Yoël Forterre. Revealing the frictional transition in shear-thickening suspensions. *Proceedings of the National Academy of Sciences*, 114(20):5147–5152, 2017.

[54] Myung Han Lee and Eric M Furst. Response of a colloidal gel to a microscopic oscillatory strain. *Physical Review E*, 77(4):041408, 2008.

[55] Eric M Furst and John P Pantina. Yielding in colloidal gels due to nonlinear microstructure bending mechanics. *Physical Review E*, 75(5):050402, 2007.

[56] Mehdi Bouzid, Jader Colombo, Lucas Vieira Barbosa, and Emanuela Del Gado. Elastically driven intermittent microscopic dynamics in soft solids. *Nature Communications*, 8(1):1–8, 2017.

Summary

In this thesis, we study the structure-function relation of colloidal gels, a class of soft materials. We combine simulations and experiments to obtain insights into the microstructural response of colloidal gels in the presence or absence of external stress. Specifically, we take a closer look at processes such as fatigue, shear and gravitational collapse and study how deformation or gravity affect the microstructure and network topology of these particle gels. We employ a recently developed particle system, which can be index- and density matched using non-hazardous polar solvents, to image large volumes of colloidal gels. This confocal microscopy data allows us to determine the network topology of these particle gels using a topology mapping algorithm described in this thesis. Simultaneously, we perform simulations to obtain a better understanding of changes in the network topology of colloidal gels during deformation.

In **Chapter 2** we study fatigue in colloidal gels by combining experiments and computer simulations. Repetitive loading of a soft solid leads to microstructural damage that ultimately results in catastrophic material failure. Even though fatigue poses a treat to the stability of virtually all materials, the microscopic origins of fatigue, especially for soft solids, remain elusive. Our results reveal how mechanical loading leads to irreversible strand stretching, which builds slack into the network that softens the solid at small strains and causes strain hardening at larger deformations. We thus find that microscopic plasticity governs fatigue at much larger scales. This gives rise to a new picture of fatigue in soft thermal solids and calls for new theoretical descriptions of soft gel mechanics in which local plasticity is taken into account.

To further investigate the role of plastic deformation prior to gel strand failure, in **Chapter 3**, we analyse whether plasticity is generally present in gel strands of different thickness and length. Our simulations show that rearrangements of particles within the strands leads to plastic lengthening and softening, which may ultimately lead to strand necking and ductile failure. This failure mechanism occurs irrespective of the thickness and length of the strands and the range and strength of the interaction potential. Here, rupture is observed to be more likely for long and thin strands and when the well width of the interaction increases.

In the following chapter, **Chapter 4**, we shifted our focus from single gel strands to the full network structure of colloidal gels, as mechanics of soft colloidal gels is determined by the network topology of the underlying rigid network. However, it is very challenging to quantifying this heterogeneous structure. In this Chapter, we describe an algorithm that reduces a colloidal gel to a network consisting of nodes and strands, which allows us to map the complete topology of the gel – both in experiments and simulations. Colloidal gels are quantified based on the number and coordination of nodes and the number, length and thickness of the segments. The described method allows for the mapping of the network topology of gels with different morphologies. For experimental and simulated gels, remarkable topological resemblance is shown. The developed topological mapping algorithm opens up a wide range of possibilities to study colloidal network physics in more detail.

In **Chapter 5** we strived to apply the algorithm presented in Chapter 4 to colloidal gels under shear. Understanding the microstructural rearrangements in the yielding transition of colloidal gels is highly relevant to understand the initiation of flow and deformation in food products, paints and coatings. Yet, it is still unexplored how the network topology of gels affects or is affected by yielding. Here, we investigate the yielding transition in colloidal gels both in simulations and experiments. We examine different gel topologies, formed at varying interaction energies and volume fractions. Upon increasing strain, the number of segments in the gel rapidly decreases, whereas strands in the network become thicker. Simulations reveal that close to percolation applying shear increases the connectivity of the network. This is due to dangling ends in the network which can form new connections. Networks at higher volume fraction, on the other hand, decrease in connectivity due to the applied deformation. These results show how the gel topology evolves during shear deformation.

In **Chapter 6**, we study another type of mechanical instability in colloidal gels, namely, the collapse of a colloidal gel due to gravity. Using confocal microscopy, the gravitational collapse of colloidal gels is followed at the single-particle level. After a short delay time, the colloidal gels are observed to detach from the top of the sample chamber and a macroscopic interface appears. The sedimentation dynamics of this interface are governed by poroelastic compression of the gel that lies beneath. Large-scale collective motions in the direction perpendicular to the gravitational field, induced by an imbalance of internal stresses in the gel, lead to shear deformation in the network that accelerate gel failure. These motions are present both during the induction period and subsequent rapid-settling stage of the gel, and subside as the gel reaches its final height. These results highlight that not only external stresses, but also internal stresses play a crucial role in the failure of these heterogeneous networks.

Finally, in **Chapter 7**, the general discussion, we place our findings in a broader scientific context and give an outlook on future colloidal gel research.

About the author

Joanne Verweij was born on the 6th of May 1991, in Bodegraven, the Netherlands. She grew up in Woerden, where she graduated from Kalsbeek College in 2009. In the same year she enrolled for the study Molecular Life Sciences at Wageningen University. After obtaining her Bachelor's degree in 2012, she continued her education with a Master in Molecular Life Sciences, with a specialization in Physical Chemistry.

During her Master she did a thesis project at the Laboratory of Cell Biology (Wageningen University). Here, she developed a Matlab tracking algorithm to follow the fluorescently labeled plus-ends of microtubuli, as a tool to study growth dynamics in wildtype and mutant strains of moss. For her Master intership she worked at the Utrecht Van't Hoff Laboratory for Physical and Colloid Chemistry (Utrecht University), where she combined experiments and Monte Carlo simulations to study depletion induced encapsulation of microspheres by smooth-rough dumbbells. In 2015 she received her Master's degree *cum laude*.

In June 2015, Joanne started as a PhD candidate in the group of Physical Chemistry and Soft Matter. Under supervision of Prof. Dr Frans Leermakers, Prof. Dr Joris Sprakel and Prof. Dr Jasper van der Gucht she studied the response of colloidal gels upon applying external fields. From October 2019 till March 2020, Joanne was a guest researcher in the group of Prof. Dr Roel Dullens in the Physical and Theoretical Chemistry Laboratory at the University of Oxford.

This thesis, entitled *"Microstructural Dynamics of Colloidal Gels"*, presents the results of the performed research.

List of publications

This thesis

- J.E. Verweij/J.M. van Doorn, J. Sprakel, and J. van der Gucht, *Strand plasticity governs fatigue in colloidal gels*, Physical Review Letters 120 (20), 208005 (2018), cover, Chapter 2

  Focus story in Physics (issue 11 (50), 2018), *Why Soft Solids Get Softer*

- J.E. Verweij, F.A.M Leermakers, J. Sprakel, and J. van der Gucht, *Plasticity in colloidal gel strands*, Soft Matter 15 (32), 6447 - 6454 (2019), cover, Chapter 3

- J.E. Verweij, T.E. Kodger, F.A.M Leermakers, J. Sprakel, and J. van der Gucht, *Simplifying Structure: Elucidating the Network Topology of Colloidal Gels*, To be submitted (2020), Chapter 4

- J.E. Verweij, T.E. Kodger, F.A.M Leermakers, J. Sprakel, and J. van der Gucht, *Colloidal Gel Networks under Shear*, To be submitted (2020), Chapter 5

- J.E. Verweij/B. van der Meer, T. Yanagishima, J. van der Gucht, J. Sprakel, and R.P.A. Dullens, *Anomalous large-scale motion during the gravitational collapse of colloidal gels*, In preparation (2020), Chapter 6

Other work

- J.E. Verweij/J.R. Wolters, G. Avvisati, M. Dijkstra, and W.K Kegel, *Depletion-Induced Encapsulation by Dumbbell-Shaped Patchy Colloids Stabilize Microspheres against Aggregation*, Langmuir 33 (13), 3270-3280 (2017).

Figure 7.4 – The Cover of Physical Review Letters 120 (20) and Soft Matter 15 (32) which show three-dimensional renderings of a gel network and a single gel strand. The mobility of particles in these structures is color-coded from low (purple) to high (yellow).

Acknowledgements

With the end of my PhD adventure in sight, I would like to thank all people that helped me along the way. Because, while research is lonely at times, the connection and collaboration with others makes it much more vibrant, successful and rewarding.

Jasper, Frans and Joris, I am thankful for the opportunity to do my PhD at PCC. Thanks for your input during the work discussions, your support during the different stages of my research and for the time and effort spend on reading and commenting on articles and thesis chapters. The fact that you allowed me to spend the final months of my PhD in Oxford, is something I highly appreciate!
Jasper, thanks for always encouraging me to take my research one step further.
Frans, I could always knock on your door to discuss scientific and personal questions, thanks!
Joris, I am very happy that you joined my PhD project. Your enthusiasm and creative ideas often motivated me to walk the extra mile.
Tom, the particle system you developed during your PhD became the basis for the experimental work in this thesis. You always made time to discuss my experimental questions and gave me lots of tips and tricks. I take it as a complement that after a while you became less scared by seeing me in the lab.
Roel, thank you for welcoming me into your group at the end of my PhD. It was inspiring to work in a group where topics are so closely related and I enjoyed it a great deal.
Jan Maarten, it was very nice to collaborate with you and to be able to combine your experiments with my simulations!
Mara en Leonie, without you the PCC lab would not run as smoothly as it does. I could always ask for help concerning administrative matters. Yet, what I appreciated most was the time you always took to ask how I was doing.
Remco, when I needed even more memory or storage space on my computer, you always took the practical approach. Often within an hour you dug up some left over hardware and plugged it in. Besides, you were always willing to help me search for new parts I wanted to add to the shear setup. Thanks!

Diane, I got to know you as a very caring colleague. It was always nice to catch up over lunch or during the coffee breaks!
Lione, you invited me to become your office mate at the start of my PhD, when PCC was still located at the Dreijen, and it stayed that way till you finished your PhD in May 2019. Due to you our office was always a lively place. I enjoyed your enthusiasm when you were busy organizing events and trips and you were always in for a nice chat, lunch or a cup of tea.
Jessica, I still remember the day that you entered our office as a postdoc and I was sad to see you go 3 years later. We had many great conversations, both in Dutch and English. I admire your dedication, both in science and learning languages!
Ruben, you always came up with ideas for technical or computer related questions and it was fun to share our enthusiasm for coding. Thanks for providing me with your beautiful thesis template!
Martijn, when you did your MSc project at PCC we shared the office. I enjoyed the enthusiasm you brought with you! It was great to see how you embarked on your own PhD adventure afterwards.
Ilse, We started our PhD project around the same time and it was always nice and motivating to catch up over a cup of tea. I am happy that you stand beside me as my paranymph today!
Justin, it was very inspiring to work with you. Even though the bead-spring-model simulations in the end did not make it into this thesis, I enjoyed our collaboration a lot!
Qimeng, it was very nice to share our PhD journey together. I enjoyed the moments that we spend together in the lab and our experimental discussions.
Ties, I entered your office many times to ask a lab related question and you always answered in the same enthusiastic way. Thanks for being such a supportive colleague!
All other colleagues at PCC, it was great to share my time with you!
Arran, Balkis, Carla, Joseph, Miranda, Nick and Taiki, thanks for making my time in the Oxford lab such a pleasant experience!
Camille, Mariana, Olivia and Johnny, thanks for welcoming me into your office in Oxford and learning me so many new things about British culture!
Andrea, Hanne, Ilse, Marleen en Nadine, ik leerde jullie kennen tijdens mijn Bachelor in Wageningen. De tijd vliegt altijd als we eens in de zoveel maanden samen gaan lunchen. Bedankt voor de gezelligheid en jullie luisterend oor. Ik hoop dat we onze lunches nog lang volhouden!
Tamara, Daniëlle en Anneke, ook al is de middelbare school al lang geleden en wonen we steeds verder uit elkaar, ik vind het heel waardevol om jullie in het echt en over Skype te spreken!
Stefan en Judith, Henk en Karin, Mirjam en Hans-Rutger, Arjon en Daphne, Henno en Marielle, het is fijn om zulke leuke buren en vrienden te hebben!
Schoonfamilie, bedankt voor jullie gezelligheid en de interesse in mijn werk!

Opa en Oma Verweij, Op de basisschool kwam ik op maandag vaak tussen de middag bij u lunchen. Ook op de middelbare school, tijdens mijn studie en PhD bleef u altijd geïnteresseerd in waar ik precies mee bezig was. Ik ben blij om nu deze mijlpaal met jullie te mogen vieren!
Erik-Jan, Leny, Ezra en Mirre, het is altijd gezellig om bij jullie op bezoek te zijn!
Peter, Ik ben heel trots dat jij vandaag als paranimf naast me staat! Als je vroeg wat ik op mijn werk aan het doen was, begreep je dat stiekem prima (alleen dan op een 'iets' grotere schaal). Het is altijd leuk om te sparren met mijn kleine/grote broer.
Paps en mams, jullie kennen mij als geen ander en staan altijd voor me klaar. Dankjewel voor jullie steun en vertrouwen in mij!
Berend, not many people can say that they collaborated with their partner on a thesis chapter, but I do. Our adventure in Oxford only just started, but it was a lot of fun to perform this research together! Dankjewel voor je onvoorwaardelijke steun en je zorgzaamheid in de afgelopen jaren. Ik ben heel blij dat ik dit bijzondere moment met jou mag vieren!

Overview of completed training activities

Discipline specific activities

19th Dutch Soft Matter Meeting	Utrecht	2015
MolSim2016 simulation school (CECAM) †	Amsterdam	2016
Physical Chemistry winterschool (WUR/TU Delft)	Hans-sur-Lesse (BE)	2016
International Soft Matter Conference †	Grenoble (FR)	2016
21th Dutch Soft Matter Meeting	Wageningen	2016
Physics@Veldhoven (NWO) †	Veldhoven	2017
Masterclass Elisabeth Bouchaud (NWO)	Veldhoven	2017
Liquid Matter Conference †	Ljubljana (SI)	2017
Physics@Veldhoven (NWO) ‡	Veldhoven	2018
CHAINS (NWO) ‡	Veldhoven	2018
Physics@Veldhoven (NWO) †	Veldhoven	2019
International Soft Matter Conference	Edinburgh (UK)	2019
Visit Physical and Theoretical Chemistry Laboratory ‡	Oxford (UK)	2019
McBain Medal Meeting (SCI)	London (UK)	2019

‡ Talk † Poster

General courses

Data Management and Planning (WUR-library)	Wageningen	2015
Taking charge of your PhD Project (ElroyCOM)	Utrecht	2015
Course XperienCentral (WUR)	Wageningen	2016
Workshop Search Engine Optimization (WUR)	Wageningen	2016
Scientific Publishing (WUR-library)	Wageningen	2016
Writing better code (L&B Tech.)	Utrecht	2016
Orientation on Teaching for PhD candidates (WUR)	Wageningen	2016

SURF Research Boot Camp – Spark (SURFsara)	Eindhoven	2017
The Art of Scientific Writing (Artesco)	Utrecht	2017
The Art of Presenting Science (Artesco)	Utrecht	2018
Career Assessment (Meijer en Meijaard)	Wageningen	2019

Optionals

Preparation of research proposal	PCC	2015
Group meetings	PCC	2015-2019
Journal club	PCC	2015-2018
Meetings Hybrid Soft Material programme	NWO/Unilever	2015-2019

The research described in this thesis is part of the Industrial Partnership Program Hybrid Soft Materials that is carried out under an agreement between Unilever Research and Development B.V. and the Netherlands Organization for Scientific Research (NWO).
Financial support from NWO for the printing of this thesis is gratefully acknowledged.

Cover: A three-dimensional visualization of an experimental colloidal gel before and after gravitational collapse (back and front, respectively). Particles are color-coded according to their number of neighbours.
Cover design: Joanne Verweij
This thesis is printed by Proeftschriftmaken.nl